SMART STRUCTURES FOR CONTROL
OF OPTICAL SURFACES

THESIS

D. Michael Sobers, Jr., First Lieutenant, USAF

AFIT/GA/ENY/02-2

DEPARTMENT OF THE AIR FORCE
AIR UNIVERSITY

AIR FORCE INSTITUTE OF TECHNOLOGY

Wright-Patterson Air Force Base, Ohio

AFIT/GA/ENY/02-2

SMART STRUCTURES FOR CONTROL
OF OPTICAL SURFACES

THESIS

Presented to the Faculty

Department of Aeronautics and Astronautics

Graduate School of Engineering and Management

Air Force Institute of Technology

Air University

Air Education and Training Command

in Partial Fulfillment of the Requirements for the

Degree of Master of Science in Astronautical Engineering

D. Michael Sobers, Jr., B.A.E.

First Lieutenant, USAF

March, 2002

SMART STRUCTURES FOR CONTROL
OF OPTICAL SURFACES

D. Michael Sobers, Jr., B.A.E.

First Lieutenant, USAF

Approved:

//Signed//

_____   _____

Major Gregory Agnes   Date
Thesis Advisor

//Signed//

_____   _____

Lt Col Robert Canfield   Date
Committee Member

//Signed//

_____   _____

Doctor David Mollenhauer   Date
Committee Member

//Signed//

_____   _____

Doctor Anthony Palazotto   Date
Committee Member

Table of Contents

List of Figures

viii

xii

AFIT/GA/ENY/02-2

Abstract

The development of lightweight, large-aperture optics is of vital importance to the Department of Defense and the US Air Force for advancing remote sensing applications and improving current capabilities. Synthetic polymer optics offer weight and flexibility advantages over current generation glass mirrors, but require active control to maintain tight surface figure tolerances. This research explores the feasibility of using imbedded piezoelectric materials to control optical surfaces. Membrane-based and stiff piezo-controlled mirrors were constructed to develop and validate control techniques. Test results verified that surface control on the order of tens of wavelengths is possible using these systems.

SMART STRUCTURES FOR CONTROL
OF OPTICAL SURFACES

I. Introduction

Men love to wonder, and that is the seed of Science.

Ralph Waldo Emerson (1803-1882)

1.1 Overview

For decades, the United States has recognized the value of placing telescopes in orbit for both research and reconnaissance. For downward-looking satellites, orbit provides the altitude required for recording the "big picture". For astronomers, Earth orbit provides a platform above the turbulent atmosphere and light pollution that plague ground-based telescopes. The resolution of the images provided by these optical systems is limited by the diameter of the primary optical surface [10:116]. Thus, there is a growing interest by the US Department of Defense (DOD), NASA, and other government organizations in developing and deploying large-aperture optical telescopes [10:116].

Many advances have been made to reduce the size and weight of satellites while increasing their capability. For optical systems, however, size and weight are almost universally determined by the size of the primary mirror. These two factors are also the most important when calculating the cost of launching payloads into orbit [18:802]. Current technology mirrors are built from heavy polished glass in a long, tedious, and expensive process. Thus, placing highly capable, large-aperture telescopes in orbit is presently expensive. In addition, the aperture of these optical systems is limited to the diameter of the largest space launch vehicles, currently about 4 meters.

As a result of these limitations, high resolution optical remote sensing systems are presently restricted to low earth orbit (LEO). Achieving global coverage from LEO requires dozens of satellites, placing them with thousands of other satellites in the most crowded region of Earth orbit. Due to their size, large-aperture optical systems in LEO would be at a higher risk of damage from orbiting debris. The development of large, lightweight systems could allow remote sensing from geosynchronous orbit (GEO) with resolutions comparable to current systems. For example, a GEO system operating in the visible range with a 30-meter aperture would have a diffraction-limited resolution of 1-2 meters [18:265]. Systems in GEO would have the added benefit of staying over the same spot on the earth and global coverage could be maintained with three or four satellites.

The development of large-aperture optics depends heavily on advances in smart structures technology. The term "smart structures" is a broad description of structures that contain integrated sensors and actuators to allow precise control of the structure's mechanical states or physical properties. These systems result from the merging of adaptive structures, which contain actuators but no sensors, and sensory systems, which contain sensors but no means for structural control [16:3]. A 30-meter diameter optical surface would need to be deployable and have a very low areal density (about 1-2 kg/m^2 or less). These requirements dictate a structure that is highly flexible, yet with surface control on the order of μm [10]. Clearly, a deployable reflector with the structural control fidelity required of optical systems requires actuators and sensors that are highly integrated into the system.

Thus, the improvement of optical remote sensing capabilities depends on advanced materials that are lightweight and have integrated, highly accurate surface control systems. In 1989, 0.9-meter composite mirror panels were developed as part of the Precision Segmented Reflector (PSR) project. These mirrors weighed as little as 5 kg/m^2 and had a surface flatness of 2μm root-mean-squared (RMS) [8:193]. Piezoelectric transducer (PZT) actuators bonded to the surface provided up to 10μm of surface movement, enabling the mirror to be warped for correction of low-order

surface figure errors [8:194]. Although the surface figure achieved was not accurate enough for operation in the visible range, these lightweight mirror panels could be assembled to create large aperture sub-millimeter or far infra-red remote sensing systems.

More recently, designs of the Next Generation Space Telescope (NGST) primary mirror achieve optical surface flatness by using a 2mm thick glass "membrane" mounted to a composite structure [1:642]. Expected to launch in 2009, the NGST is designed with a folded, 8-m deployable primary mirror to alleviate launch vehicle size limitations. A 2-meter hexagonal mirror segment demonstrator was constructed in 2000 to test the composite design. The glass faceplate was controlled by 50 screw-type actuators per square meter, enabling local control of the mirror surface. The entire demonstrator mirror had a weight of 40kg and an areal density of 15.4kg/m^2 [1]. Further improvements in the actuated faceplate design should enable the NGST to meet its goal of a 13kg/m^2 primary mirror [12:9]. While the design is lightweight (compared to solid glass mirrors), extensive polishing of the mirror is still required to produce an optical-quality surface.

Promising advances in materials, combined with smart structures technology, seek to overcome the limitations faced by current lightweight mirror programs. Recent experiments have shown that mirrors cast from liquid polymers have a surface flatness suitable for optical imaging [14]. Polymer mirrors are much lighter than their glass counterparts and are easier and less expensive to manufacture. Due to their flexible nature, these mirrors can also have built-in actuators for surface control and vibration suppression. Current large-aperture glass mirrors use voice-coils for surface actuation. These coils are heavy, require significant electrical power (compared to piezoceramics), and only provide global shape control. Active polymer mirrors could have smaller, more efficient piezo actuators that would allow local, high-order surface control as well as global control.

Polymers could also be used to design a membrane-based optical telescope (see Figure 1.1). A membrane primary mirror would greatly enhance remote sensing capabilities, overcoming today's size and weight limitations. These extremely lightweight mirrors ($<2\text{kg/m}^2$) would drastically decrease the cost of placing large-aperture optical remote sensing systems into orbit. A control layer imbedded in the membrane could maintain global shape control and correct manufacturing flaws remotely. In addition, membrane optics can be folded for launch, allowing larger systems to be placed on orbit using smaller launch vehicles [10].
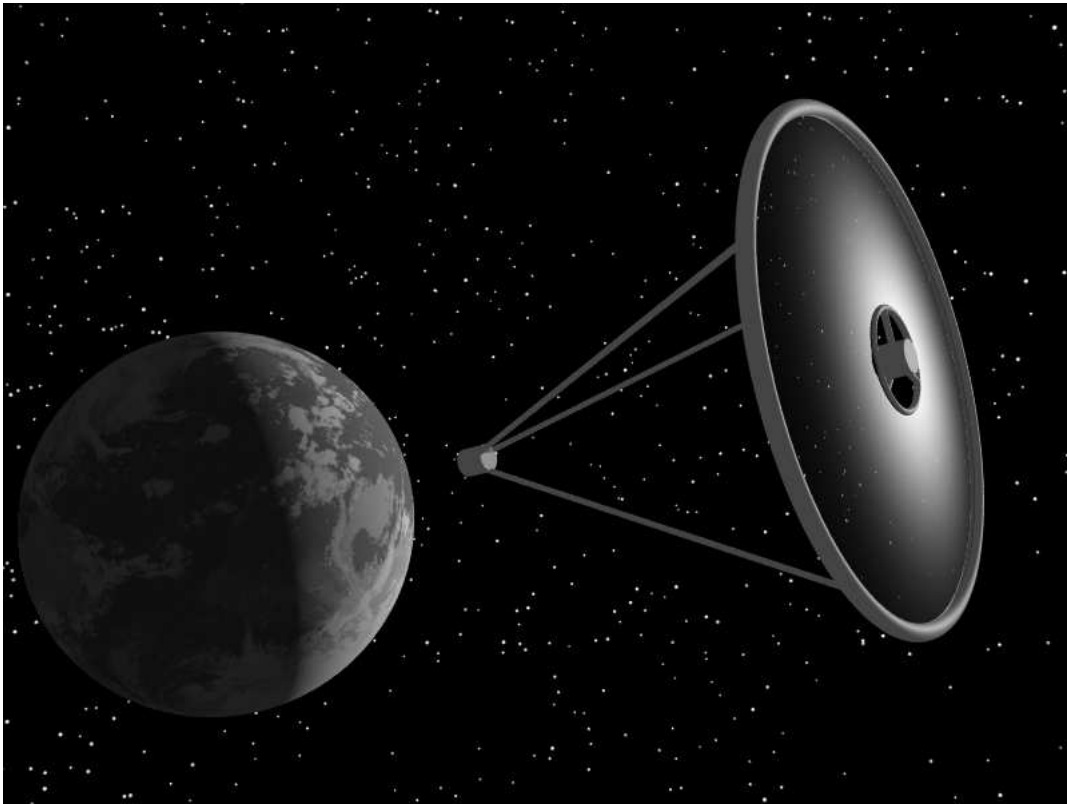
Figure 1.1   Author's concept of optical membrane remote sensing satellite.

Unfortunately, folding an optical membrane could introduce creases and wrinkles that would likely remain present after deployment [10]. In addition, membranes will not maintain their required shape without some internal or external support structure. Success of the Inflatable Antenna Experiment (IAE) and advances in the development of near net-shape optical membranes suggest that an inflatable structure

would be suitable for membrane support [5]. However, the system would still require a mechanism for controlling the flexible surface of the primary mirror to the exacting tolerances required for optical sensing.

1.2   Problems

The primary challenge of using alternative materials for optical surfaces is to ensure that a suitable shape is maintained and that surface flaws are small relative to the wavelength being measured. For uncompensated optical systems, the mirror surface must be manufactured to sub-λ tolerances, where λ = 400-700 nm. With the advent of real-time holography and other advanced adaptive optics techniques, the surface shape tolerance can be relaxed to tens of μm [10]. Taking advantage of smart structures technology, lightweight polymer mirrors may be able to meet these requirements. Local surface flatness is primarily determined by material selection and manufacturing techniques, while high-order figure correction and global curvature can be maintained by employing imbedded actuators for shape control. Piezoceramics mounted to a stiff substrate could be used to control a polymer surface. Similarly, membrane surfaces may be controlled by using a piezopolymer film integrated into the membrane. These techniques must be tested in order to determine their viability for use in operational systems.

1.3   Scope

The objective of this research is to manufacture and test two emerging mirror designs that employ smart structures technology to determine the level of surface control achieved by each system. The experiments will determine the effectiveness of a controllable membrane system and a polymer mirror with imbedded actuators in maintaining and correcting optical surface shape. This research will focus on the adaptive capabilities of the polymer mirrors, rather than closed-loop active control of the mirror surfaces.

Several new manufacturing techniques were developed in an attempt to solve problems discovered during previous research, particularly in the arena of membrane optics. In addition, different control system layouts will be tested to determine their effect on surface control. In addition, the membrane mirror tests will generate data that may be useful for validating recent developments in piezo-controlled membrane modelling.

1.4   Summary of Thesis

The remainder of this thesis discusses the previous work that supports this research and presents the details and results of the experiments performed.

The second chapter reviews recent literature in various fields that contributed to the designs tested during this research. Included is a discussion of bimorph piezo mirrors, recent advances in membrane optics, and the results of previous attempts to manufacture controllable membrane mirrors. Chapter Two also describes a new layered approach to designing polymer mirrors and explains the process of spin-casting.

The third chapter details the experimental test setup and the manufacture of the different mirrors. Chapter three also outlines the test methodology and describes the data gathered during the tests. The results of the mirror tests are documented in chapter four, followed by conclusions and recommendations for further research in chapter five.

II. Review of Relevant Literature

A thousand times every day I remind myself that my inner and outer life depends on the labors of other men, living and dead, and that I must exert myself in order to give in the same measures as I have received. And I am still receiving.

Albert Einstein (1879-1955)

2.1   Overview

Prior to recent advances in adaptive optics, the use of membranes for optical reflectors was considered impossible. Thus, the field of membrane optics is a fairly recent one. Some research has been completed using pressurized systems to maintain membrane curvature [10]. Other approaches suggest the use of spin-casting to create net-shape curved membranes. The results of these experiments and the relative impact to this research are discussed below.

2.2   Pressurized Lenticular Optics

Experiments performed by the Air Force Research Laboratory (AFRL) using vacuum pressure to maintain the required membrane curvature were highly successful [10]. For space applications, however, a similar technique would require a pressurized transparent canopy. This technique was proved feasible for radio wavelengths on the IAE mission. During ground tests, the precision reflector was measured to be within 7mm ($\lambda/15$ at the 3GHz operating frequency) of the designed parabolic shape. The pressurized lenticular failed to inflate during orbital tests, however, preventing surface measurements during the flight [3]. While theoretically possible (see Figure 2.1), transferring this technology to optical systems poses major manufacturing challenges. Due to the shorter wavelengths involved, the canopy would have to be manufactured to thickness tolerances considered impossible with current technology [10]. In addition, the canopy must be transparent across a wide range of wavelengths
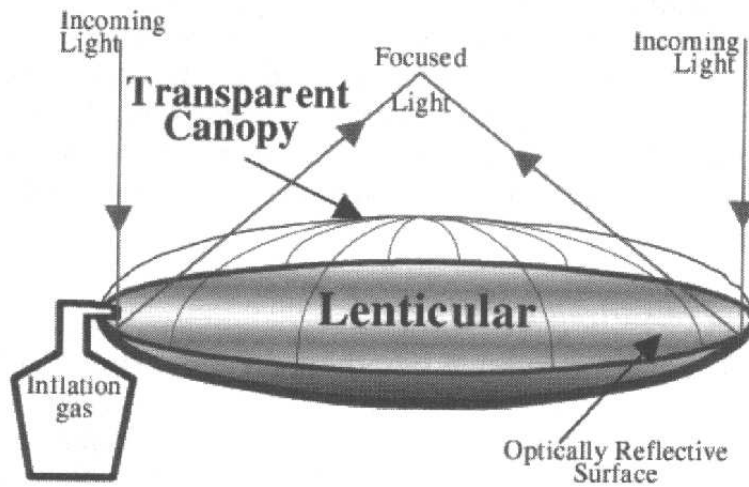
Figure 2.1   Theoretical pressurized optical lenticular. [10]

to be useful for optical sensing. The optical density of the material must be constant across wavelengths to prevent dispersion of the light as it passes through the membrane.

Not only would the pressurized lenticular be difficult to manufacture, the shape of the reflector (controlled by the pressure) must be maintained to micrometer-level accuracy. Changes in canopy pressure caused by solar heating, leaks caused by micrometeoroids, and the eventual exhaustion of inflation gas pose major challenges to this type of optical membrane system. Fortunately, AFRL is pursuing techniques of producing net-shape, self-supporting membranes for possible use in optical systems [10:197]. However, these systems would still require control of the membrane surface to meet optical performance requirements.

2.3   Bimorph Piezo Mirrors

Flexible mirror technology has been developed over the past decade primarily for use in adaptive optics techniques. Current active mirrors rely on micro-electromechanical (MEM) manufacturing processes that do not easily scale upward. As a result, MEMs adaptive mirrors are fragile and designs are typically limited to diam-
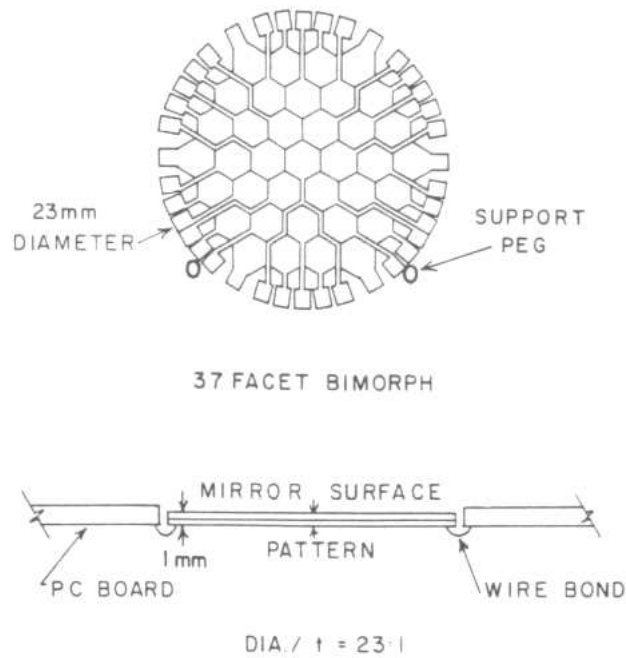
Figure 2.2   Schematic of 37-element piezo bimorph mirror. [4]

eters on the order of tens of centimeters [15:118]. Some flexible mirror technology
may, however, be applied to global shape control of much larger mirrors. One such
example is the piezoelectric bimorph mirror.

A bimorph is constructed from two piezo wafers bonded together that produce
a curvature when voltage is applied to either or both faces [7]. Experiments were
conducted on a bimorph mirror with 37 individually actuated piezo elements arranged
in a hexagonal pattern (see Figure 2.2). The bimorph surface was then polished to
produce a relatively flat surface (0.53 λ RMS). By adjusting the voltage applied to
each element, the overall surface flatness of the mirror was improved by a factor of
four to 0.12λ RMS (see Figure 2.3)[4]. The 37-element mirror was designed as a
focus controller and wavefront correction mirror for an adaptive optics system. A
similar shape control technique could be used to construct a larger active mirror by
imbedding piezo actuators in a lightweight flexible polymer. The polymer optical
surface would reduce cost and production time for the same mirror by eliminating
surface polishing.

NO VOLTAGE   VOLTAGE   APPLIED
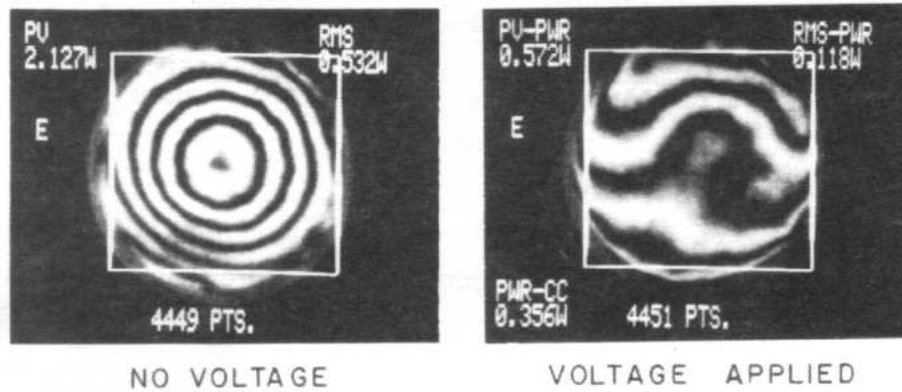
Figure 2.3   Surface flatness improvement due to individual tuning of the bimorph elements. [4]

2.4   PVDF Control of Membrane Surfaces

The use of polyvinylidene fluoride (PVDF) as the active control layer of a membrane mirror has been tested in the past with limited success. PVDF is a piezopolymer that is commercially available and used for lightweight strain gauges. It is manufactured in a thin clear sheet which is then coated on both sides with a metallic layer to create a conductive surface. Because of its piezoelectric properties, the material may also be used as an actuator by applying a charge to the membrane. An electrode pattern can be etched on the surface to allow charge to be confined to specific regions of the surface. When a charge is applied, the PVDF thickness changes, causing a deformation of the membrane's surface. In the past, the primary difficulty using PVDF has been the manufacture of a composite optical membrane, specifically the bond between the PVDF layer and the optical membrane surface [17].

In an experiment conducted at the Air Force Institute of Technology, test mirrors were constructed by stretching a piece of Upilex® optical-quality membrane and mounting it on a 6" diameter aluminum ring. A piece of PVDF was then bonded to the rear surface of the Upilex®. Several mirrors were constructed using different bonding techniques and different electrode patterns were etched on the PVDF to allow actuation of specific regions of the mirrors [17]. Due to thickness variations in the

2-4

bond layer, print-through of electrical connections, and shear lag between the PVDF and Upilex®, overall surface roughness was higher than could be effectively measured. However, upon examination of specific regions controlled by the PVDF layer, surface motion of 39μm peak-to-valley (PV) and 8.9μm root mean squared (RMS) was observed. Thus, the PVDF layer provided a large amount of surface deformation (relative to the wavelength) in the membrane system [17].

Another experiment at the University of New Mexico attempted global control of a pressurized membrane system using PVDF. A 51cm diameter low-density polyethylene membrane was constructed with a 1.25cm × 23cm PVDF strip bonded to the rear surface using adhesive transfer tape [9]. Initial interferometric techniques, which were limited to measuring surface movement of 0.1mm or more, showed observable deformation at the PVDF bond site. However, no noticeable surface movement occurred with changes in voltage applied to the PVDF strip. A more advanced measurement technique was developed for the system, and motion on the order of 10 μm was eventually recorded [9]. These experiments suggest that using PVDF to control optical membranes is possible, but manufacturing suitable mirrors to test this technique has been a challenge in the past.

2.5   Multi-Layered Polymer Mirror Experiment

While glass mirrors have always been the standard in telescope construction, there are several successful examples of alternative materials used for the primary reflecting surface. The astronomer Wood first utilized the knowledge that a spinning liquid has a parabolic surface to construct a mirror using liquid mercury in 1908. This technique was duplicated several times later in the twentieth century, and eventually gave birth to the idea of using this property to create curved mirrors from liquid polymer resin [14].

This technique, called spin-casting, was explored by the Air Force Research Laboratory, Materials and Manufacturing Directorate, in the attempt to create lightweight polymer mirrors. Initial experiments used a composite foam substrate that contained
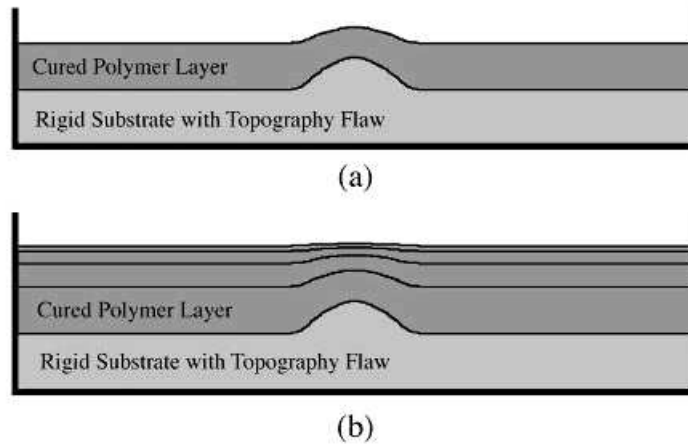
Figure 2.4   Illustration of the multiple polymer layer process: (a) First layer has large surface flaw due to substrate; (b) Subsequent layers significantly reduce surface flaw. [14]

the liquid polymer as it was spun and cured [14]. Two mirrors were manufactured with "substantially parabolic surface features" using this process [14]. Unfortunately, the mirrors contained unexpected local surface flaws. It was concluded that these flaws were likely due to resin cure shrinkage, incomplete resin mixing, and premature curing of the resin [14]. Thus, an experiment was designed to determine the effects of resin mixing and cure shrinkage on the polymer mirror surface and to test the theory that multiple polymer layers may reduce the effects of substrate topography flaws (see Figure 2.4).

The Multi-Layered Polymer Mirror Experiment examined how surface flaws on the solid substrate affected the final surface of the cured resin. Two test mirrors were constructed from 12.7mm thick aluminum plates with raised walls (see Figure 2.5). Each mirror was machined to create a depression in the surface, representing manufacturing surface flaws in the substrate. Uncured resin was then poured onto the aluminum plates and contained within the raised walls. The mirrors were placed on a flat surface and allowed to cure [14].

After curing, the mirrors were tested using a Twyman-Green interferometer to determine the surface flatness. The first mirror, which contained a 0.18mm deep flaw
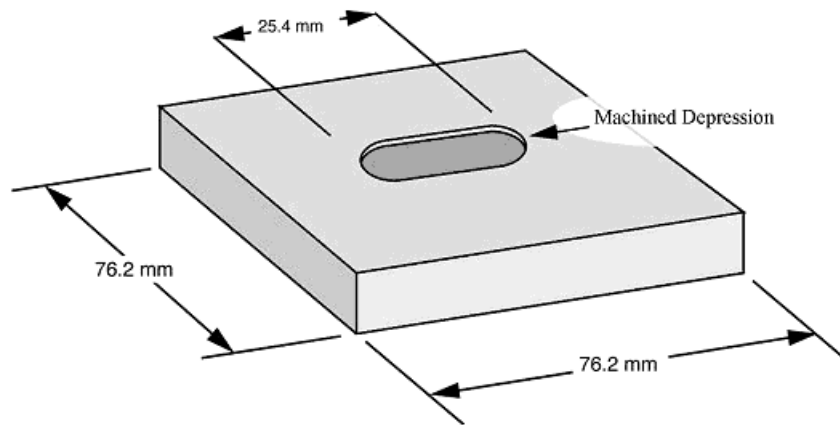
Figure 2.5   Diagram of the aluminum plate substrate used for the multi-layered polymer mirror experiment. [14]

in the substrate, showed an outline of the substrate flaw in the mirror surface as well as random surface flaws in other regions of the mirror. The random flaws were likely due to poor resin mixing, as careful mixing in subsequent tests produced much flatter surfaces outside the flaw area [14]. The overall surface flatness was 2.90λ PV (0.45λ RMS), where $\lambda = 632.8$nm. The second mirror, which had a 0.25mm deep surface flaw was similarly tested. It also showed a clear outline of the substrate flaw and was flat to 1.56λ PV (0.50λ RMS). Thus, the substrate flaws were transferred through the polymer layer to the free surface due to cure shrinkage of the resin (see Figure 2.6). However, the effect of the surface flaws was reduced to only 0.4% of the initial flaw depth. It was theorized that each polymer layer applied would further reduce the surface flaws to 0.4% of the previous layer. A second layer was applied to each mirror and the resultant surfaces showed little evidence of any substrate flaw (see Figure 2.7). The resultant mirrors had an average surface flatness of 0.23μm PV (0.03μm RMS).

These experiments suggest that liquid polymers may be used for optical surfaces, if proper care is taken in the preparation and handling of the polymers. This research takes advantage of lessons learned in previous experiments with PVDF control membranes by using liquid polymers for the optical surface. This eliminates the

2-7
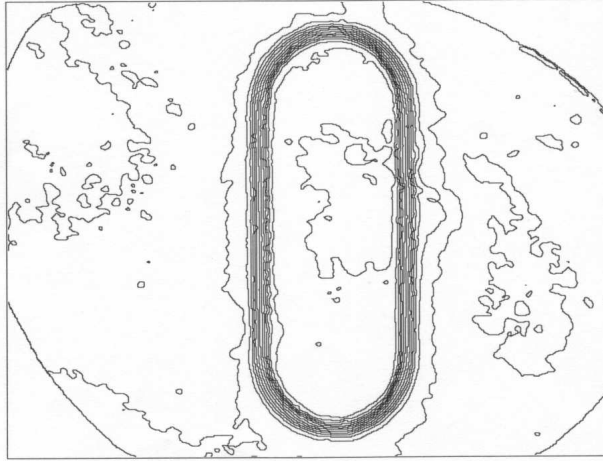
Figure 2.6   Surface topography map of mirror with 0.25mm depression after one polymer layer. The interval between contours is $\lambda/10$. [14]
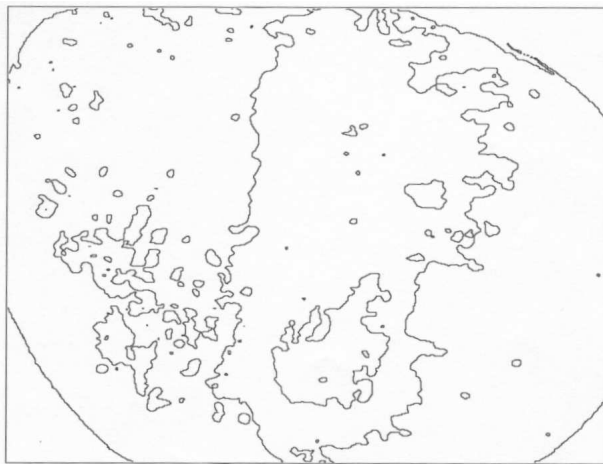
Figure 2.7   Surface topography map of mirror with 0.25mm depression after second polymer layer. The interval between contours is $\lambda/10$. [14]

imperfections caused by bonding the PVDF and wire leads to an otherwise optically flat membrane. In addition, the polymer layering technique was used to create flat optical surfaces with imbedded piezoelectric actuators. The next chapter describes the mirror construction and provides details of the test setup used to measure the mirror surfaces.

III. Mirror Construction and Test Methodology

Although nature commences with reason and ends in experience it is necessary for us to do the opposite, that is to commence with experience and from this to proceed to investigate the reason.

Leonardo Da Vinci (1452-1519)

3.1   Overview

The application of smart structures to optical surfaces has thus far been limited to global shape control of polished glass surfaces or small, expensive MEM devices. This research will expand the boundaries of optical smart structures by introducing the use of flexible polymer-based optical surfaces. Four mirrors were constructed and tested to determine the effectiveness of several different control techniques. Two of the mirrors were constructed of piezo-ceramic materials bonded to copper-clad circuit board. The other two mirrors were constructed from a stretched PVDF membrane bonded to an aluminum ring. All of the optical surfaces were created by pouring a liquid polymer over the controllable substrates to produce flat, semi-reflective surfaces. Several of the mirrors were coated with a layer of gold to enhance reflectivity. All mirrors were tested using Shack-Hartmann sensing to determine surface flatness.

3.2   Construction of Membrane Mirror 1

The first membrane mirror (M1) was constructed from a "blank" piece of PVDF membrane. A previously-developed membrane stretching and mounting system was used to keep the membrane under tension while a 6" diameter aluminum ring was bonded to the membrane using epoxy [17]. The stretching system consisted of a 14" diameter aluminum ring with a rubber o-ring attached, an aluminum faceplate, and four bar clamps (see Figure 3.1).

The PVDF membrane was placed between the o-ring and the faceplate. The bar clamps were then tightened incrementally until the membrane was taut (see Figure

Figure 3.1   Membrane stretching system.

3.2). Five-minute epoxy was applied to the 6" aluminum mounting ring (see Figure 3.3), which was then bonded to the membrane (see Figure 3.4). A 0.5" thick aluminum disk was placed on top of the ring along with a 1 lb. weight to ensure a good bond between the membrane the ring (see Figure 3.5).

After the epoxy had thoroughly cured, the clamps were loosened and the excess membrane was cut away from the mounting ring. A small tab was left on one edge of the membrane to serve as an electrical contact. Leads were constructed by soldering wire to small pieces of copper tape. The tape was then stuck to the membrane tab, providing a means of applying voltage to specific regions of the PVDF control layer. Mirror M1 was originally constructed to test the membrane mounting procedures only. After its construction, however, the membrane etching procedures were developed and a control pattern was etched on the back surface (see Figure 3.6).

The electrode pattern consisted of a 1" diameter circle in the center with a 3" diameter concentric ring. The two control areas were separated by a 0.125" gap, and leads were etched from each electrode to the tab on the membrane edge. See Appendix A for more details on the membrane etching process. The mirror was then spray-painted on the side opposite the electrodes (inside the mounting ring).
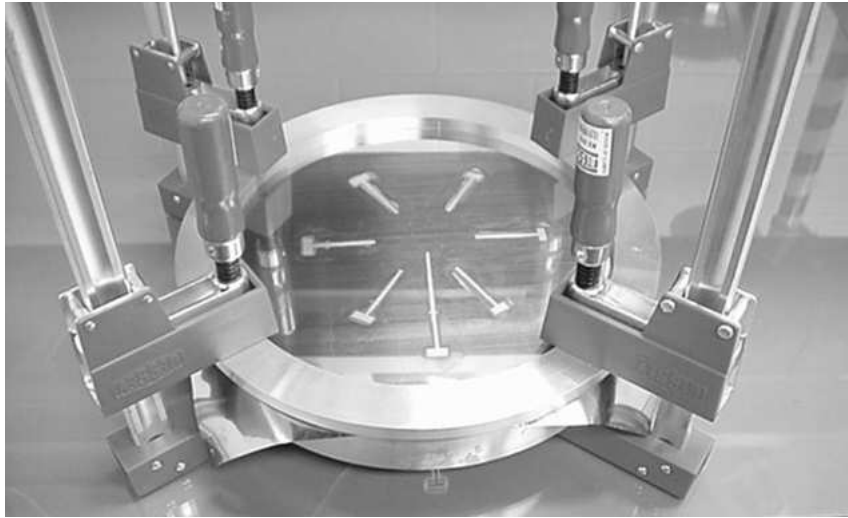
Figure 3.2   Membrane M2 in the stretching ring.

Figure 3.3   The 6" diameter membrane mounting ring.
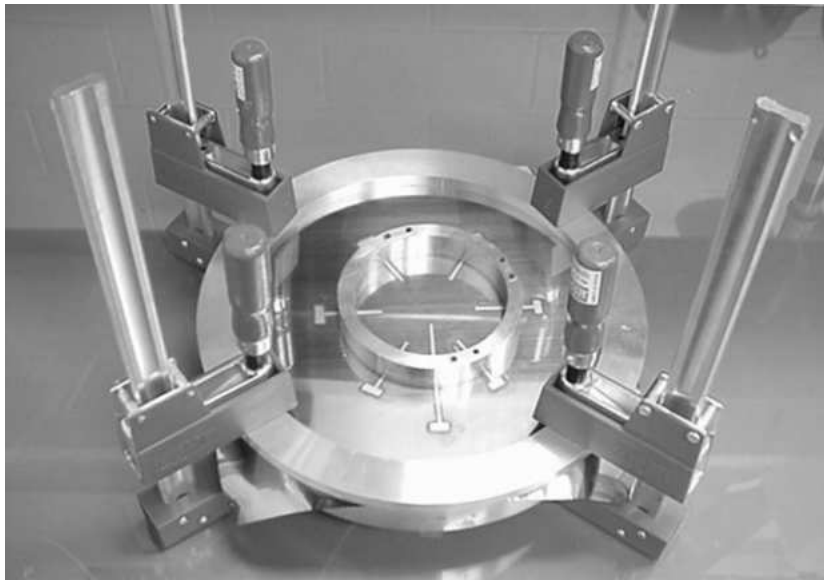
Figure 3.4   The mounting ring bonded to the stretched membrane.
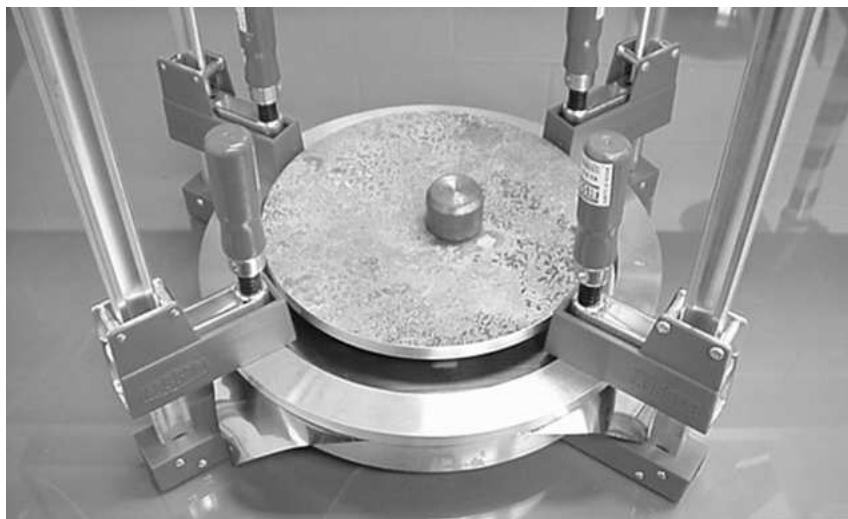
Figure 3.5   Weights were placed on top of the mounting ring while the epoxy cured.
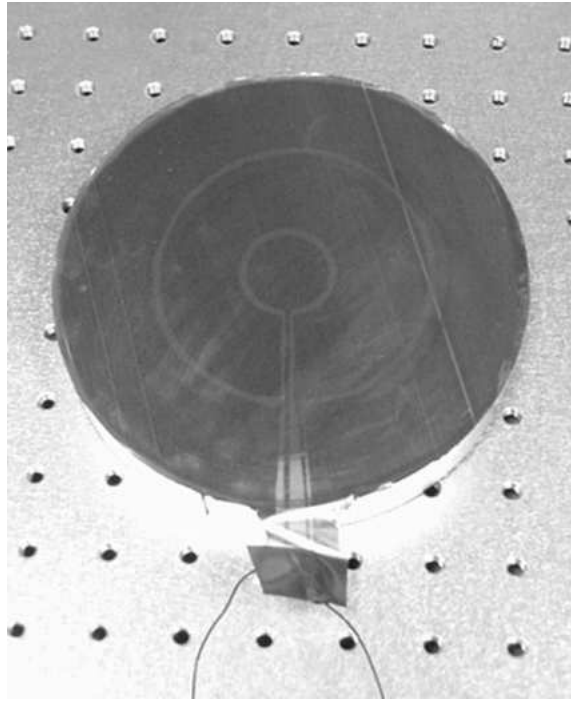
Figure 3.6   Mirror M1 with etched control pattern.

The painted surface prevented the reflective PVDF from causing interference during testing. Once the paint had dried, silicone rubber primer was applied and a layer of GE Silicones® RTV615 approximately 3mm thick was poured into the mounting ring. RTV615 was chosen for the mirror surface due to its low cure shrinkage and its long working time. In addition, previous experiments showed that RTV615 had very flat surface after curing [14]. See Appendix A for more details on resin mixing procedures. After the polymer was poured, the mirror was supported by the edges of the mounting ring while the resin cured. Bubbles visible in the resin were carefully removed with a dental pick prior to cure. Figure 3.7 shows the mirror after the first polymer layer had cured.

The first layer was tested and found to have a slight curvature. A second layer was applied to the mirror while the membrane was supported by placing it on top of a flat piece of glass. This technique improved the surface figure and subsequent mirrors were constructed using the glass for support. The total thickness of the final membrane was measured to be 6mm. After the second layer of RTV615 was tested
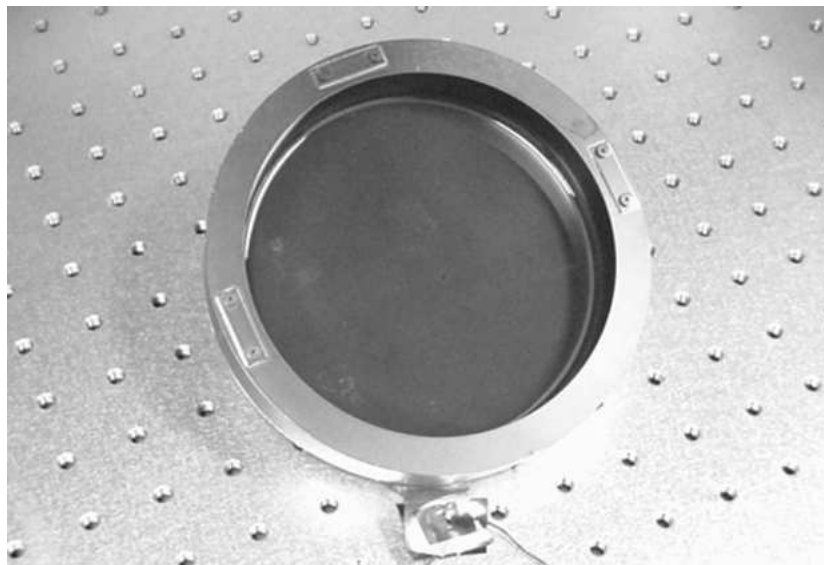
Figure 3.7   Mirror M1 after application of the first polymer layer.

and found to be suitable, M1 was vapor coated with a layer of gold to enhance its reflectivity (see Figures 3.8 through 3.10). The mirror was suspended in the vacuum chamber above the heating element and the vacuum chamber was allowed to run overnight to ensure that the pressure was as low as possible. A 1" length of gold wire was used for this mirror, and the coating produced was completely opaque and highly reflective. After construction of the mirror was complete, the mirror was weighed and compared to an empty mounting ring. The weight of the membrane alone was then divided by the area to calculate the areal density. The areal density of M1 was measured to be 3.55 kg/m^2.

3.3   Construction of Membrane Mirror 2

The second membrane mirror (M2) was constructed using the techniques developed during the construction of M1. However, the PVDF membrane used for M2 was thicker (52μm versus 32μm for M1). In addition, the control pattern was etched on the PVDF prior to stretching and mounting the membrane. The keystone pattern used for M2 enabled actuation of individual sections of the membrane. This pattern was designed to provide high-order surface control upon actuation of individual sec-

Figure 3.8   M1 mounted in the vapor deposit vacuum chamber.

Figure 3.9   The glowing heating element is visible during the gold evaporation process.

Figure 3.10   M1 after a reflective layer of gold has been applied.

tions and low-order surface control upon actuation of the outer sections in unison (see Figure 3.11). The pattern was applied by first creating a full-size template and printing it on stiff photographic paper. The electrode sections (dark areas in Figure 3.11) were then removed using an x-acto® knife, and the electrodes were drawn on the PVDF with a Sharpie® marker using the template as a guide.

Once the electrodes were drawn with the protective marker, the nickel-copper layer surrounding them was removed using a Q-tip® dipped in Ferric Chloride etchant. Thus, the electrodes were electrically isolated from each other and from the back surface, which was used for grounding the membrane. The etchant residue was then removed using damp cotton balls, taking care not to use too much pressure when wiping the surface. Once all of the etchant had been cleaned from the membrane surface, the permanent marker covering the electrodes was removed with cotton balls saturated with isopropyl alcohol. After the electrodes had been etched, the metal on the reverse of the membrane was removed behind the leads so that a charge applied to a particular electrode would not produce a piezoelectric effect along the lead as well (see Figure 3.12).
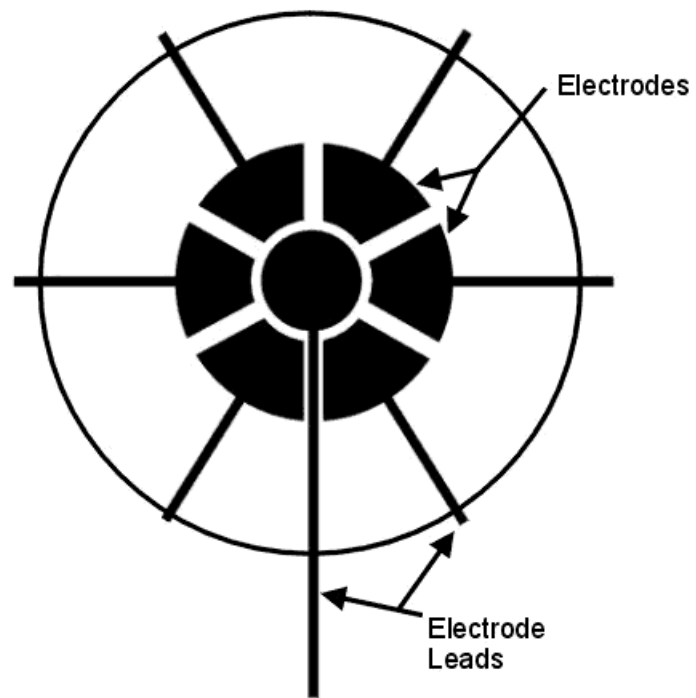
Figure 3.11   The control pattern used for mirror M2.
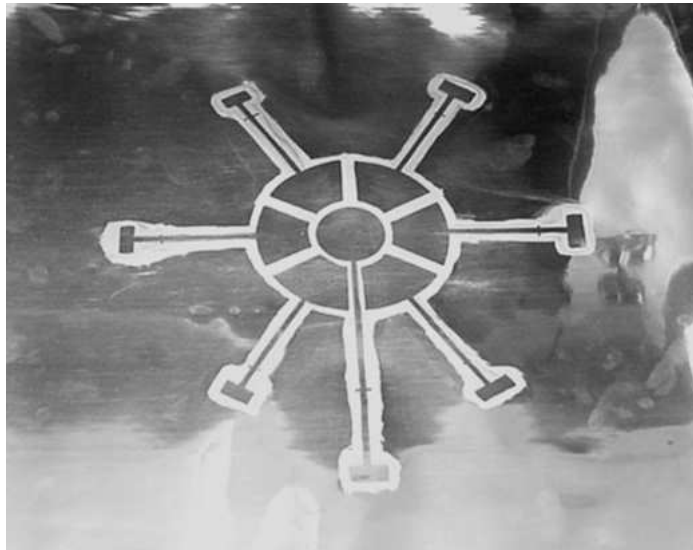
Figure 3.12   M2 PVDF membrane control pattern (inner region 3cm diameter, outer region 8cm diameter).
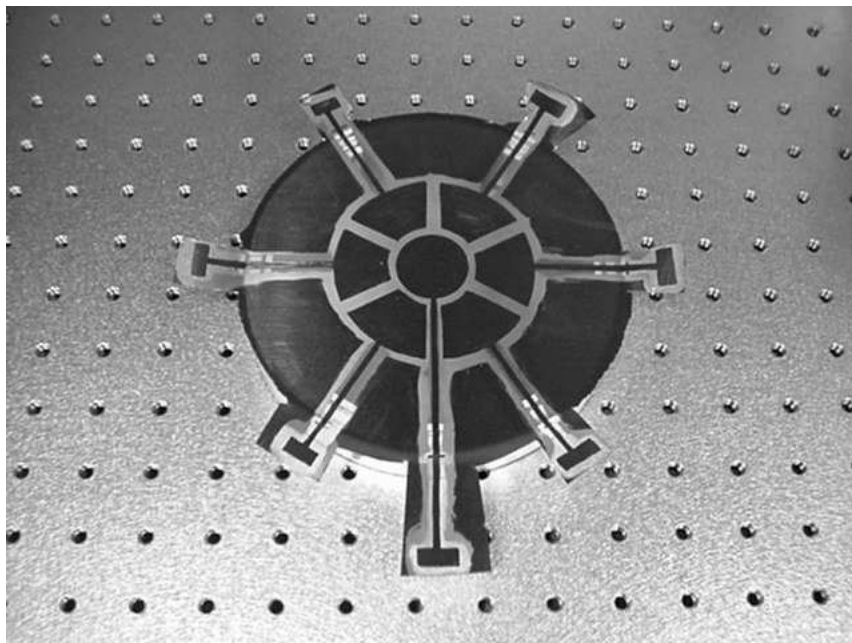
Figure 3.13   M2 after mounting the PVDF membrane.

The membrane was then stretched and bonded to the mounting ring using the procedure described above for M1 (see Figures 3.1 through 3.5). Once the epoxy had cured, the excess PVDF membrane was removed using scissors and an x-acto® knife. The PVDF is manufactured in long sheets, resulting in unidirectional properties. As a result, the thicker PVDF used for M2 had a high tendency to "run" along the grain (lengthwise) when it was being cut. Thus, great care was taken when cutting out the electrode leads to prevent tearing them (see Figure 3.13).

The mirror was then painted and two layers of RTV615 were poured, allowing several days between layers for the polymer to cure. During the cure of each layer, the mirror was placed on top of a flat glass plate to support the membrane. After the liquid polymer was poured for each layer, bubbles were carefully removed with a dental pick. After the top layer had cured, the membrane thickness was measured to be 4mm. The mirror was tested successfully without a reflective coating. The areal density of membrane mirror M2 (minus the mounting ring) was measured to be 1.97 kg/m².

3.4   Construction of Stiff Mirror 1

The first piezo-driven stiff mirror (S1) was constructed to develop mirror build-ing techniques and identify any potential problems. A 3" square copper-clad fiberglass board was used for the mirror substrate. The piezo driver element was removed from a small plastic speaker and bonded to the center of the copper board with epoxy. A small hole was drilled in the board for the piezo element wires. A 0.5" wide open section was cut from the center of a 20 oz. plastic soda bottle to serve as a form for the polymer resin. The plastic ring was bonded to the copper board and the wire hole was filled with epoxy to prepare the mirror for the first polymer layer.

Mirror S1 was also constructed from GE Silicones® RTV615 silicone rubber. After the epoxy had thoroughly cured, the mirror substrate was placed on a flat surface and the resin was poured over the piezo element to about 0.25" thick. After the first layer of resin had cured, an additional 0.25" thick layer of RTV615 was added. The mirror was then vapor-coated with a layer of gold to enhance reflectivity. Figure 3.14 shows the mirror prior to application of the reflective coating. The finished mirror weighed 4.14 kg/m^2.

3.5   Construction of Stiff Mirror 2

The second stiff mirror (S2) was more complex than S1 or either of the mem-brane mirrors. A 1mm thick 6" diameter copper-clad baseplate was used for the substrate, which was then mounted to a membrane mounting ring to facilitate test-ing in the membrane mirror test setup. An electrode pattern was designed using CAD software and milled into the baseplate using an automated circuit board milling ma-chine (see Figure 3.15). The baseplate was then bonded to the mounting ring using conductive epoxy to provide a ground for the interior actuators.

Two 1" diameter disc-shaped and two 1.5" diameter washer-shaped piezoce-ramic elements were used to actuate the surface of S2. The piezos were purchased from in-stock material to reduce shipping time, and were 5mm thick. Thinner ma-
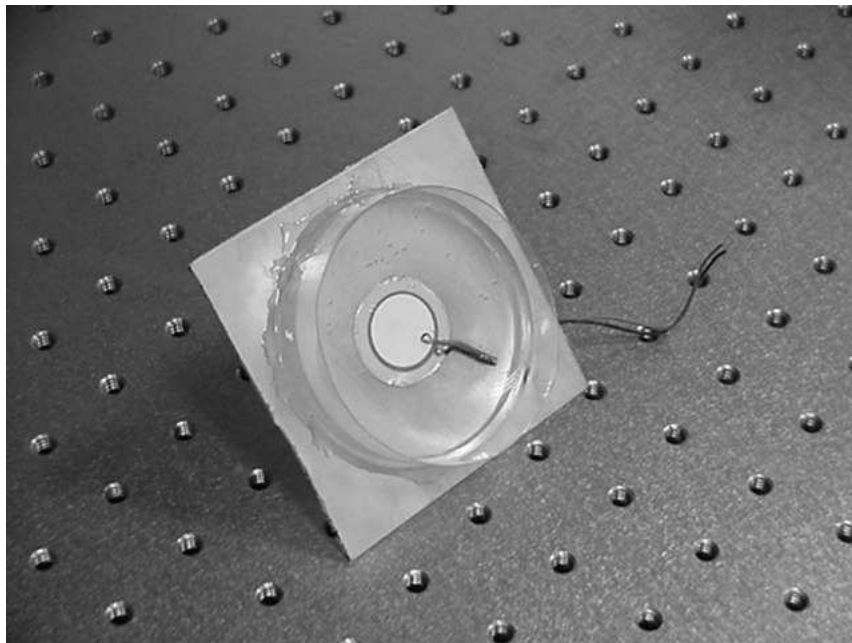
Figure 3.14   Mirror S1 prior to application of gold reflective coating.

Figure 3.15   The copper baseplate used for mirror S2.

Figure 3.16   The interior actuators of mirror S2.

terials would probably be better suited to this application, since the number and thickness of the polymer layers is proportional to the size of the substrate surface features [14]. A disc and washer piezo pair were bonded to the front of the baseplate using conductive epoxy. Holes were drilled for the wire leads, and a wire was bonded to each of the piezos (see Figure 3.16).

Once the epoxy on the front actuators had cured, an identical pair of piezos was bonded to the rear of the mirror. The second pair of actuators was designed to allow testing of the front surface with or without bending caused by the interior actuators. Since actuation of the interior piezos would create local surface deflection as well as global bending, applying the appropriate voltage to the rear actuators could remove the bending if desired. Wire leads were then soldered to the rear actuators (see Figure 3.17).

Before the liquid polymer was poured into mirror S2, the front actuators were grounded by soldering a piece of 0.25" wide copper tape to the front of them and then running it along the copper plate and soldering it to the plate and the mounting

Figure 3.17   The rear actuators of mirror S2.

ring. Thus, the rear actuators each had a positive lead and shared a grounding lead, and the front actuators each had a positive lead and shared the mounting ring as the ground.

Due to availability, a different polymer, GE Silicones® RTV656 was chosen for mirror S2. It is nearly identical to RTV615, but it is slightly more viscous. The polymer was mixed, the bubbles were removed by vacuum, and it was poured into the mirror over the front actuators to a height of about 1mm above the top of the piezos. The mirror was then placed in the vacuum chamber to ensure there were no bubbles trapped around the actuators. The mirror was removed from the vacuum chamber and allowed to cure overnight.

After curing, the surface of S2 appeared flat upon visual inspection, except for surface flaws above the actuators. These flaws were expected due to the thickness of the piezos. Because several layers were required to achieve the desired flatness, and each layer required seven days to fully cure, the curing process was accelerated using an elevated temperature process. The polymer was post-cured in a 250°F oven

for several hours to ensure that the polymer had completely cured before adding additional layers. After the mirror was removed from the oven, the wire leads arced when initially touched together. The piezos had built up a charge due to thermally-induced stresses during the heating and cooling of the mirror. In addition, the first polymer layer showed signs of debonding from the copper substrate.

As a result, the first layer of RTV656 was carefully removed from the mirror. Upon removal of the initial layer, some uncured resin was noticed surrounding the piezoceramic actuators. It is unknown what inhibited the cure of the resin, although some solder flux residue may have been present. The mirror was thoroughly cleaned with acetone and a primer was applied to the surface to ensure proper bonding of future layers. Another layer of polymer was then applied as described above. This layer also showed the expected surface flaws caused by the actuators. The mirror was then post-cured in the oven and a second layer of RTV656 was applied to the mirror. Upon cure, the second layer appeared very flat until the actuator leads shorted again, discharging the piezos. Since the polymer had cured while the piezos were charged, this discharging caused a change in the actuator thickness and mirror surface.

Several days later, a third layer of RTV656 was applied as described above. All leads were grounded prior to curing the polymer, and the bubbles were removed by putting the mirror in the vacuum chamber. Upon cure, the mirror surface had many sticky spots where the resin had not completely cured. Upon further testing, this phenomenon was attributed to the vacuum debulking process by which the bubbles were removed. Although previous layers were not affected by this process, all subsequent layers placed in the vacuum chamber resulted in the same curing problems. To prevent contamination of future layers with uncured resin, S2 was thoroughly cleaned with acetone and a layer of GE Silicones® RTV627 was applied to seal the surface and help fill in surface flaws. An additional layer of RTV656 was applied, but bubbles were removed by spinning the polymer in a centrifuge instead of using the vacuum chamber.

Upon cure, this layer appeared very flat by visual inspection of the surface, and S2 was moved to the testing lab to verify its shape. The testing occurred several days after initial cure, however, and the reflection revealed surface flaws consistent with uneven substrate topography (caused by the actuators). Upon visual inspection, the surface flaws were readily apparent. Voltage was applied to the actuators in an attempt to correct the surface. Although the surface features improved as voltage was increased (up to 700 Volts), the flaw depth was larger than the deflection attainable by the actuators.

Possible causes for the change in surface features were differences in temperature and humidity, as well as the possibility that the initial flatness was observed before the polymer had fully cured. The polymer is solid after 24 hours, but it requires seven days to fully cure at room temperature. Steps were taken to rule out these possible problems by heating the mirror for several hours to ensure it had fully cured, allowing it to cool, discharging the actuators, and then pouring the last layer of resin in the lab where the mirrors were tested. The final areal density of the mirror, excluding the mounting ring weight, was 30.4 kg/m^2.

3.6   Test Setup

All tests were conducted using variations of a setup previously designed for measuring the surface flatness of membranes mounted to the 6" diameter aluminum rings (see Figure 3.18) [17]. All specimens were illuminated using a 20mW helium-neon laser, which has a wavelength of 632.8nm. All surface measurements were made using a WaveScope® Shack-Hartmann wavefront sensor built by Adaptive Optics Associates (AOA). The WaveScope® measured the reflection of each test specimen and compared it with a reference source. The WaveScope® software then calculated the optical path difference between the test surface and the reference surface. The data was used to calculate a surface plot of the specimen, a synthetic interferometric fringe pattern, and the first 35 coefficients of the Zernike polynomial describing the surface shape (see Appendix C for plots of the first 35 Zernike coefficients). To

facilitate comparison of different test data and enhance the display of the test surfaces, the surface data and Zernike polynomials were exported to a file and then plotted using MATLAB®.
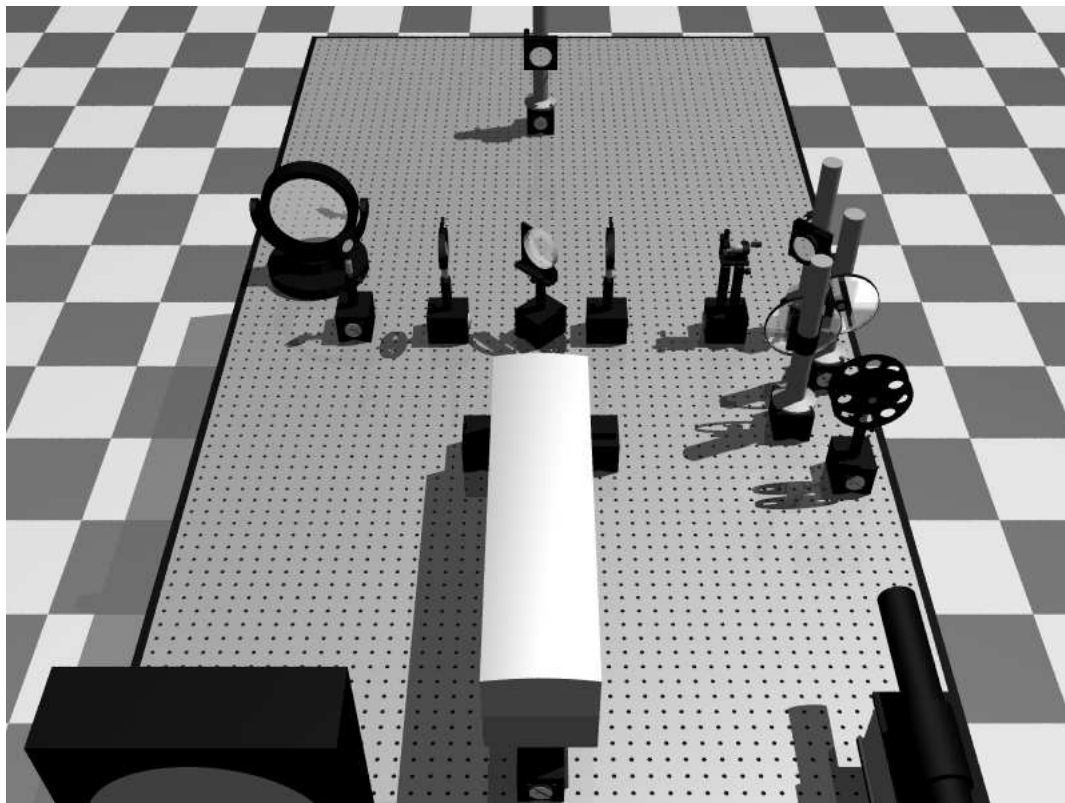
Figure 3.18   The basic test setup.

Several different configurations of the test setup were used to measure the mirror surfaces. In all tests, the beam path initiated at the laser output and passed down the length of the optics table through a set of filters (see Figure 3.19). Because the WaveScope® is very sensitive, the light reflected from the reference mirrors or test specimens with reflective coatings had to be dimmed. Since reflectivity of the uncoated specimens was reduced, however, a higher intensity test beam was required for some tests. Beam intensity control was achieved using a filter wheel (F1) that contained neutral density filters ranging from 10% to 80% transmission. In addition, two gradient wheel filters (F2,F3) were required for fine control of beam intensity. The beam was then turned 90° using a $\lambda/20$ flat mirror (FM1) and passed through
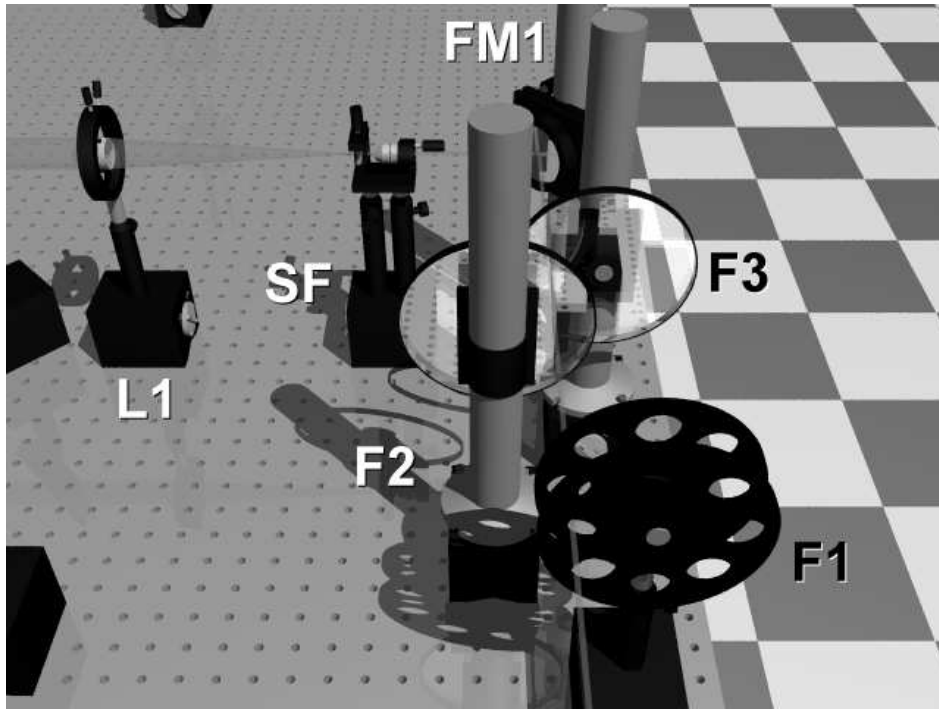
Figure 3.19   The beam path from the laser to the collimating lens (L1).

a spatial filter (SF) to produce a clean Gaussian wavefront. The expanding beam was then collimated using a 1" achromatic doublet lens (L1) with a focal length of 200mm. Figure 3.19 shows the beam path from the laser to L1.

Once the collimation of the beam from L1 was verified, the beam was passed through a 3" diameter $\lambda/5$ wedge beam splitter (BS). Early tests were attempted using a cube beam splitter, but testing was difficult due to ghost images caused by the parallel surfaces of the cube. The wedge beam splitter was chosen to eliminate the ghost images. Figure 3.20 shows the path of the beam through the beam splitter. The incoming beam was divided into two equal intensity beams at 50% of the incoming beam intensity. The beam splitter turned one of the outgoing beams 90° down the length of the table. This half of the beam was reflected off a $\lambda/20$ flat mirror (FM2) back through the beam splitter and into the WaveScope® (WS) to serve as the reference beam.
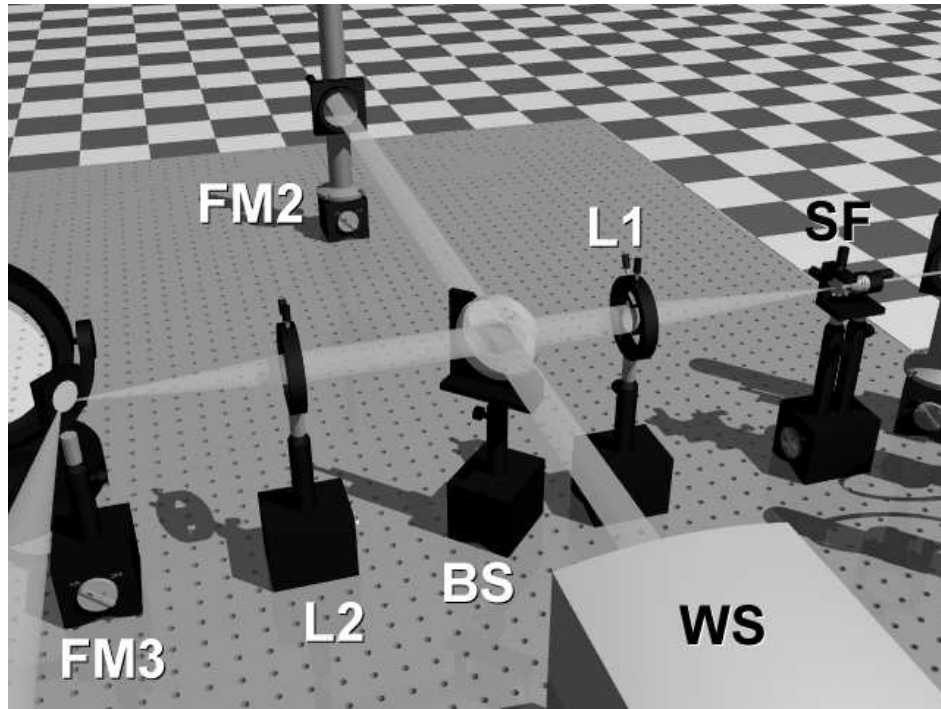
Figure 3.20   The beam path from the spatial filter (SF) through the beam splitter
              (BS).

The half of the beam that passed through the beam splitter was then expanded
using a 1" doublet lens with a focal length of 250mm (L2). The expanding beam
was reflected off a $\lambda/10$ flat mirror (FM3), which turned the beam down the length
of the table towards a 12.5" diameter parabolic reflector (PR) with a focal length of
75.125" (1908.175mm). The expanding lens and turning mirror were placed such that
the beam expanded as a point source located near the focal point of the parabolic
mirror (see Figure 3.21). Thus, the expanded beam was collimated into a beam wide
enough to illuminate the test specimens. Light reflected from the test specimen then
travelled along the same path back to the beam splitter, where it was recombined
with the reference beam and turned into the WaveScope®. The expansion ratio is
given by the following formula:

$$\text{Expansion Ratio} = \frac{\text{PR Focal Length}}{\text{L2 Focal Length}} = \frac{1908.175\text{mm}}{250\text{mm}} = 7.6327$$
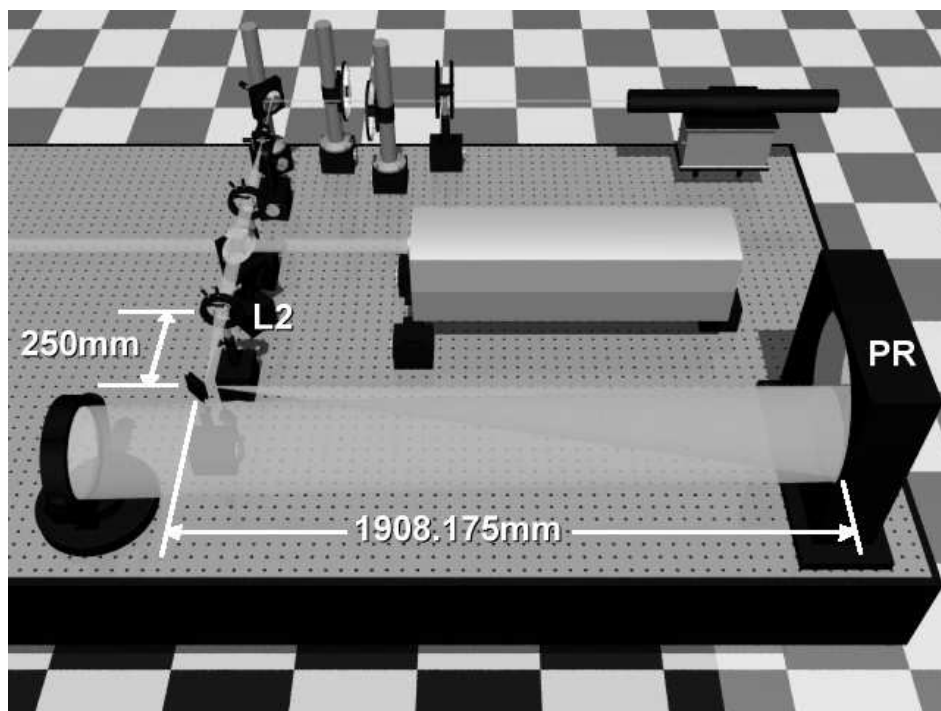
Figure 3.21   The 1" collimated test beam was expanded to 7.6" to illuminate the test section.

Initial testing revealed that the membrane mirrors deformed when mounted vertically. Thus, the 6" mirror mount was reconfigured to enable testing of the membranes in a horizontal position. The 6" mount was bolted to a large post and flat mirror (FM4) was mounted at 45° to turn the test beam path downward. The membrane mirrors were then placed on the table supported by spacers under the mounting ring. Full-aperture test were accomplished using this setup (see Figure 3.22).

3.7   Data Collection and Processing

Measuring optical surfaces can be accomplished using Twyman-Green interferometry or a Shack-Hartmann sensor, among other techniques. Interferometry requires that the test and reference surfaces be illuminated simultaneously, and that the reflection from each have comparable intensity. In addition, the test and reference beam paths must be approximately the same length (within one laser tube length) to avoid pulsation of the interference pattern. Because the reflectance of the uncoated mir-
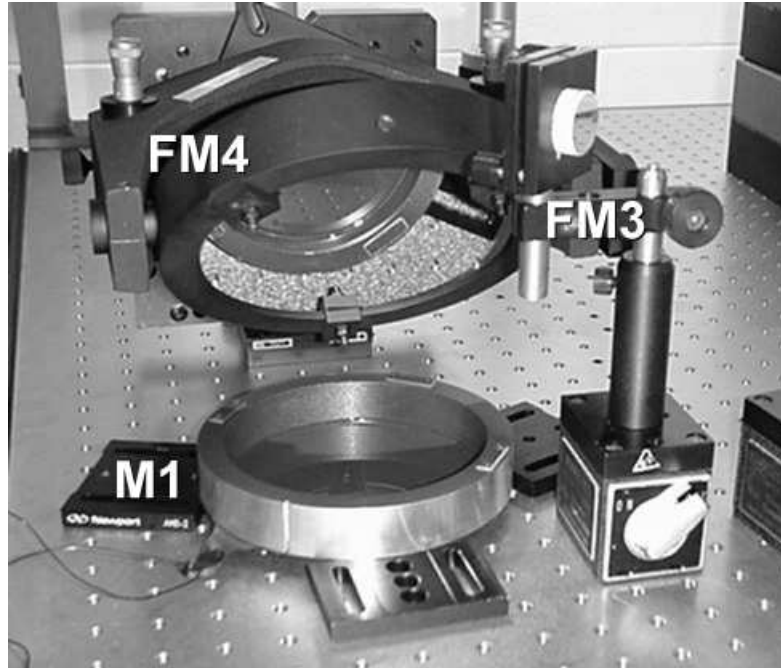
Figure 3.22   The membrane mirrors were tested in a horizontal configuration.

rors was significantly less than the reference mirrors, interferometry was infeasible for measurement of the uncoated specimens. A Shack-Hartmann sensor, however, measures the test and reference reflections independently. Thus, the intensity of the beam can be adjusted using a filter wheel to switch between the high intensity reference reflection and the low intensity test reflection.

As a result of the independent measurement of the test and reference beams, a single reference measurement can be used to measure different test articles. This allows comparison between different specimens and the removal of most of the test equipment bias from surface measurements. In addition, there is no restriction on the reference beam path length. This allows a shorter reference path, which is more convenient and more accurate due to fewer reflections required. These properties of Shack-Hartmann sensing were crucial for measuring the active mirror surfaces. In addition to absolute surface measurement, independent beam sampling allowed measurement of a mirror's surface relative to itself. Testing of the active mirrors

M2 Surface Flatness vs. 6" λ /10 Reference
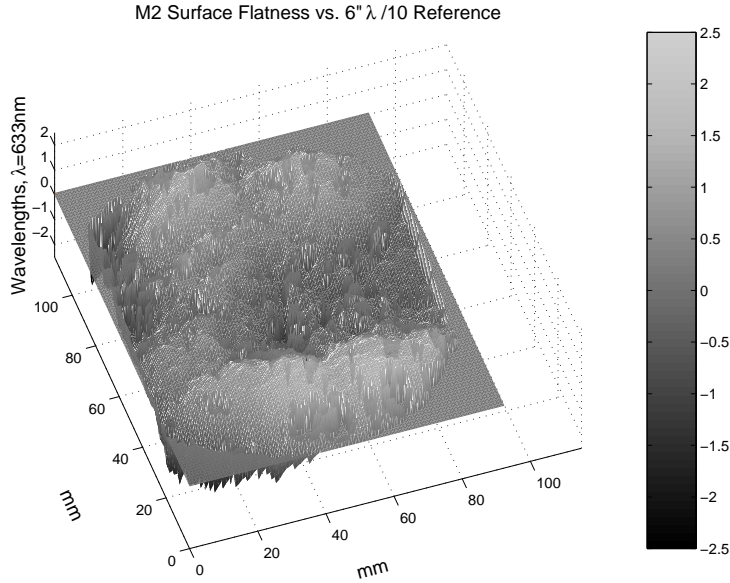
Figure 3.23   M2 surface compared to a $\lambda/10$ reference flat (3.95λ PV, 0.63λ RMS).

was accomplished by using the unactuated mirror surface as a reference and then measuring surface deformation relative to the unactuated state.

Figure 3.23 shows the surface flatness of membrane mirror M2. A 6" flat mirror ($\lambda/10$) was used for the reference beam. This measurement was made after some testing of the mirror (but prior to test T3), and residual surface deflection is clearly visible (see Figure 3.11 for the M2 control pattern). Although the surface was relatively flat (3.95λ PV, 0.63λ RMS), the initial surface shape could have affected test results. The relative flatness, however, was measured by using the unactuated test mirror as the reference. Figure 3.24 shows that the surface flatness with M2 self-referenced was greatly improved (0.59λ PV, 0.07λ RMS). Using this method, highly accurate relative surface measurements are achieved. In addition, the self-referenced surface flatness serves as an approximate measurement of the error associated with each test.

Light entering the WaveScope® passes through a monolithic lenslet module (MLM) that focuses the light onto a CCD sensor. During testing, the CCD camera is traversed forward and backward, measuring the light at different focal planes. The
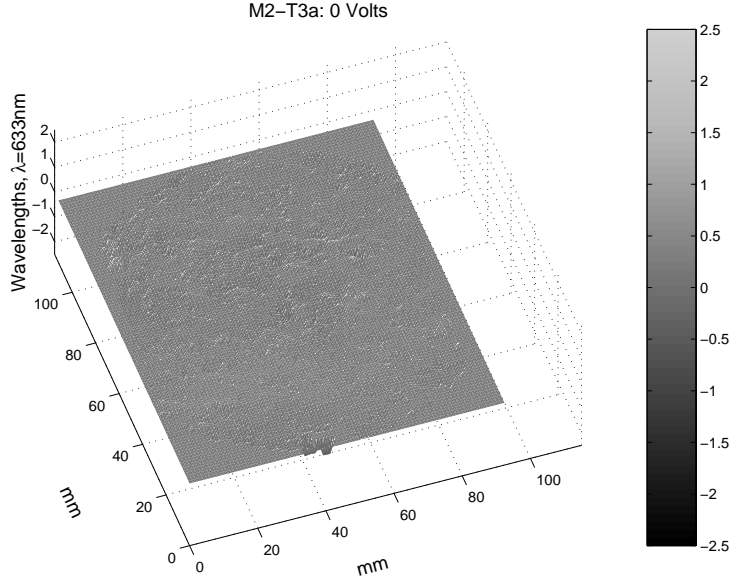
Figure 3.24   M2 surface self-referenced (0.59λ PV, 0.07λ RMS).

fidelity of the data collected using the WaveScope® depends on the size of the lenslets in the MLM [19]. Two different MLM sizes were used for this research. A low-fidelity array, with lenslets measuring 480μm across, was used during initial testing. Once testing procedures were refined and mirror construction had improved, tests were performed with a higher fidelity, 133μm MLM.

For each test, the WaveScope® software allows the user to set the number measurements, the number of frames captured for each measurement, and the frame rate. During initial tests, five measurements were taken for each test. Each measurement consisted of an average of the five frames collected at 30Hz. The WaveScope® collected one data point for each of the MLM lenslets. As a result, later tests using the finer 133μm MLM produced much more data. Since the data took longer to process, the frame rate was switched to 5Hz. In addition, initial testing revealed that fewer measurements were necessary to accurately capture the mirror surface. As a result, tests using the 133μm MLM consisted of three measurements with five frames per measurement taken at 5Hz.

3-23

During testing, the surface shape of the test article was viewed using the WaveScope® software. For each test the surface flatness was recorded, both peak-to-valley (PV) and root mean squared (RMS). To facilitate viewing and comparing the data, a representative sample (one of the three or five measurements collected for each test) was selected and the surface shape and Zernike polynomial coefficients were imported into MATLAB. For each test, the surface data and Zernike polynomials were plotted. Because the Zernike polynomial plot is only valid for the area enclosed by the test data, a mask was created using the data from each test. This mask was applied to the Zernike plots to allow comparison between the plots and the surface data.

For every test, there were regions within the test pupil that the WaveScope® could not accurately measure. The wavefront path difference for these data points is recorded as zero. As a result, the masks created for the Zernike plots also mask out small sections of the Zernike surface corresponding to the areas where no data was collected. This results in "spikes" or "wells" in the otherwise continuous Zernike surface. Compare the unmasked Zernike plot in Figure 3.25 with the masked Zernike plot in Figure 3.26. An algorithm could be written to exclude interior points from the Zernike mask, but this would increase processing time for each data set.

In some tests, the WaveScope® assigned light coming from a certain lenslet to a neighboring lenslet. This misclassification resulted in a spike on the surface that differed by as much as an order of magnitude from the surrounding data. These anomalies were very rare (only 4 or 5 tests exhibited this phenomenon) and were removed manually from the data sets (see Figure 3.27). To aid in the qualitative analysis of the data, the high fidelity (133μm MLM) test results were also "smoothed" using a simple interpolation algorithm. Surface smoothing was only performed for qualitative analysis of the data. All surface data plots presented in this thesis are unsmoothed, raw data. Appendix B contains examples of the MATLAB® code written for analysis of the data collected using the WaveScope®.
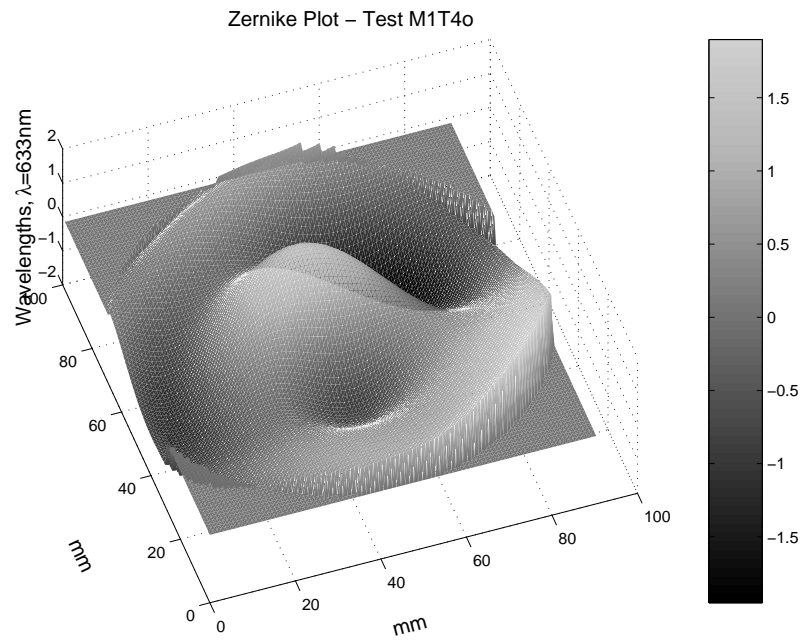
Figure 3.25   An example of a Zernike polynomial plot.
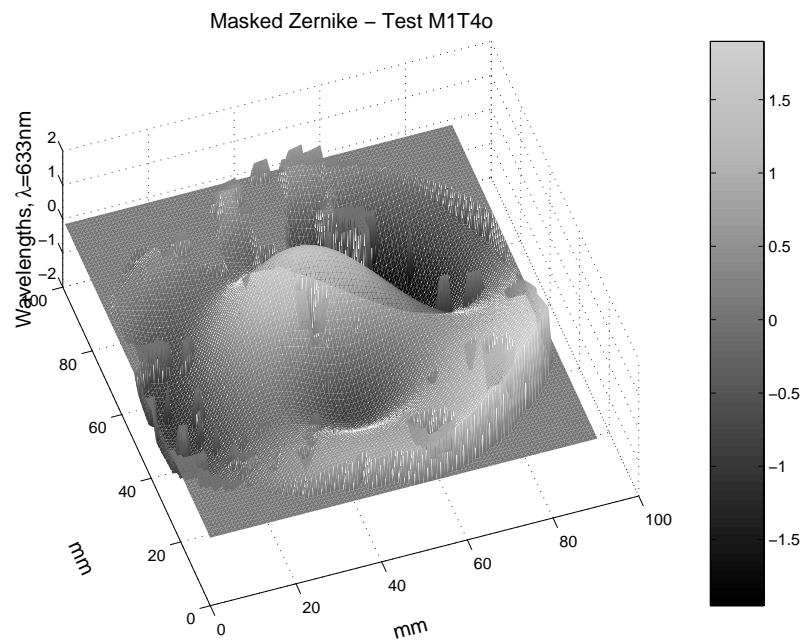
Figure 3.26   The Zernike plot after applying the data mask.
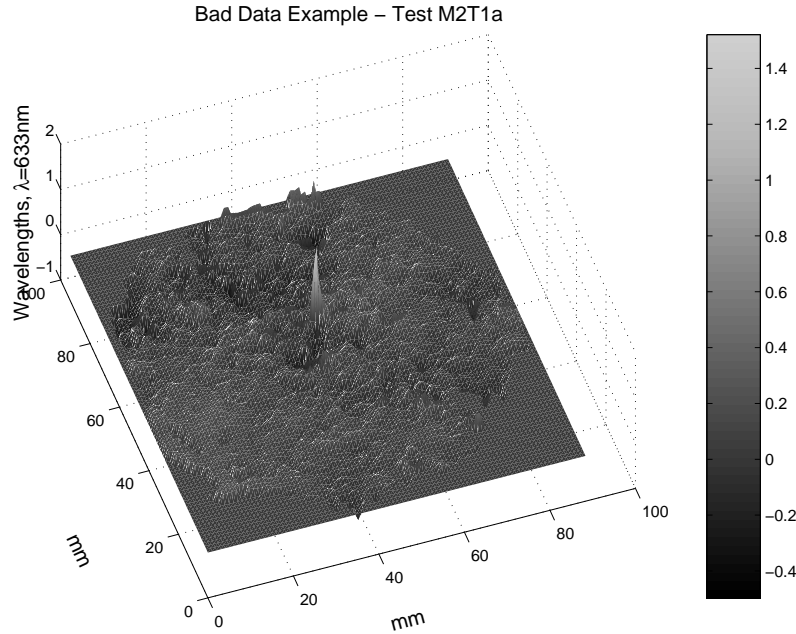
Figure 3.27   An example of lenslet misclassification by the WaveScope®.

Once all of the data had been imported for each test, the height data was converted from μm to λ by dividing by 0.6328 (the wavelength in μm). In addition, the width and length of the data plot was adjusted to match the actual mirror surface. One data point was recorded for each lenslet in the MLM array. To convert the data to match the mirror surface, the data spacing was multiplied by the lenslet size (0.133mm or 0.480mm) and then by the beam expansion ratio (1:1, 2:1, or 7.6327:1, depending on the setup). As a result of the data output format and the subsequent import into MATLAB®, the plotted data is rotated counterclockwise 90° from the image recorded by the WaveScope®. Once the data was plotted, the the vertical scale on the graphs was adjusted to allow comparison between relevant tests. As a result, the minimum and maximum values on the color bar and vertical scale may exceed the minimum and maximum values plotted on any given graph. All surface plots have units of λ for the surface height and color bar, and horizontal distance is plotted in millimeters on the mirror surface. All PV and RMS surface flatness values are averages of the measurements taken for each test.

3.8   Summary

Four mirrors were constructed to test piezoelectric control of polymer optical surfaces. Two mirrors were manufactured using PVDF membrane control layers, and two mirrors had copper-clad circuit board substrates with piezoceramic actuators. The mirrors were coated with silicone rubber polymers to create optically flat surfaces and gold vapor deposits were applied to enhance reflectivity.

The surface flatness of the mirrors was measured using a WaveScope® Shack-Hartmann sensor. The mirrors were measured in both actuated and unactuated states. The data was then imported into MATLAB® and the surface shape and Zernike polynomials were plotted for comparison. The next chapter presents the test data recorded for each of the mirrors.

IV. Test Results

A few observations and much reasoning leads to error; many observations and a little reasoning to truth.

Alexis Carrel (1873-1944)

4.1 Overview

Surface measurements were collected for each of the mirrors using the AOA WaveScope® Shack-Hartmann sensor. Initial tests were conducted using a 480μm MLM and a 1" diameter test beam to check the local surface flatness and observe deformation of the mirrors during actuation. A horizontal, full-aperture testing method was later developed which provided a 4" diameter test spot. In addition, a 133μm MLM was utilized to improve test data fidelity. Each mirror was tested using the unenergized state as a reference, taking measurements of the surface shape with different regions of the mirror actuated at different voltages. Average surface deviation measurements and surface plots for each test are presented in the following sections.

4.2 Membrane Mirror M1

Initial testing of M1 revealed that the mirror had net surface curvature. The curvature prevented measurement of the mirror's surface by causing the test beam to expand as it returned to the WaveScope®. As a result, the first layers of M1 were tested using a modification of the setup described above. The expanding lens L2 was removed, allowing a 1" section of the mirror to be tested. The turning mirror FM3 was replaced with a 2" $\lambda/10$ flat mirror similar to FM2. The beam was then turned directly to the membrane surface, which was mounted vertically in the 6" mirror mount (see Figure 4.1). After the testing process had been refined and a second layer of RTV615 and a gold coating had been applied to M1, the mirror was tested using the expanded beam. Details of the results from each test are recorded in Appendix
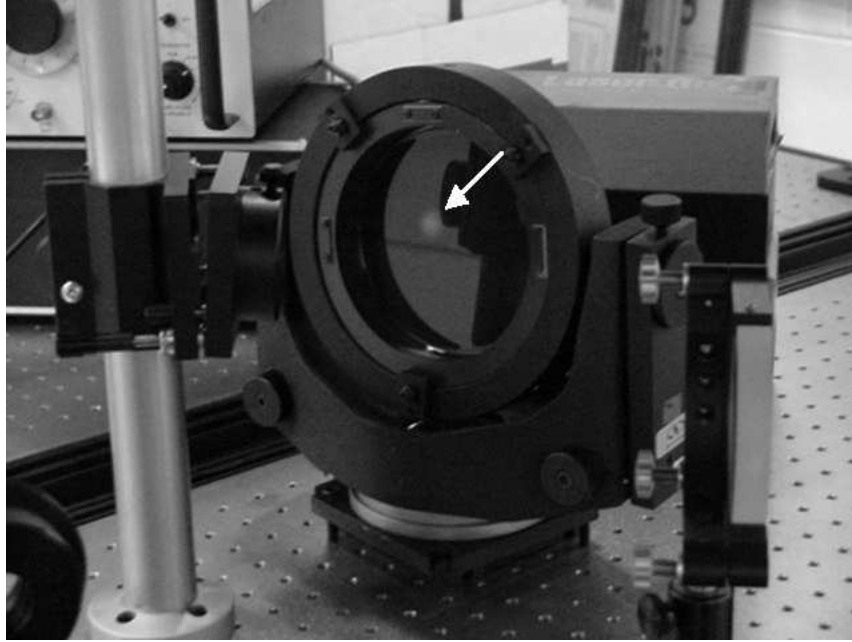
Figure 4.1   M1 in the test setup (note location of test beam spot).

A. The first set of tests were inconclusive as a result of improper WaveScope® setup and calibration.

4.2.1   M1 Test 2.   The second test was designed to measure the surface deflection of the actuated membrane. The test section was limited to a 1" diameter spot. The test spot was placed on the border of a control region (see Figure 4.2). The surface flatness was measured to be 0.53λ PV (0.10λ RMS) at the test location (Test 2a - see Figure 4.3). The test beam at the WaveScope® slightly overfilled the MLM aperture, which resulted in only about half of the test spot being measured (1" diameter test beam versus 10mm diameter surface measurement).

The WaveScope® was then re-calibrated using the membrane surface as the reference. The self-referenced surface flatness was measured to be 0.16λ PV (0.02λ RMS) at the test spot location (Test 2b). The magnitude of the surface flatness measured in the self-referenced tests provides a measurement of the relative error for this technique. To check these results, the WaveScope® was again re-calibrated. The self-referenced surface flatness after re-calibration was found to be 0.11λ PV
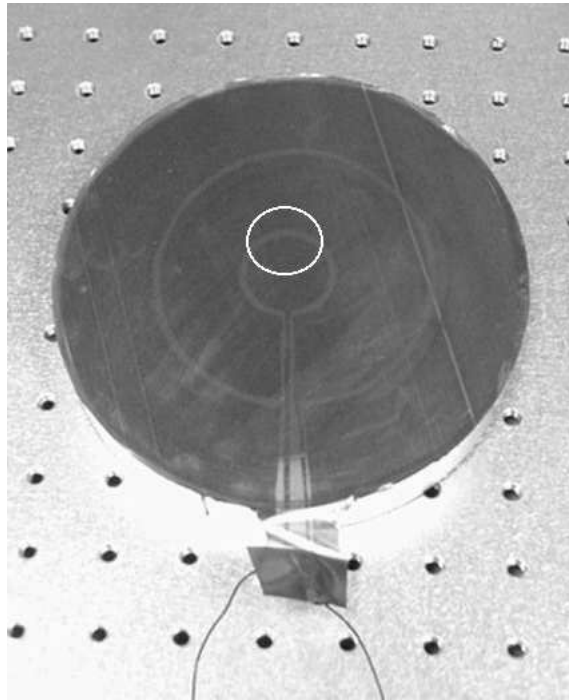
Figure 4.2   Test location for M1 tests T2 and T3.
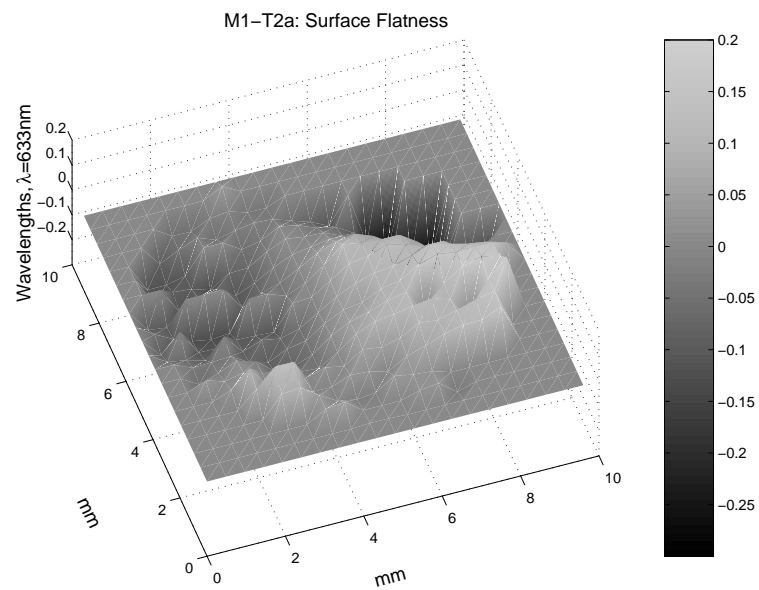
Figure 4.3   M1 surface flatness (0.53λ PV, 0.10λ RMS.)
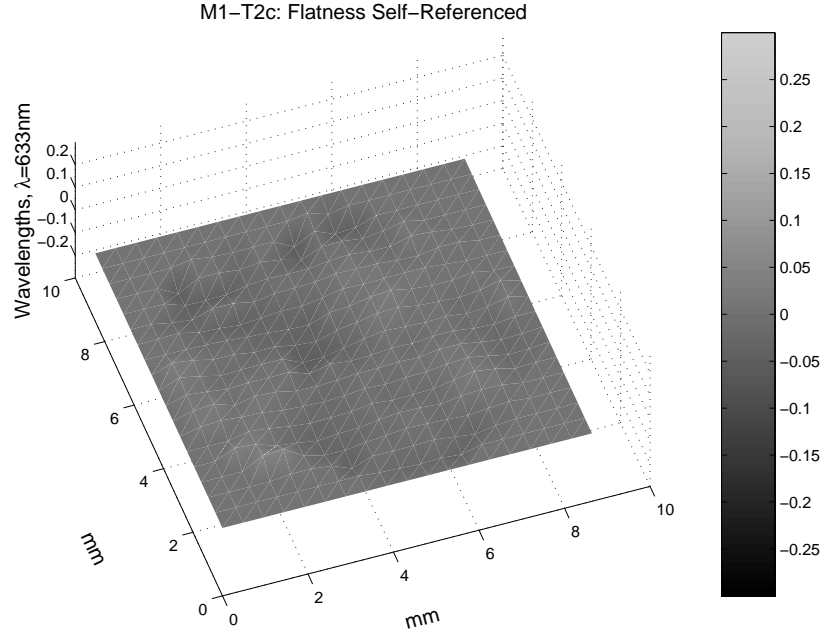
Figure 4.4   M1 Self-referenced surface flatness (0.11λ PV, 0.02λ RMS).

(0.02λ RMS) (Test 2c - see Figure 4.4). Voltage was applied to the center control section on the order of several hundred volts (no voltmeter was available during this initial test), and the surface was recorded (Test 2d). The voltage was then reversed, and the surface was measured again (Test 2e). Figures 4.5 and 4.6 show the surface measurements of the test spot in during T2.

Although this initial test was performed with unknown voltages and the data collected was low-fidelity over a small section of the mirror, the test clearly showed that the mirror surface is affected by the PVDF control layer. Figures 4.5 and 4.6 show that reversing the voltage applied to the control layer reversed the surface deformation. In addition, the magnitude of the deflection is on the same order of the magnitude as the unactuated surface flatness. Thus, these initial results indicate that the PVDF membrane control system is viable for correcting and maintaining local surface figure.

4.2.2   M1 Test 3.   Test 3 was performed using the same setup as Test 2, with the test beam spot located in approximately the same location. A voltmeter was
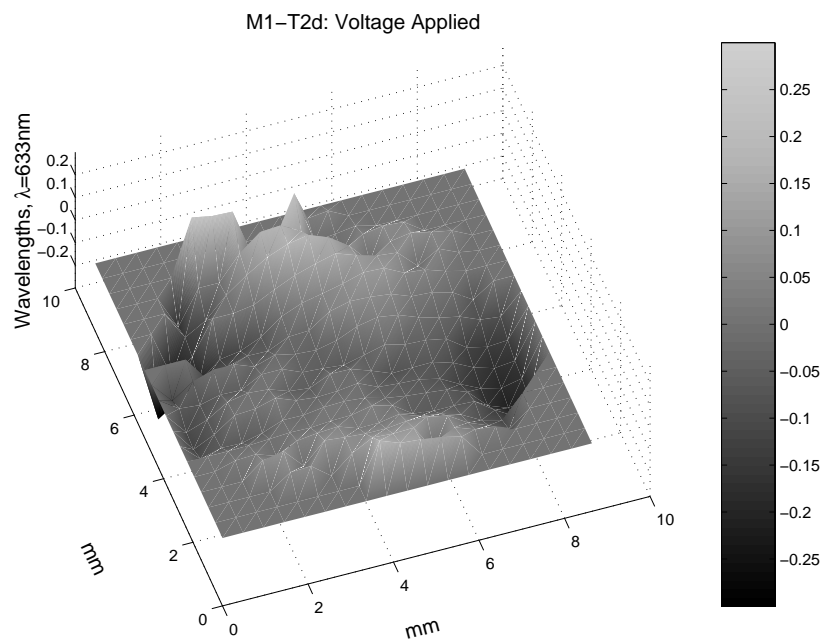
Figure 4.5　M1 surface with voltage applied (0.55λ PV, 0.09λ RMS).
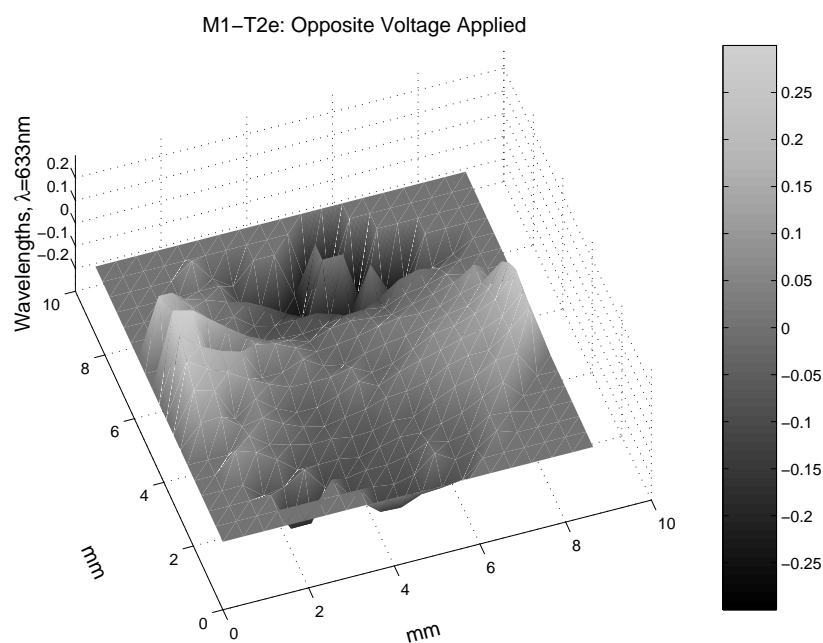
Figure 4.6　M1 surface with opposite voltage applied (0.61λ PV, 0.11λ RMS).

obtained to measure the applied voltage. Prior to the test, the voltage was measured along the etched leads and at the control pattern to determine how much of the applied voltage was present at the control surface. A voltage of 300V was applied at the wire leads. The voltage was measured to be 300V at the etched leads, but only about 20V at the center electrode.

After further testing, it was determined that when measuring the voltage at the etched leads an arc occurred between the voltmeter lead and the PVDF surface. The metal coating was vaporized, resulting in an open in the circuit. In future tests, more care was taken to create wider etched leads and to avoid arcing at the PVDF surface. The open was repaired using conductive copper tape and the voltage at the control electrodes was measured again to verify that the applied voltage was reaching the control surface.

Before measuring surface actuation, the electrodes were grounded to ensure that no charge was present on the control layer. The surface flatness was measured to be 0.62λ PV (0.12λ RMS) at the test location (see Figure 4.7). The WaveScope® was then calibrated using the un-energized state as the reference, and measurements were taken at 100V intervals from 0V to 500V (tests T3b through T3g - see Figures 4.8 through 4.10). The surface deflection increased with increasing voltage from 0.16λ to 0.34λ PV (0.02λ to 0.06λ RMS) (see Figure 4.11).

After testing the change in surface deflection with increasing voltage, the voltage was reversed on the control region. The surface was measured with an applied voltage of -600V (Test 3k) and +600V (Test 3l). Figures 4.12 through 4.15 show the surface deflection and a plot of the associated Zernike polynomials. A reversal of surface deflection is clearly visible when the voltage is reversed.

4.2.3 M1 Test 4.   After a second coat of RTV615 was applied to M1, the surface was flat enough to test using the expanded test beam. The mirror was also coated with a layer of gold to enhance reflectivity. The mirror was tested in a horizontal position by mounting the 6" mirror mount at 90° and tilting the mirror
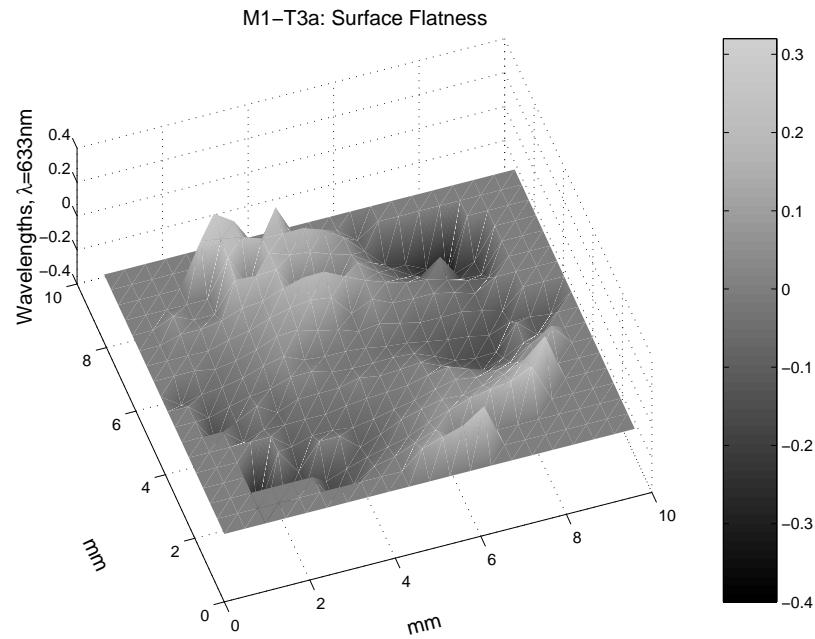
Figure 4.7   Test T3a - Surface flatness of M1 (0.62λ PV, 0.12λ RMS).
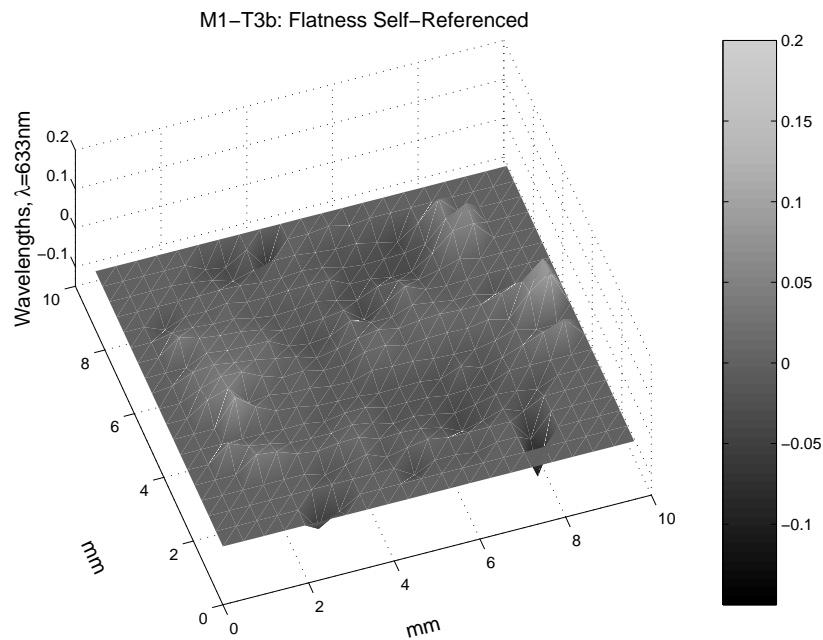
Figure 4.8   Test T3b - Surface flatness of M1 at 0V (0.16λ PV, 0.02λ RMS).
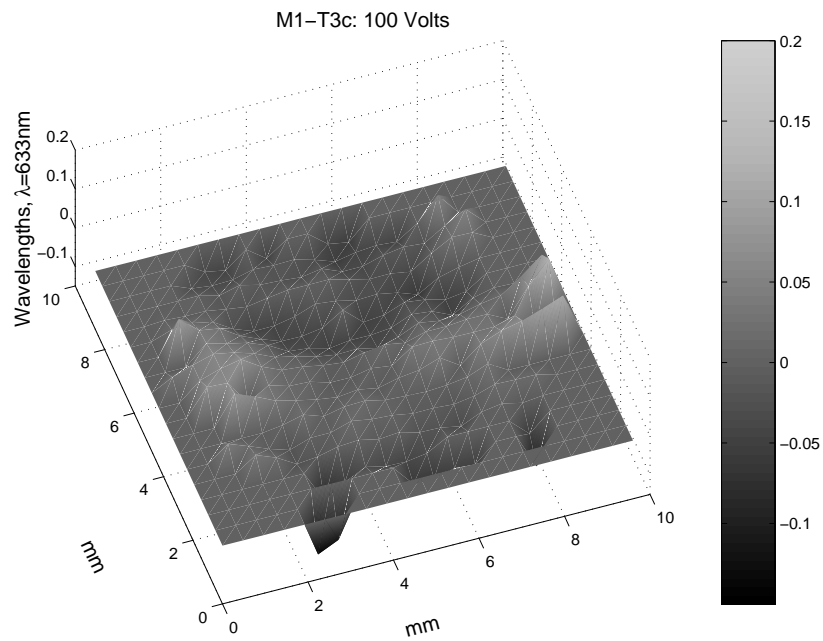
Figure 4.9   Test T3c - Surface flatness of M1 at 100V (0.24λ PV, 0.04λ RMS).
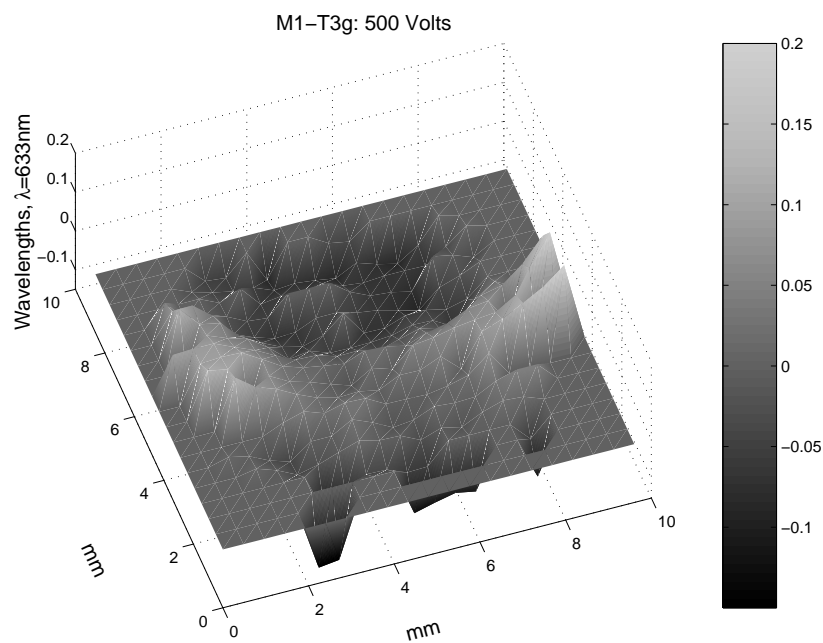
Figure 4.10   Test T3g - Surface flatness of M1 at 500V (0.33λ PV, 0.06λ RMS).
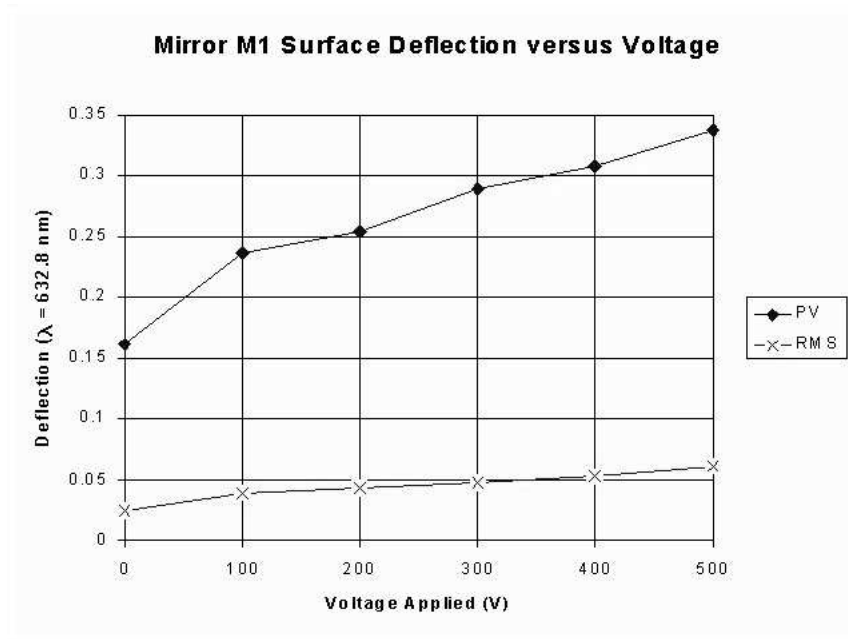
Figure 4.11   Surface deflection of M1 with varying voltage.
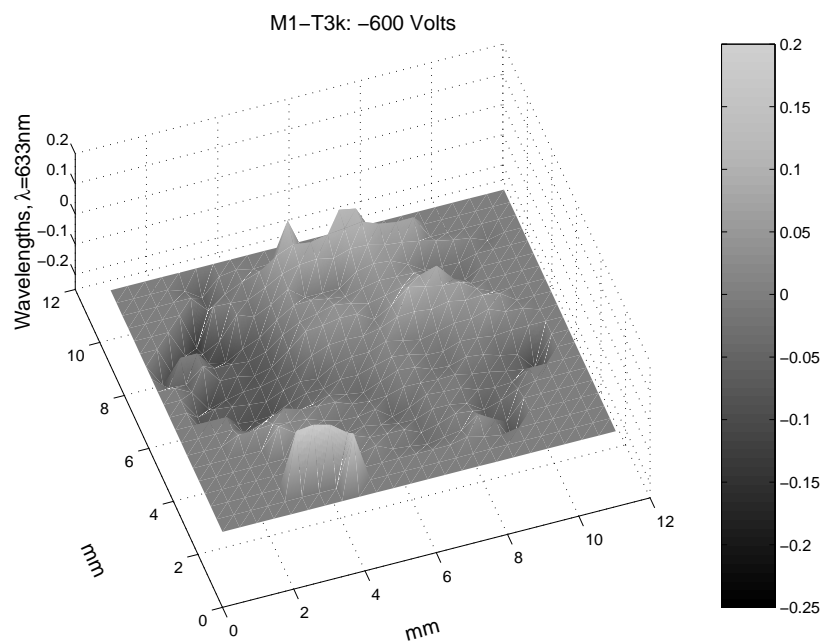
Figure 4.12   Test T3k - Surface flatness of M1 at -600V (0.29λ PV, 0.05λ RMS).
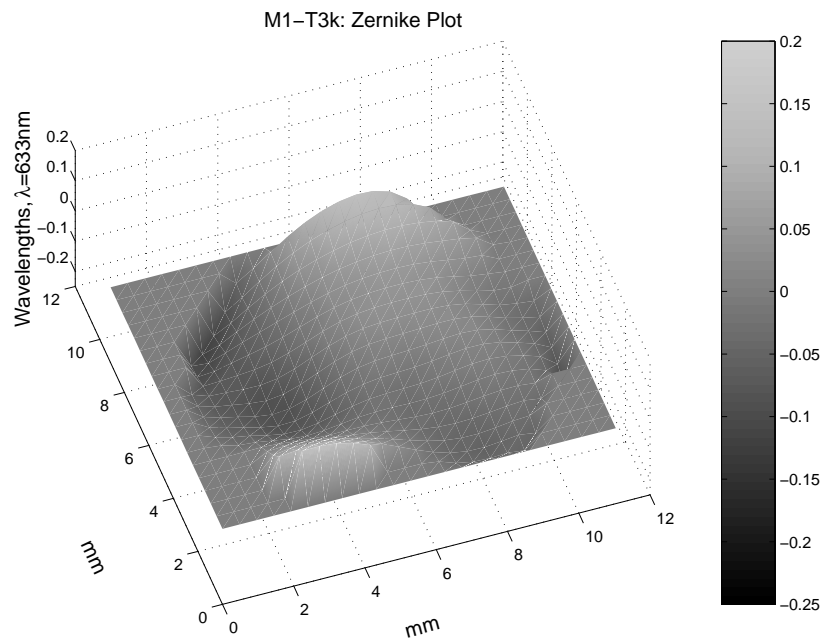
Figure 4.13   Test T3k - Zernike Polynomial
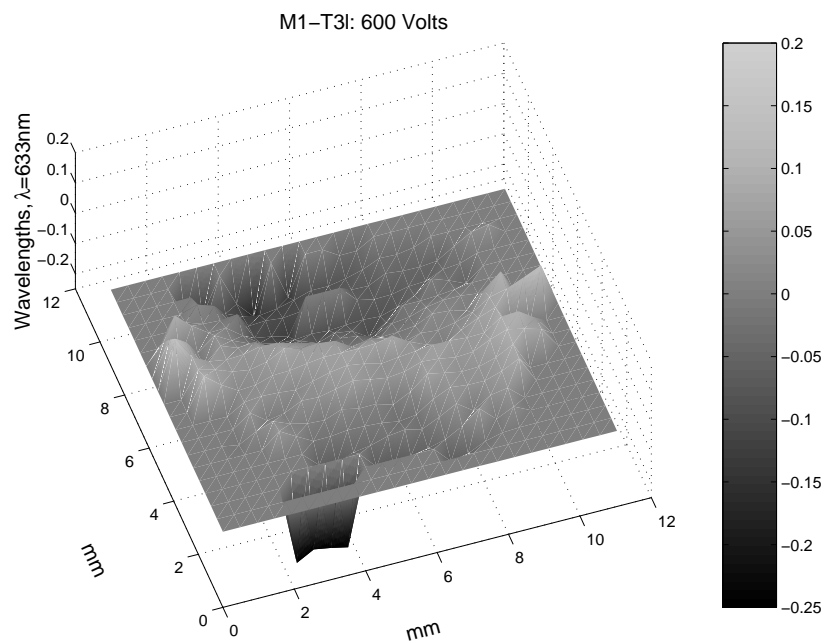
Figure 4.14   Test T3l - Surface flatness of M1 at +600V (0.51λ PV, 0.07λ RMS).
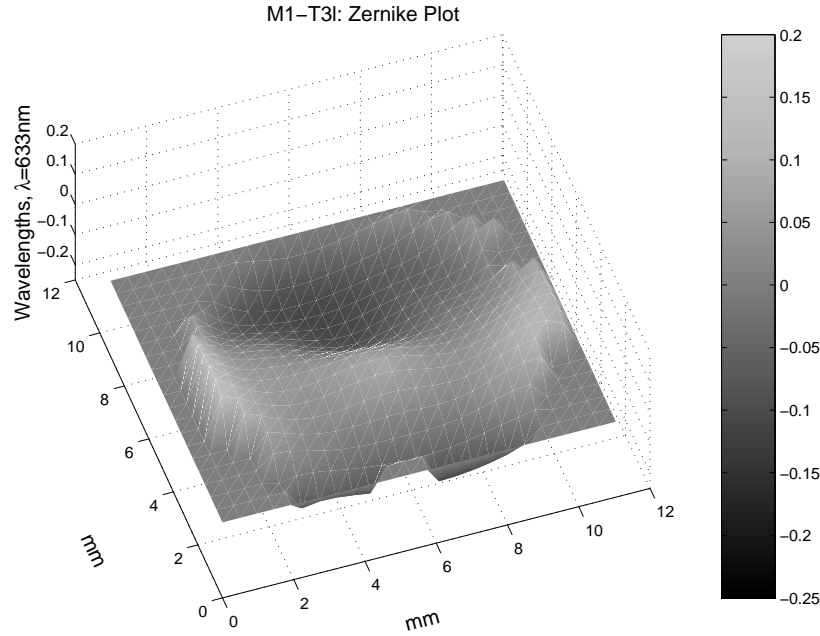
Figure 4.15   Test T3l - Zernike Polynomial

45° to reflect the test light downward (see Figure 4.16). All further membrane mirror tests were conducted using this configuration. The tilted 6" mirror reduced the test beam to an ellipse 4" by 6". For maximum fidelity, the optics were selected such that the test beam completely filled the MLM aperture, which resulted in a 10cm diameter test section. In addition, the 133μm MLM was used for Test 4 to increase the number of test points recorded.

To check the fidelity of the system for absolute surface measurements, a $\lambda/10$ 6" flat mirror was placed horizontally in the test section and measured relative to FM2. The total distortion in the test beam was measured to be 3.0λ PV (0.36λ RMS), mostly 45° astigmatism (see Figure 4.17). The surface flatness of M1 was then measured in the same manner (Test 4a) and determined to be 10.4λ PV (1.6λ RMS). The surface measurements were repeated after re-calibrating the WaveScope® (Test 4b) and the surface flatness was measured to be 6.6λ PV (1.2λ RMS). The same overall shape was observed for both Test 4a and 4b. (see Figure 4.18). A more accurate method for absolute surface measurements would have been to use the 6" flat placed horizontally in the test section as the reference. Using this configuration, errors
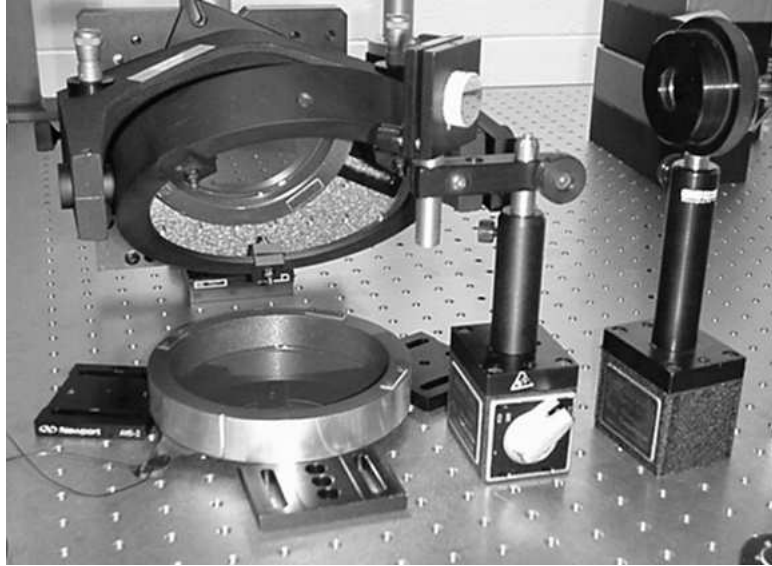
Figure 4.16   Horizontal mirror testing configuration.

introduced by the optics in the test leg would be the same for the test and reference reflections, thus cancelling when the WaveScope® compared the two beams.

The surface flatness was then tested using M1 as the reference (Test 4c) and the flatness was found to be 1.14λ PV (0.13λ RMS). Because the membrane mirrors were stored "face-down" when not in use, M1 was allowed to rest in the "face-up" position for approximately one hour. This ensured that any relaxation of the membrane had reached steady state before continuing the testing. The self-reference test was repeated (Test 4d) resulting in a surface flatness measurement of $0.80~\lambda$ PV ($0.08~\lambda$ RMS) (see Figure 4.19).

The inner region of the mirror was then actuated with 300V (Test 4e) and 600V (Test 4f) and the surfaces were measured for each case. Following actuation with positive voltage, the surface flatness was re-checked at 0V (Test 4g). The surface flatness measured during Test T4e clearly shows the outline of the center control region when energized with 300V (see Figure 4.20). When energized with 600V, however, the surface figure changed unexpectedly (see Figure 4.21). After comparing the data to later test results, it appears that the etched electrodes shorted, allowing charge to bleed onto the outer region of the M1 control pattern instead of remaining
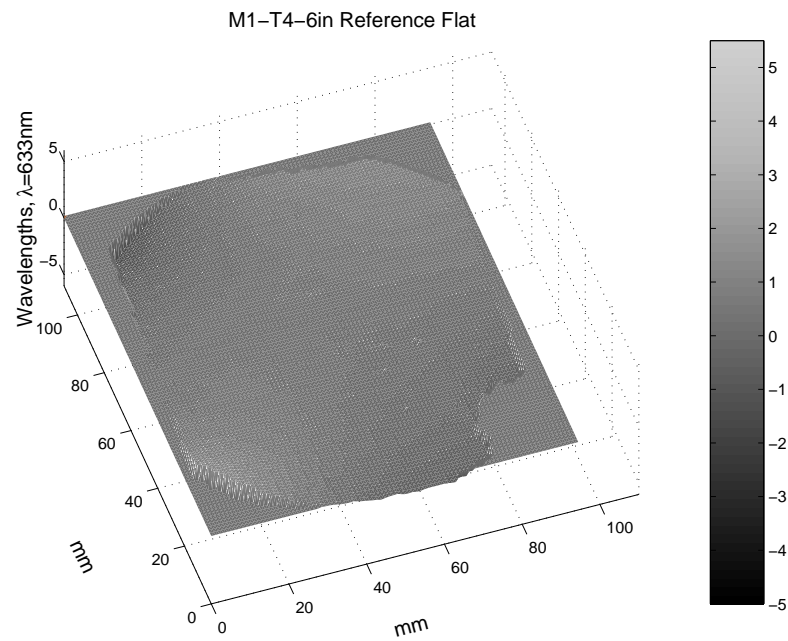
Figure 4.17   6" $\lambda/10$ flat mirror. Note slight 45° astigmatism (3.0λ PV, 0.36λ RMS).
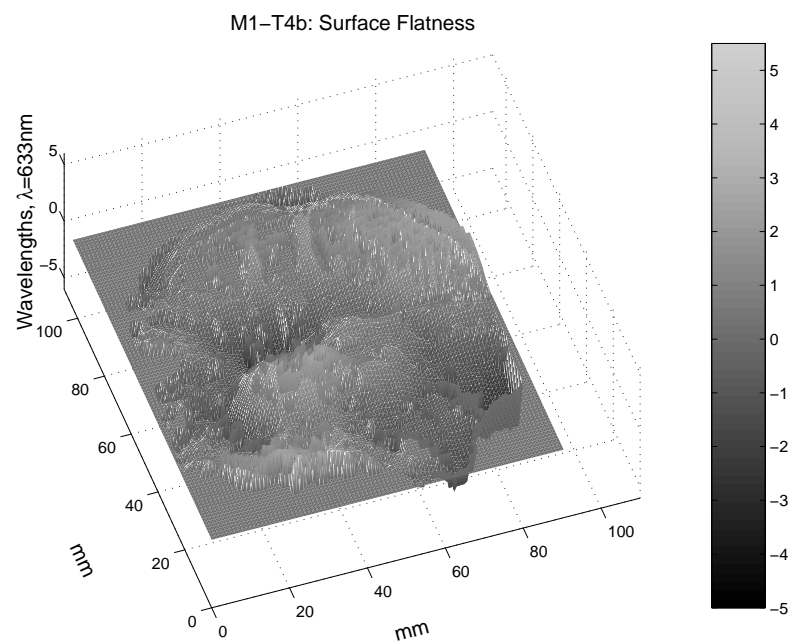
Figure 4.18   Surface flatness, compared to $\lambda/20$ mirror FM2 (6.6λ PV, 1.2λ RMS).
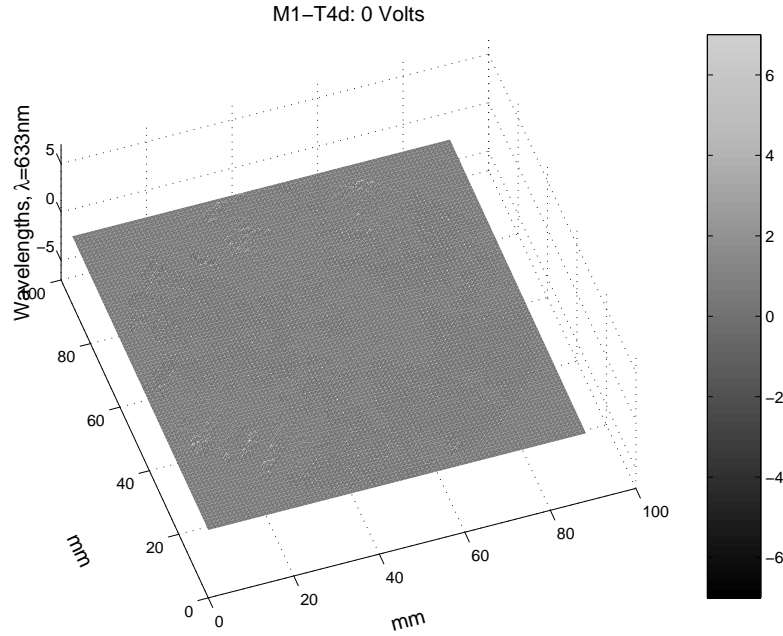
Figure 4.19   M1 self-referenced surface flatness (0.80λ PV, 0.08λ RMS).

in the inner region. Compare Figure 4.21 to Figure 4.27, the surface shape when actuating the outer region with 300V.

The tests of the center region were repeated using -300V, -600V, and 0V (Tests 4h-4j, respectively). Figures 4.23 through 4.25 show the surface flatness for Tests 4h-4j. The magnitude of surface displacement for these tests is lower than that observed for the positive voltage tests. Shorting of the etched electrodes during earlier tests may have prevented proper charge containment, allowing charge to bleed to other areas of the control layer.

The surface showed residual displacement after surface actuation, indicating possible residual charge on the control membrane surface. To compensate, the Wave-Scope® was re-calibrated before continuing to test the outer control region using the same series of voltages (Tests 4k-4q). Figures 4.26 through 4.32 show the surface flatness measured during Tests 4k-4q.

The surface shape of M1 during Test 4m shows an isolated region of control, compared to the surface actuation in Test 4l. The same control region was actuated,
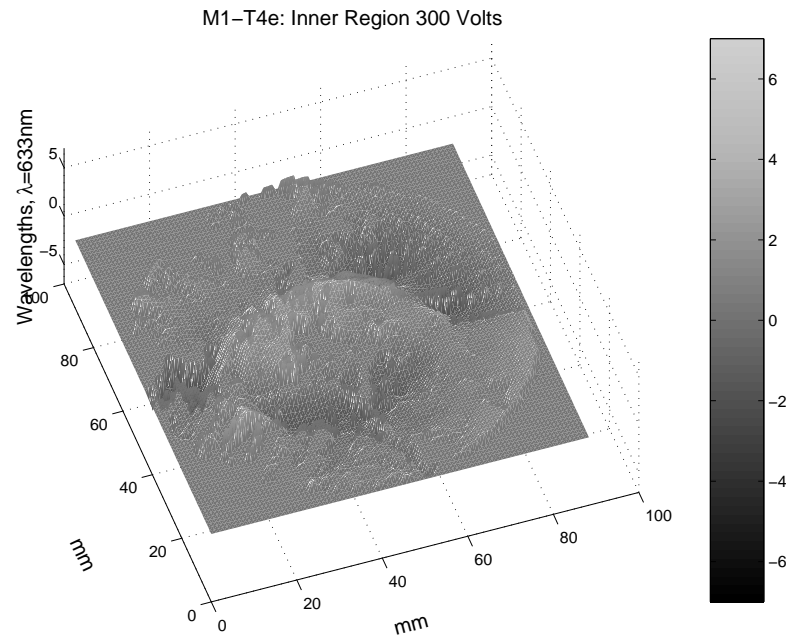
Figure 4.20   M1 inner region actuated with 300V (5.37λ PV, 0.87λ RMS).
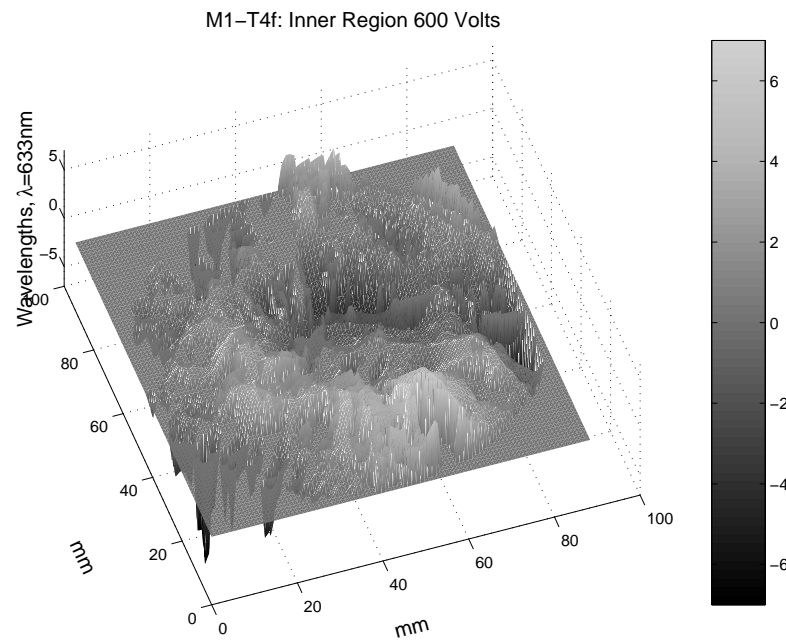
Figure 4.21   M1 inner region actuated with 600V (16.5λ PV, 2.26λ RMS).
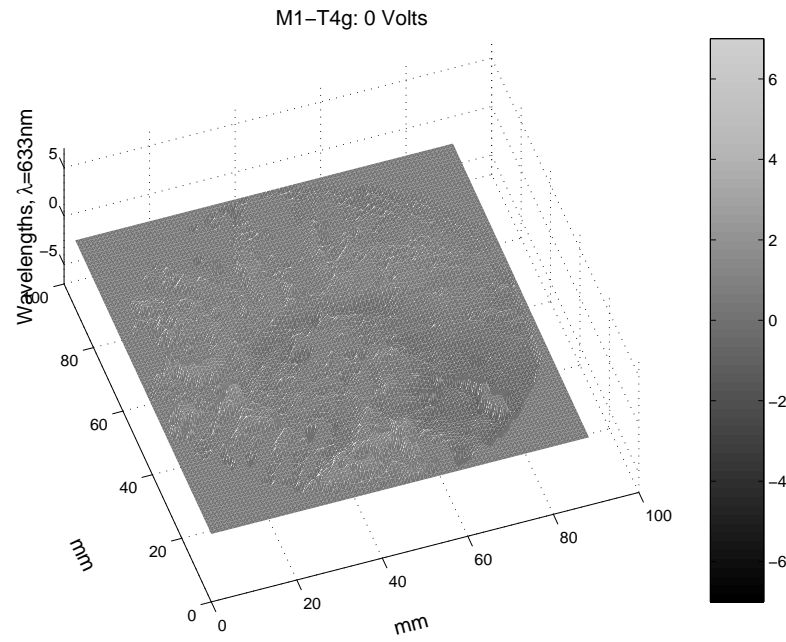
Figure 4.22   M1 at 0V after applying positive voltage (3.10λ PV, 0.43λ RMS).
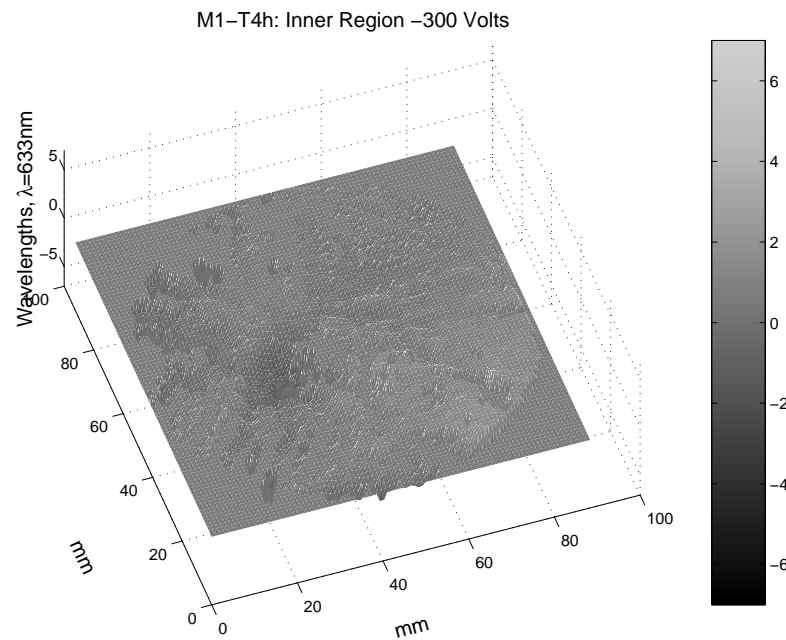
Figure 4.23   M1 inner region actuated with -300V (4.16λ PV, 0.59λ RMS).
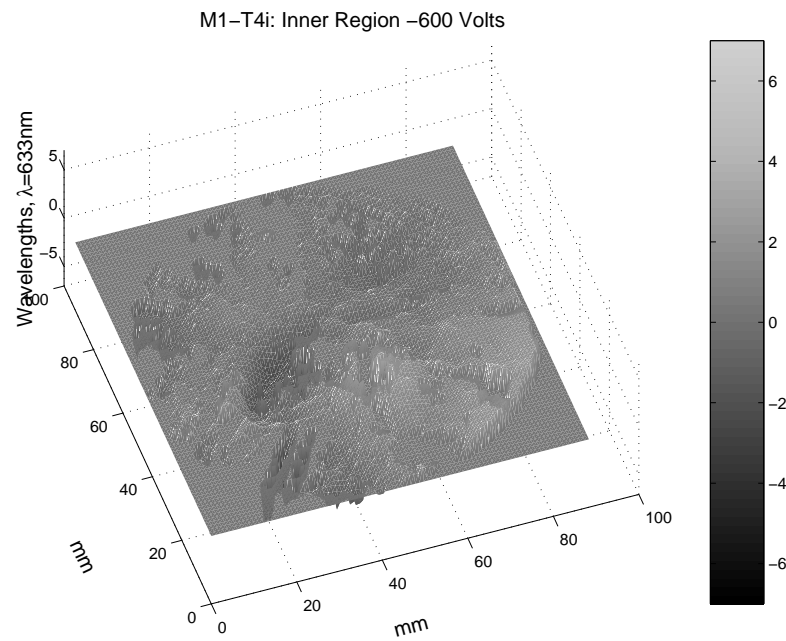
Figure 4.24   M1 inner region actuated with -600V (7.05λ PV, 0.95λ RMS).
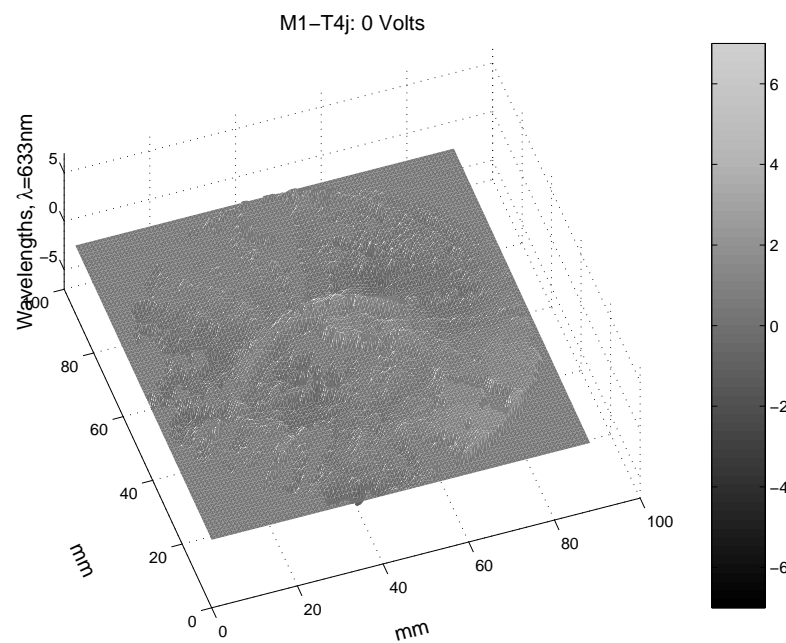
Figure 4.25   M1 at 0V after applying negative voltage (2.79λ PV, 0.46 λ RMS).
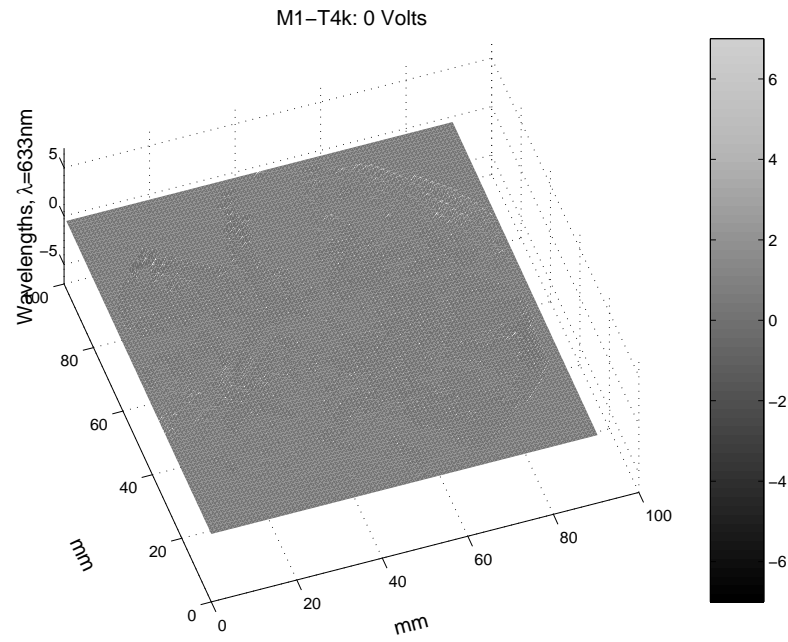
Figure 4.26   M1 at 0V after re-calibration (0.97λ PV, 0.12λ RMS).
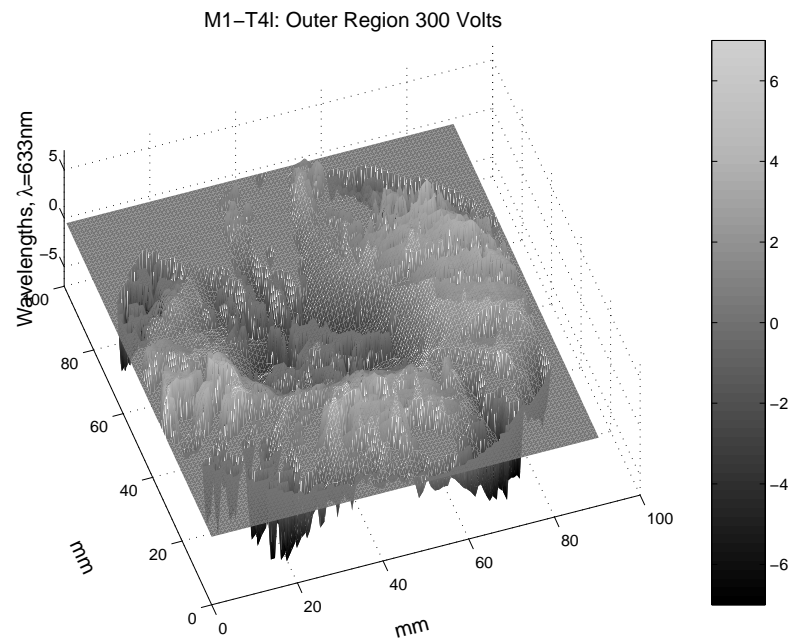
Figure 4.27   M1 outer region actuated with 300V (13.6λ PV, 2.28λ RMS).
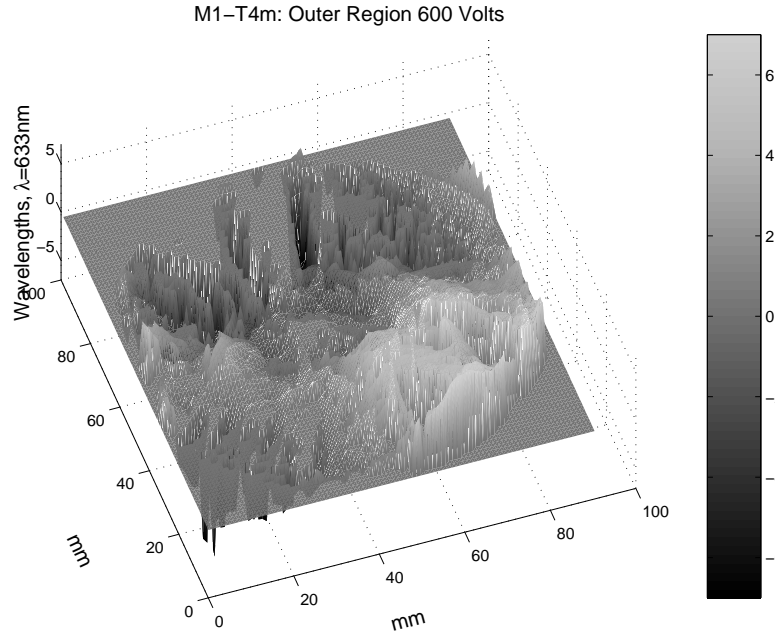
Figure 4.28   M1 outer region actuated with 600V (18.6λ PV, 3.34λ RMS).

but the higher voltage used in Test 4m may have allowed the leads to short. Thus, only the section of the membrane with the etched leads was actuated instead of the control section. Future membranes were etched on both sides to isolate the leads and prevent actuation of the membrane except in the desired control regions.

Tests 4l and 4p show the best response of the outer region of M1 to positive and negative voltage. For qualitative comparison, plots of the Zernike polynomials for these two tests are shown below. Figure 4.33 shows the +300V case, and Figure 4.34 shows the -600V case. Note that the areas inside and outside of the control region are deflected in the opposite direction as the control region. This indicates that the energized PVDF not only deflects out of plane, but exhibits bending at the control boundaries when voltage is applied.

The results of the tests performed on M1 prove that low-order, global shape control of lightweight membrane mirrors can be achieved using a piezopolymer control layer, such as PVDF. The level of control achieved was on the same order of magnitude as the mirror surface features, indicating that shape control could be used to correct
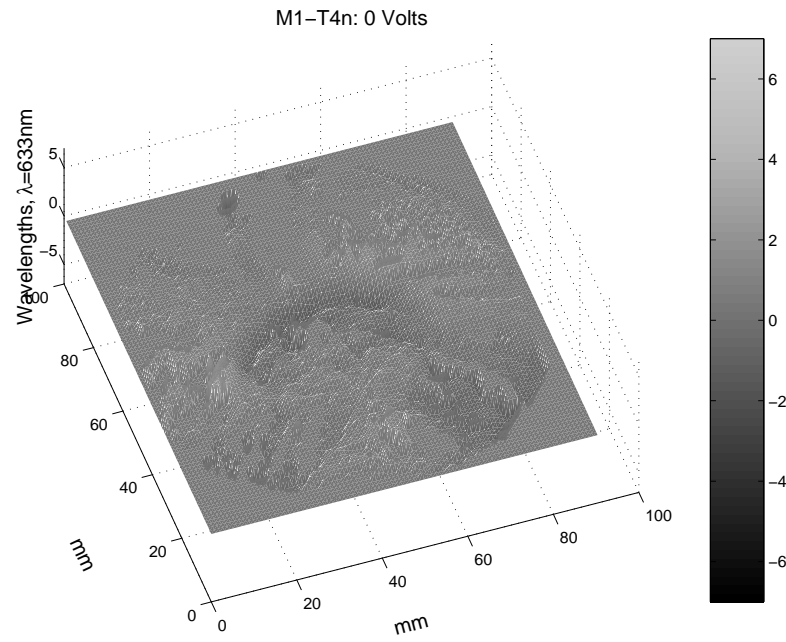
Figure 4.29   M1 at 0V after applying positive voltage (3.78λ PV, 0.59λ RMS).
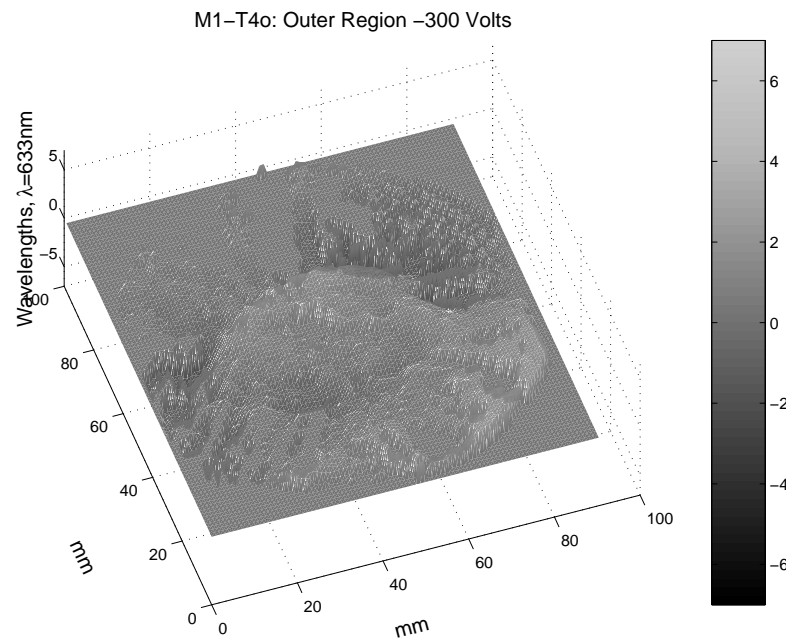
Figure 4.30   M1 outer region actuated with -300V (5.12λ PV, 0.90λ RMS).

M1−T4p: Outer Region −600 Volts
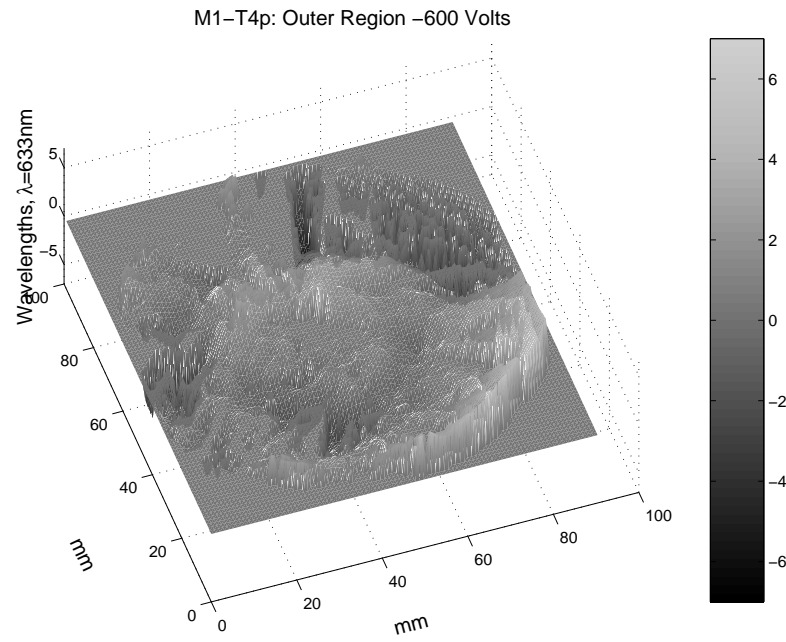
Figure 4.31   M1 outer region actuated with -600V (10.7 λ PV, 1.81 λ RMS).

M1−T4q: 0 Volts
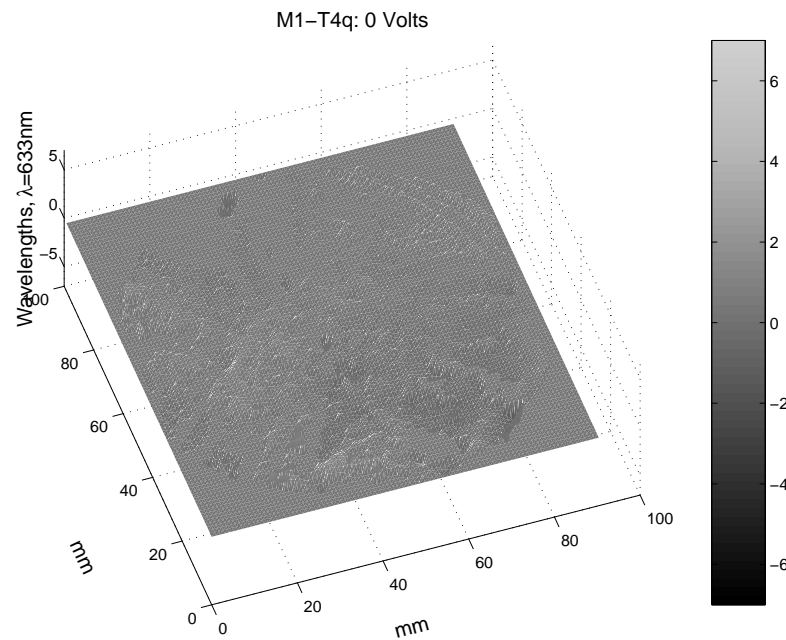
Figure 4.32   M1 at 0V after applying negative voltage (3.24λ PV, 0.344λ RMS).

M1−T4l: Zernike Plot
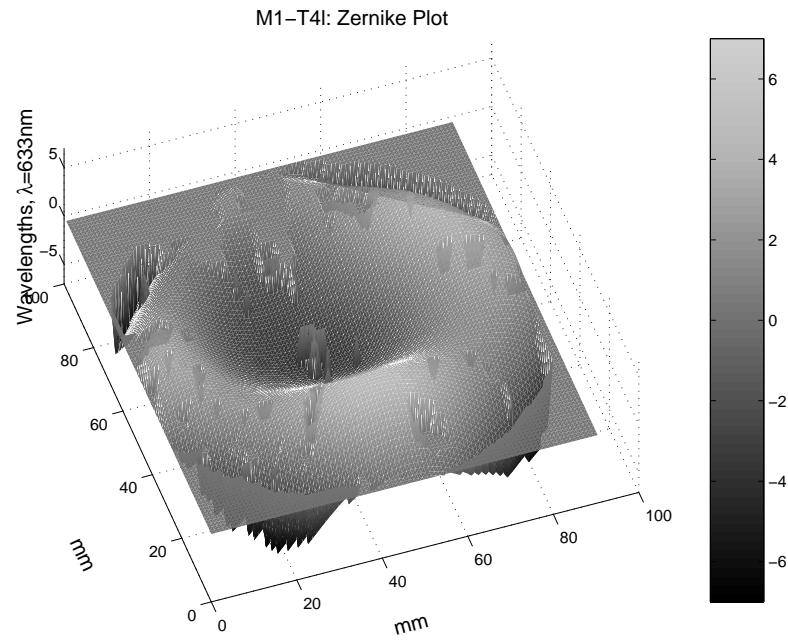
Figure 4.33   M1 outer region actuated with 300V (Zernike).

M1−T4p: Zernike Plot
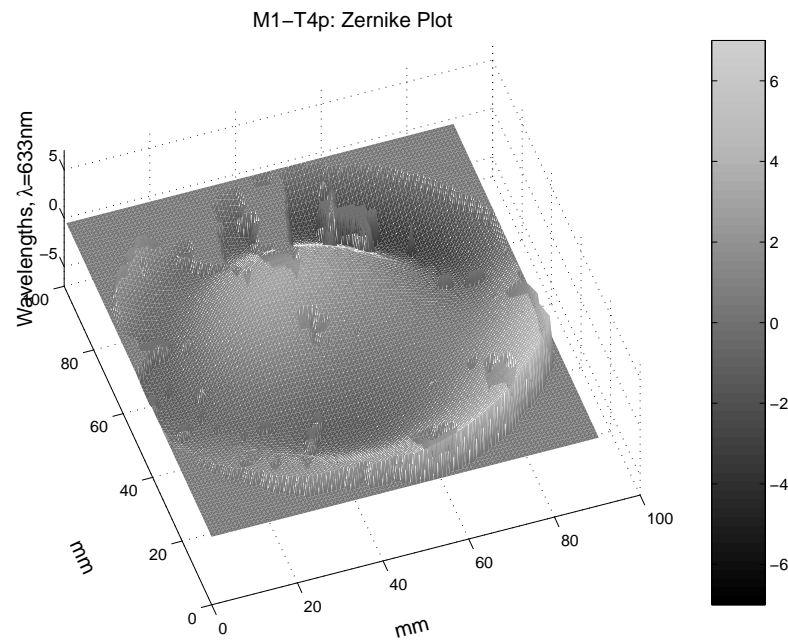
Figure 4.34   M1 outer region actuated with -600V (Zernike).

Figure 4.35   M2 control pattern.

these features. Net-shape membrane optics could employ similar control techniques to alter mirror focal length and make other global curvature corrections while in orbit, thus loosening the manufacturing tolerances on the optical membranes.

4.3   Membrane Mirror M2

Mirror M2 was tested in a horizontal configuration, with a beam expansion ratio of 7.6327 (see section 3.6 for details), enabling a 10-cm section of the surface to be tested. Several tests were conducted by energizing different regions of the control pattern and recording the surface deflection. Figure 4.35 shows the control pattern etched on the M2 PVDF layer and identifies the regions actuated during the following tests. The first test measured the actuation of region 7, the center of the control pattern. Two opposing regions, 3 and 6, were actuated in the second test. The third test of M2 shows actuation of each of the control regions in sequence.
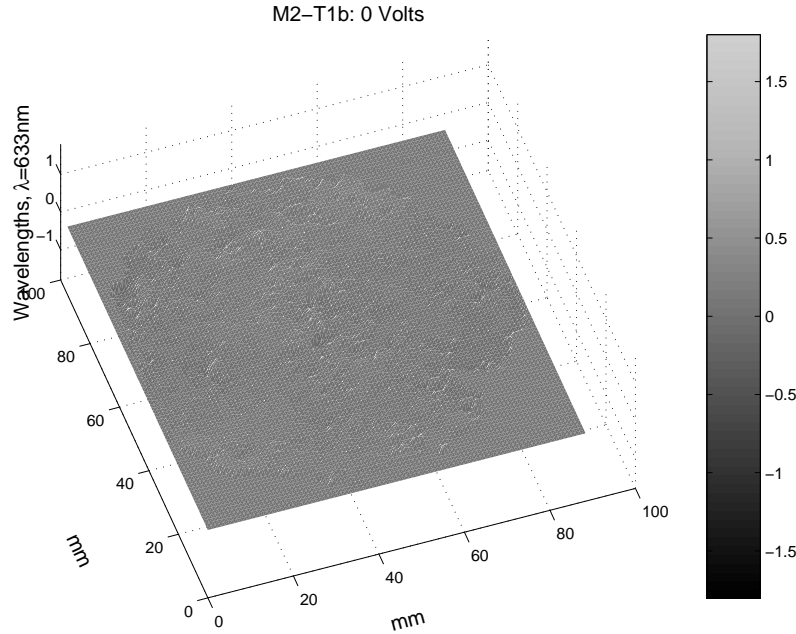
Figure 4.36   M2 self-referenced surface flatness (0.71λ PV, 0.05λ RMS).

4.3.1   M2 Test 1.   The first test of M2 shows the effect of different voltages applied to the center region of the control pattern. The mirror surface was first measured at 0V, using itself as the reference. On the first test, the WaveScope®️ misclassified one of the center data points (see Figure 3.27 for example), resulting in a large spike and erroneous surface flatness measurement (1.9λ PV). The WaveScope®️ was re-calibrated and the test was repeated with acceptable results (see Figure 4.36).

The center leads were connected to the power supply, and voltage was applied to control region 7. The surface flatness was measured at 300V and 600V. The surface plots and corresponding Zernike polynomial plots (see Figures 4.37 through 4.40) show a clearly defined depression located in the center region. The magnitude of the depression increased by almost one wave (2.33λ PV for 300V versus 3.22λ PV for 600V) while remaining fairly smooth (0.27λ RMS versus 0.30λ RMS). The effect of the control region actuation is clearly localized to the etched pattern.

After the mirror had been tested with positive voltage applied, the control leads were grounded to discharge the PVDF layer. The surface flatness was measured at 0V,
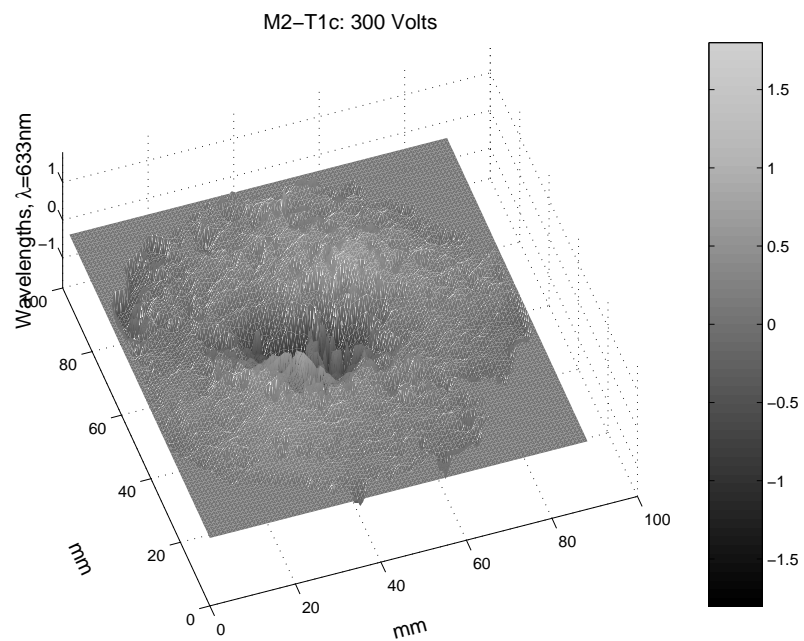
Figure 4.37   Center region of M2 actuated with 300V (2.33λ PV, 0.27λ RMS).
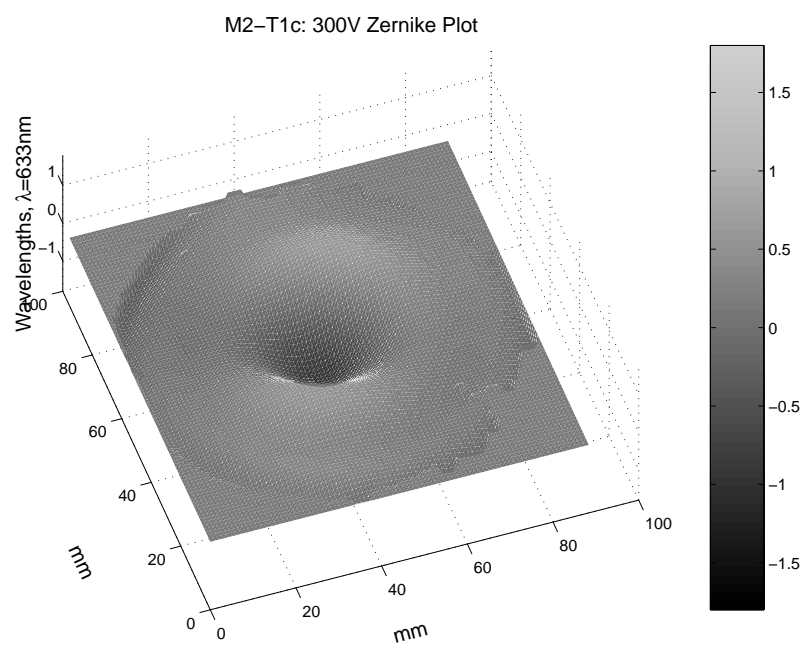
Figure 4.38   Center region of M2 actuated with 300V (Zernike).

4-25
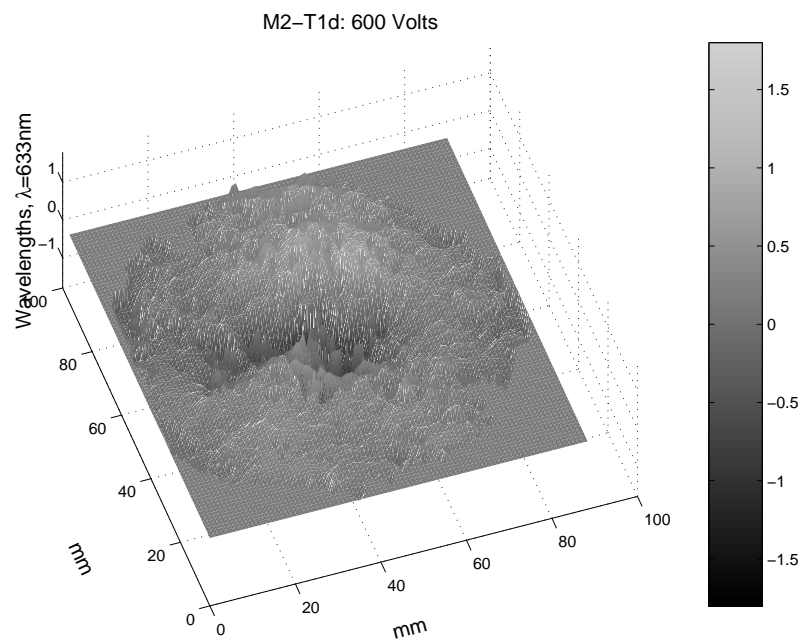
Figure 4.39   Center region of M2 actuated with 600V (3.22λ PV, 0.30λ RMS).
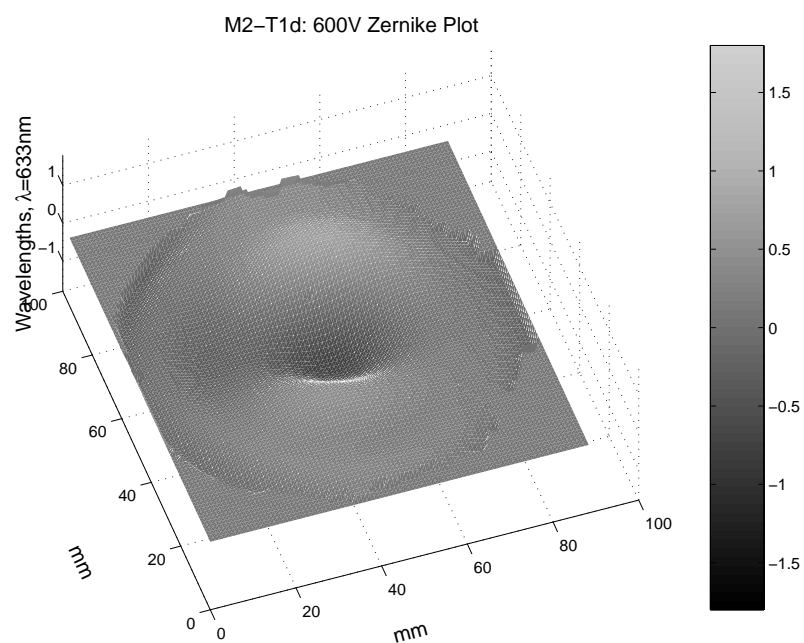
Figure 4.40   Center region of M2 actuated with 600V (Zernike).
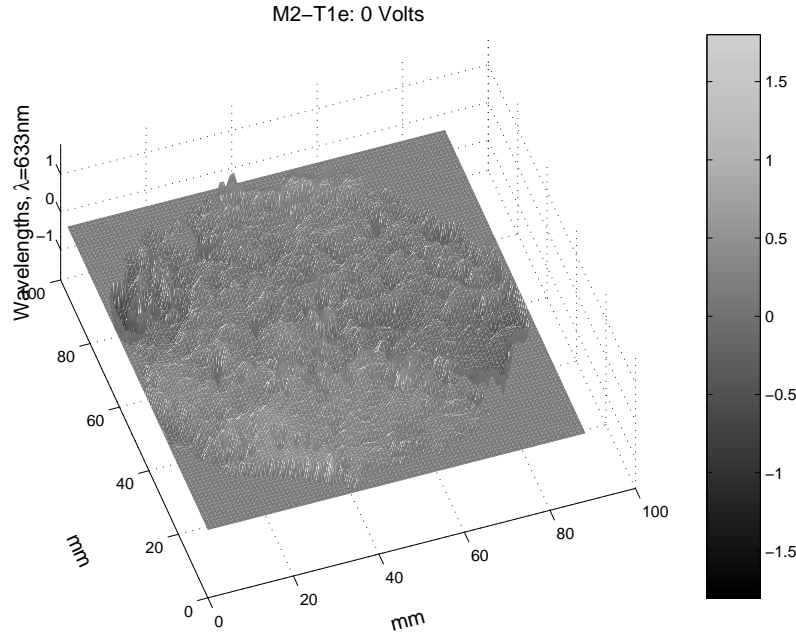
Figure 4.41   M2 at 0V after applying positive voltage (2.60λ PV, 0.20λ RMS).

still referenced to the original undeformed state. As seen in Figure 4.41, the surface retained some deformation as a result of control layer actuation. While there were some isolated regions of large peak-to-valley deformation (2.6λ PV near the edges), the overall surface remained smooth (0.20λ RMS). Figure 4.42 shows the Zernike plot for the 0V state after the series of positive actuation voltages.

Region 7 of M2 was then actuated using -300V and -600V to compare the surface deflection in the opposite direction. Figures 4.43 through 4.46 show the clearly defined center section raised above the surface of the surrounding membrane. The deflection was measured to be 2.39λ PV and 3.40λ PV for the -300V and -600V cases, respectively. In addition, the width of the deformed region increased from about 40mm for the -300V case to about 50mm for the -600V case. The deformed region of the mirror extended slightly beyond the control region, which measured 30mm across. Thus the magnitude and the deformed area increased with increasing voltage.
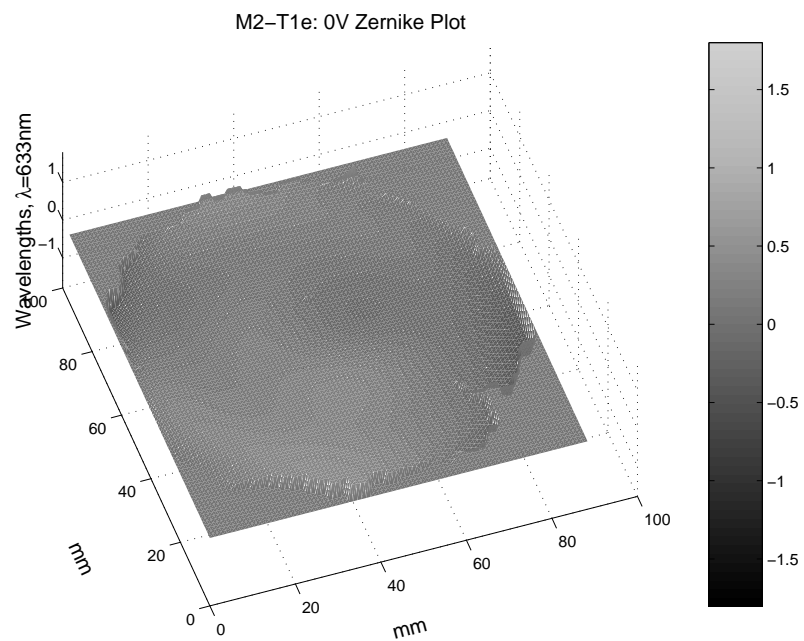
Figure 4.42   M2 at 0V after applying positive voltage (Zernike).
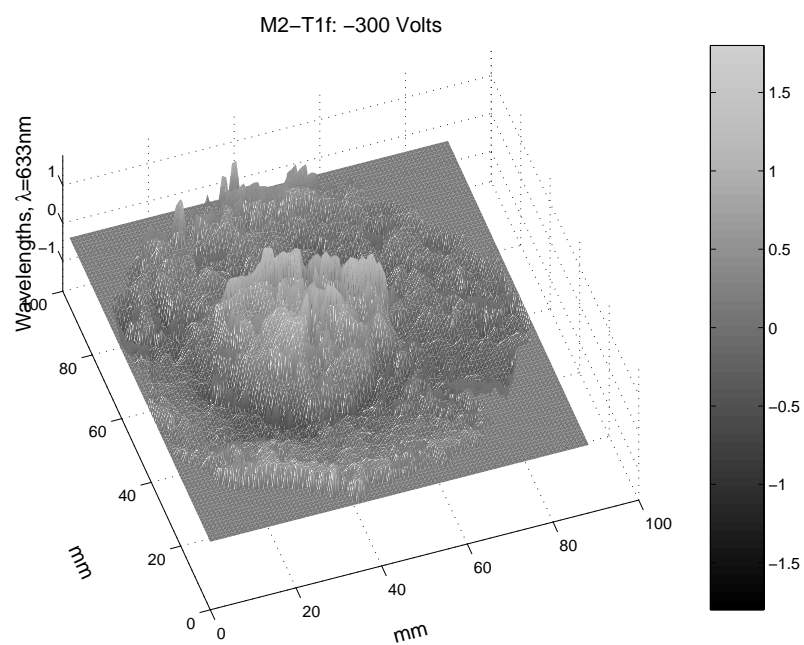
Figure 4.43   Center region of M2 actuated with -300V (2.39λ PV, 0.36λ RMS).

M2−T1f: −300V Zernike Plot
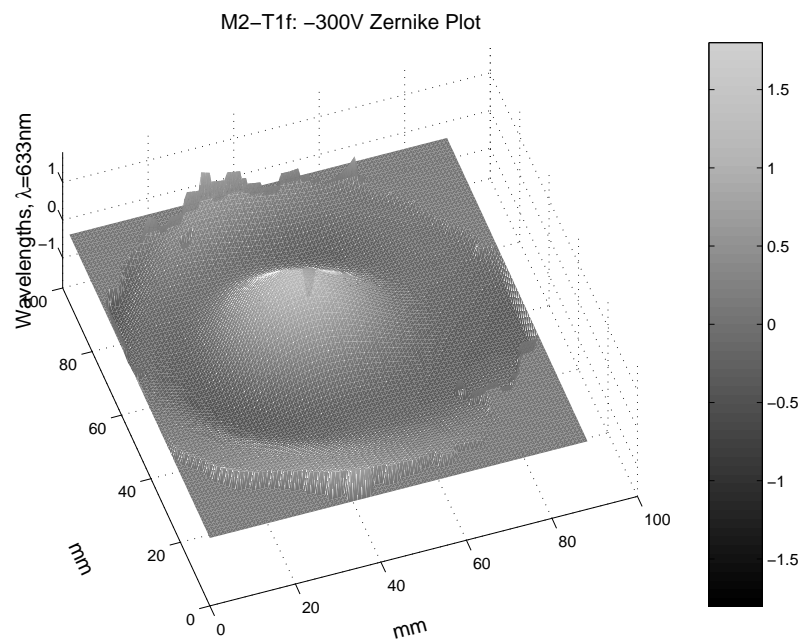
Figure 4.44   Center region of M2 actuated with -300V (Zernike).

M2−T1g: −600 Volts
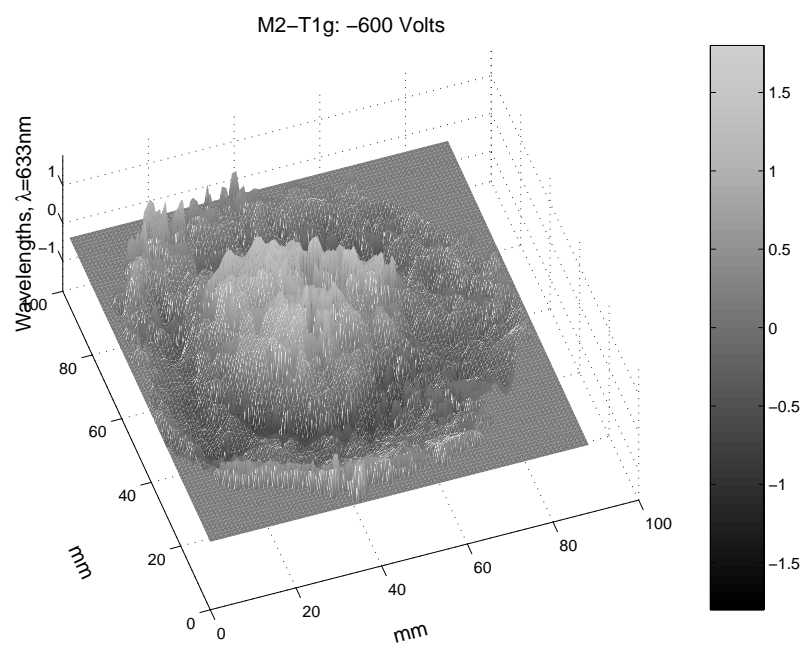
Figure 4.45   Center region of M2 actuated with -600V (3.40λ PV, 0.47λ RMS).

4-29
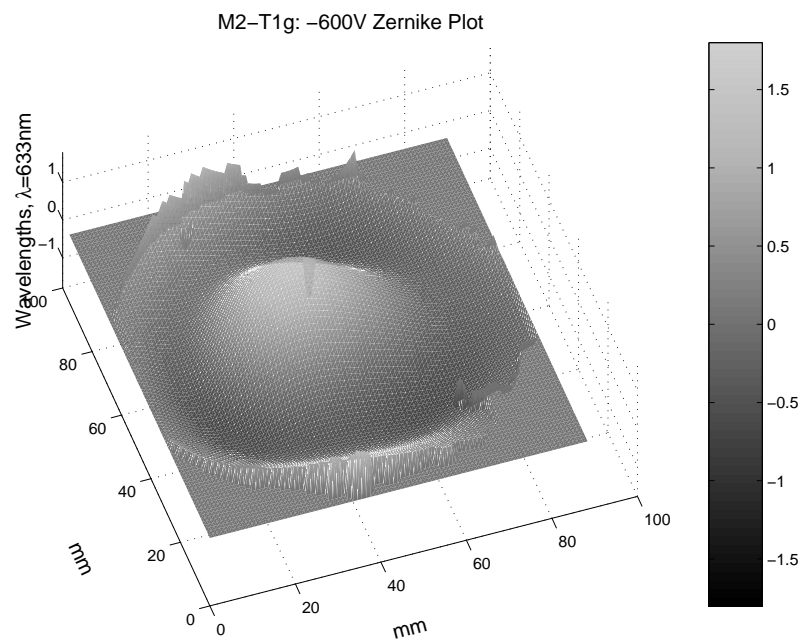
Figure 4.46   Center region of M2 actuated with -600V (Zernike).
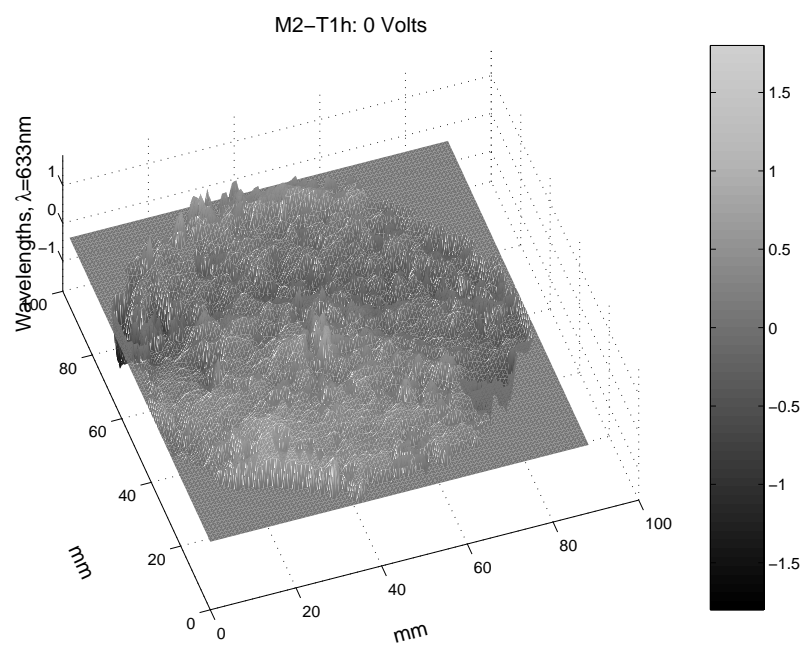
Figure 4.47   M2 at 0V after applying negative voltage (3.52λ PV, 0.29λ RMS).
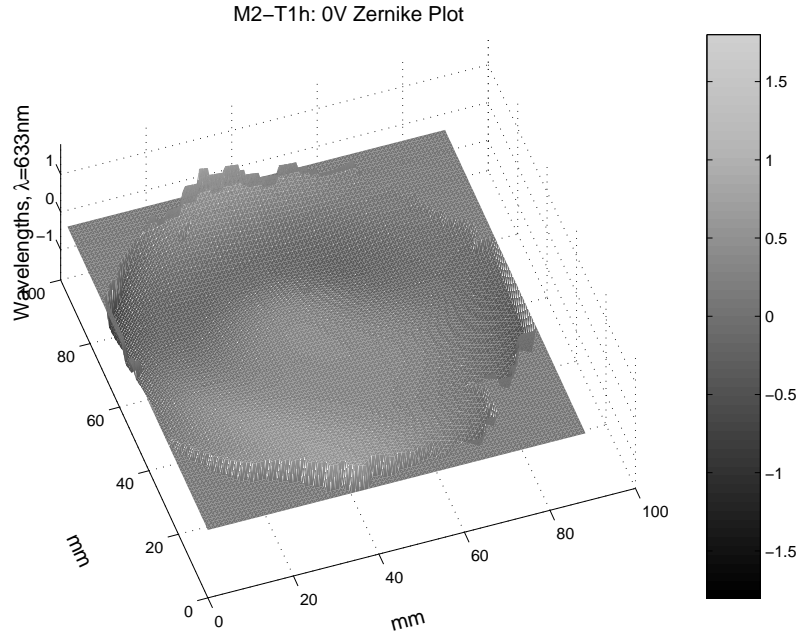
Figure 4.48   M2 at 0V after applying negative voltage (Zernike).

After completing the tests of region 7, M2 was re-tested at 0V to check residual surface deformation. The surface had returned to an overall flat shape (0.29λ RMS), although there were some large, localized areas of residual deformation (3.52λ PV). These were again located near the edges, with only minor shape differences near the center. Figure 4.47 shows the surface shape measured relative to the original 0V state. The Zernike plot in Figure 4.48 shows the residual deformation of the surface shape due to actuation of the center region during Test 1.

4.3.2   M2 Test 2.   The second set of tests for M2 consisted of applying voltage to two of the outer regions and measuring the surface displacement. The leads for regions 3 and 6 were connected to the power supply and the membrane deflection was measured from 600V to -600V in 300V increments. Before applying voltage, the WaveScope® was re-calibrated with the membrane at 0V. The self-referenced surface flatness was measured to be 0.68λ PV (0.09λ RMS), as shown in Figure 4.49.

The 300V actuation of regions 3 and 6 produced localized surface deflection at the control regions. Figure 4.50 clearly shows an isolated depression at each of the

4-31
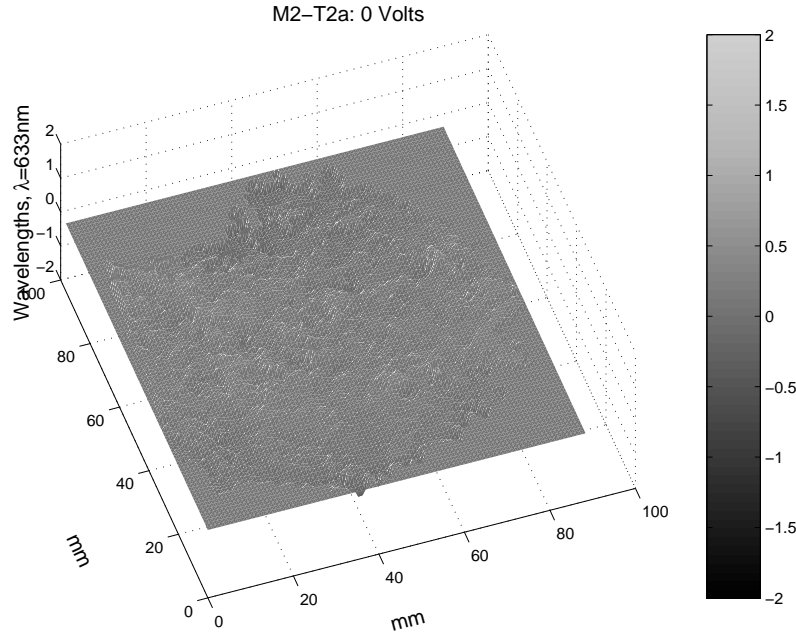
Figure 4.49   M2 self-referenced surface flatness (0.68λ PV, 0.09λ RMS).

regions. The surface flatness was measured to be 2.88λ PV (0.42λ RMS). Figure 4.51 shows a plot of the Zernike polynomials for the 300V actuation.

The voltage to regions 3 and 6 was increased to 600V, producing an increased membrane surface deflection. Figure 4.52 shows that the control regions affect the surrounding membrane more at the higher voltage. This phenomenon was also observed in the first test of M2. The surface flatness was measured to be 4.46 λ PV (0.76λ RMS), but the deflection was no longer confined to the control regions. The width of the affected area had increased to include the center portion of the mirror. In addition, the regions outside the etched control pattern were deflected upward. The Zernike plot in Figure 4.53 shows the increased control region area of influence created by the higher voltage.

The membrane control leads were then grounded and the surface flatness was measured at 0V. Although there was still some residual deformation, the surface overall remained fairly flat. Figure 4.54 shows the surface after actuation with positive
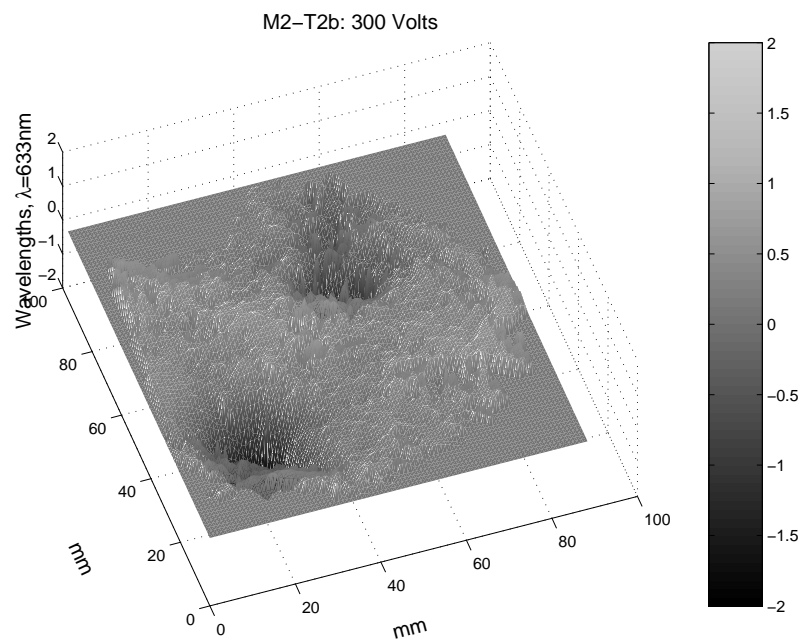
Figure 4.50   M2 regions 3 and 6 actuated with 300V (2.88λ PV, 0.42λ RMS).
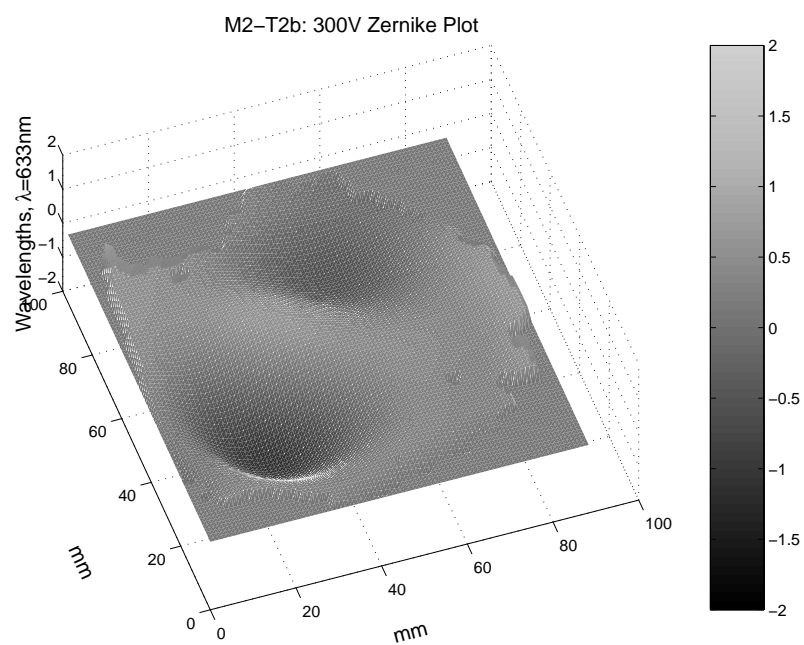
Figure 4.51   M2 regions 3 and 6 actuated with 300V (Zernike).
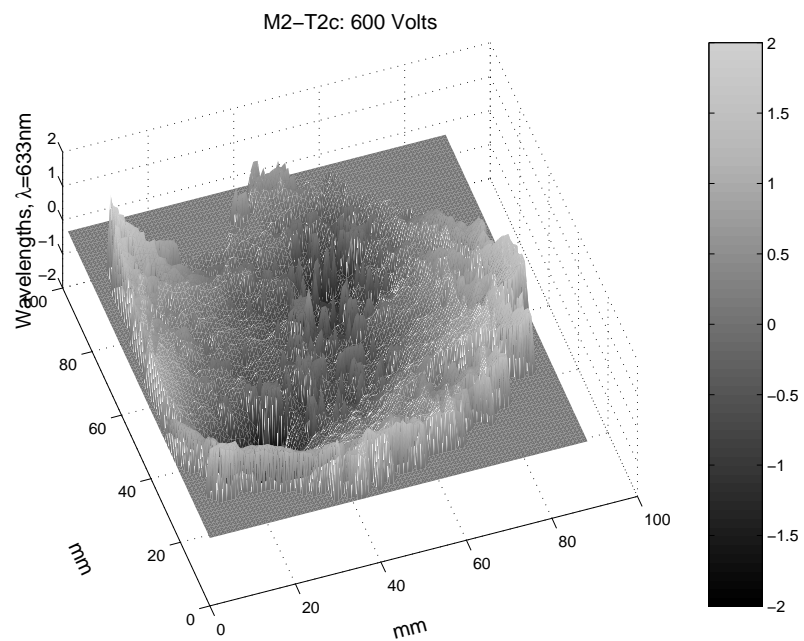
Figure 4.52   M2 regions 3 and 6 actuated with 600V (4.46λ PV, 0.76λ RMS).
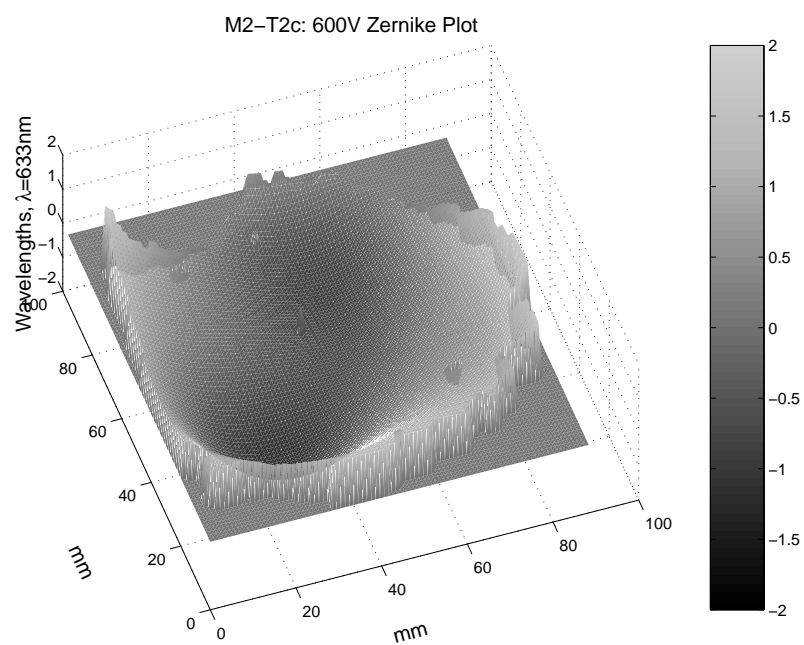
Figure 4.53   M2 regions 3 and 6 actuated with 600V (Zernike).
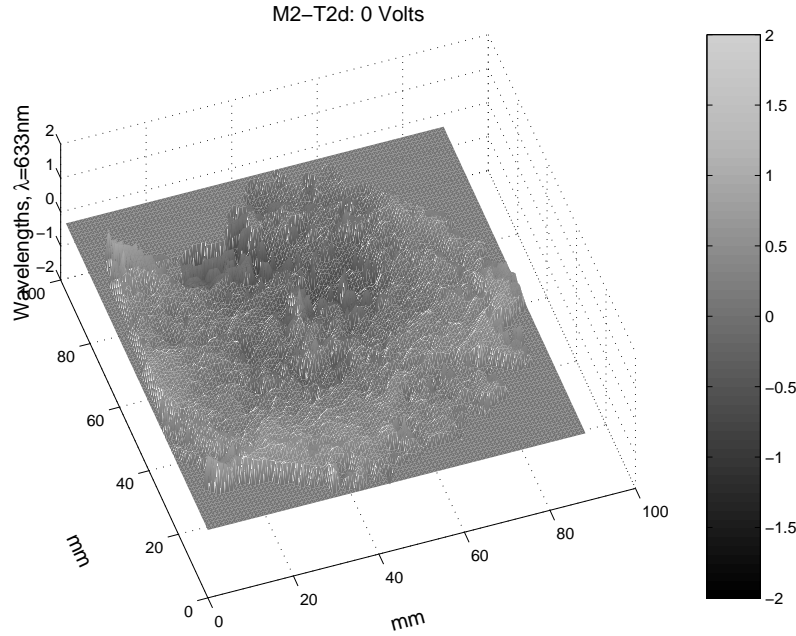
Figure 4.54   M2 at 0V after applying positive voltage (2.28λ PV, 0.31λ RMS).

voltage applied to the control regions. The Zernike plot in Figure 4.55 shows the minor surface deviations as a result of membrane actuation.

The control regions were then actuated with -300V, causing surface deflection in the opposite direction. Figures 4.56 and 4.57 show the clearly defined control regions raised above the surrounding surface. The flatness was measured to be 3.50λ PV (0.49λ RMS) for the -300V actuation. The voltage was then increased to -600V, causing the surface deflection to increase to 5.25λ PV (0.77λ RMS). Figures 4.58 and 4.59 show the increased magnitude of deflection for regions 3 and 6 at the higher voltage. The area of influence also increased with voltage, as observed for the +600V case.

After the -600V test was complete, the control leads were grounded and the surface flatness was measured again at 0v. Figures 4.60 and 4.61 show that the surface retained residual deformation after surface actuation. It is unknown whether the deformation was caused by charge leakage to the region of the PVDF membrane
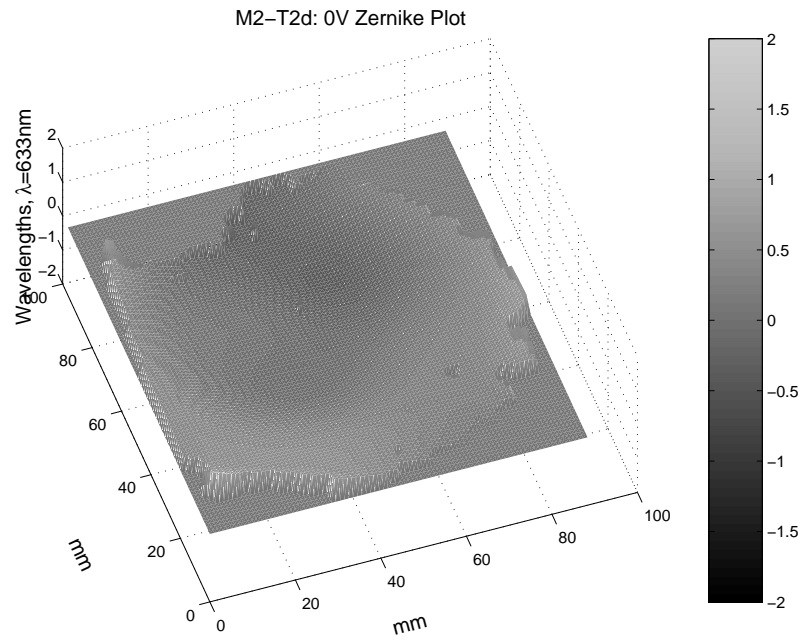
Figure 4.55   M2 at 0V after applying positive voltage (Zernike).
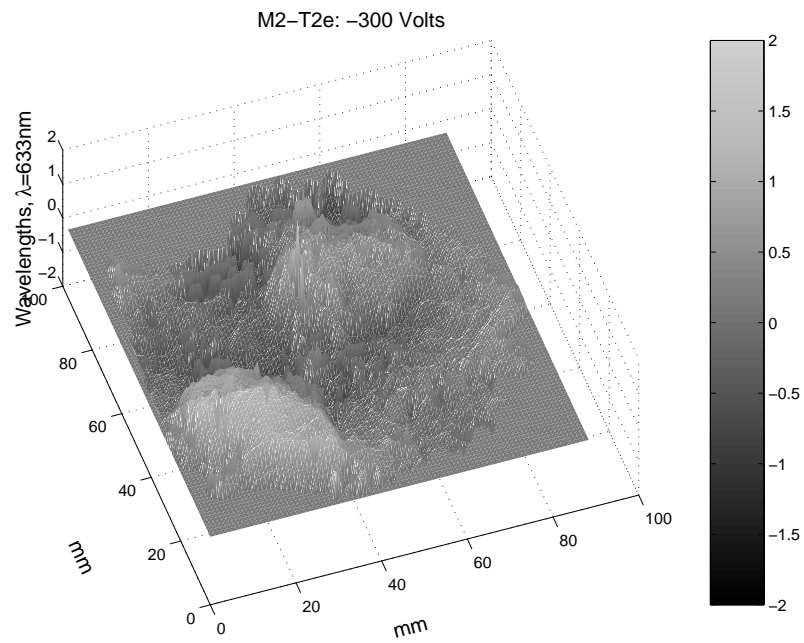
Figure 4.56   M2 regions 3 and 6 actuated with -300V (3.50λ PV, 0.49λ RMS).
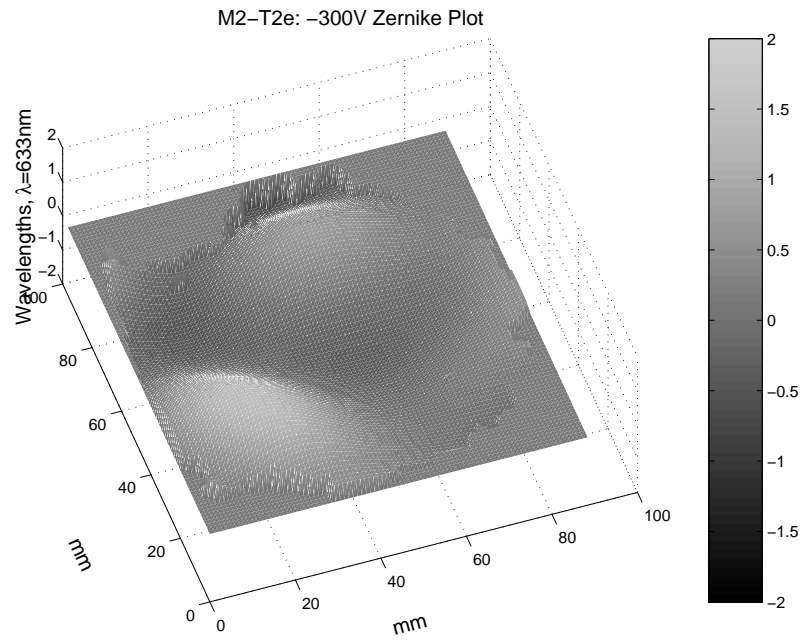
Figure 4.57   M2 regions 3 and 6 actuated with -300V (Zernike).
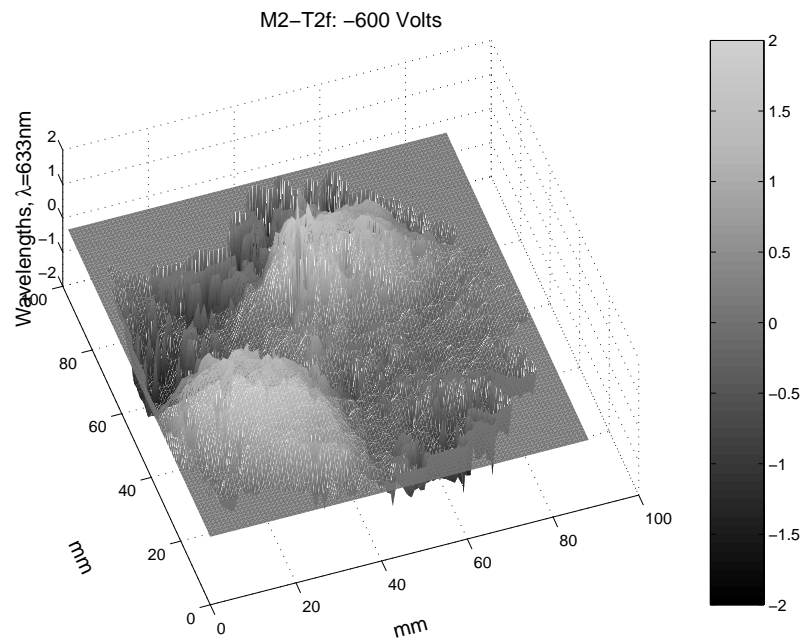
Figure 4.58   M2 regions 3 and 6 actuated with -600V (5.25λ PV, 0.77λ RMS).
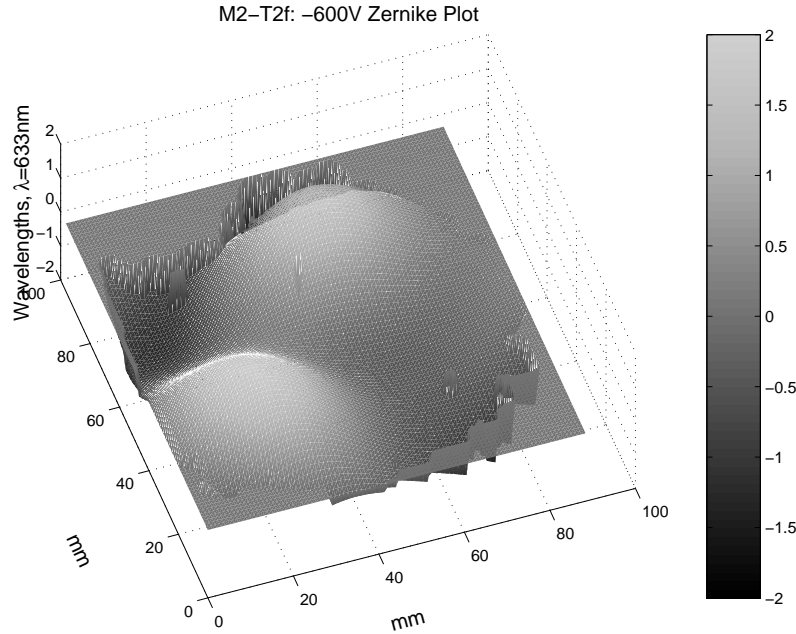
Figure 4.59   M2 regions 3 and 6 actuated with -600V (Zernike).

outside the control pattern or was a result of changes in the mechanical properties of the mirror, possibly causing the membrane to sag due to gravity.

Before continuing to test the other regions of mirror M2, the absolute surface flatness was measured relative to a 6" diameter $\lambda/10$ flat mirror. The flat mirror was placed horizontal in the test section and the surface reflection was recorded as the reference. The flat mirror was then replaced with mirror M2 and the surface flatness was measured to be 3.95λ PV (0.63λ RMS). Figures 4.62 and 4.63 show the surface flatness and the Zernike plot, respectively. The actuated regions (3, 6, and 7) are clearly visible as depressions in the surface. Again, it is unknown whether the deformation is a result of uneven residual charge distribution or changes in the mechanical properties of the mirror. Note that the orientation of the mirror is rotated clockwise by about 60°. This orientation was also used for Test 3.

4.3.3 M2 Test 3.   After measuring the surface flatness referenced to a flat mirror, the WaveScope® was re-calibrated using M2 as the reference. The self-referenced flatness was then measured at 0V to be 0.59λ PV (0.07λ RMS) (see Figure
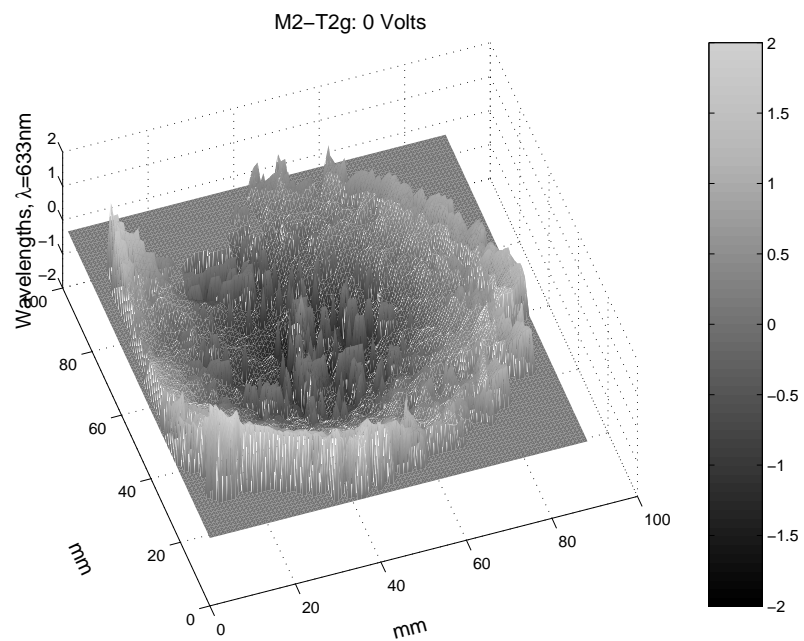
Figure 4.60   M2 at 0V after applying negative voltage (4.42λ PV, 0.72λ RMS).
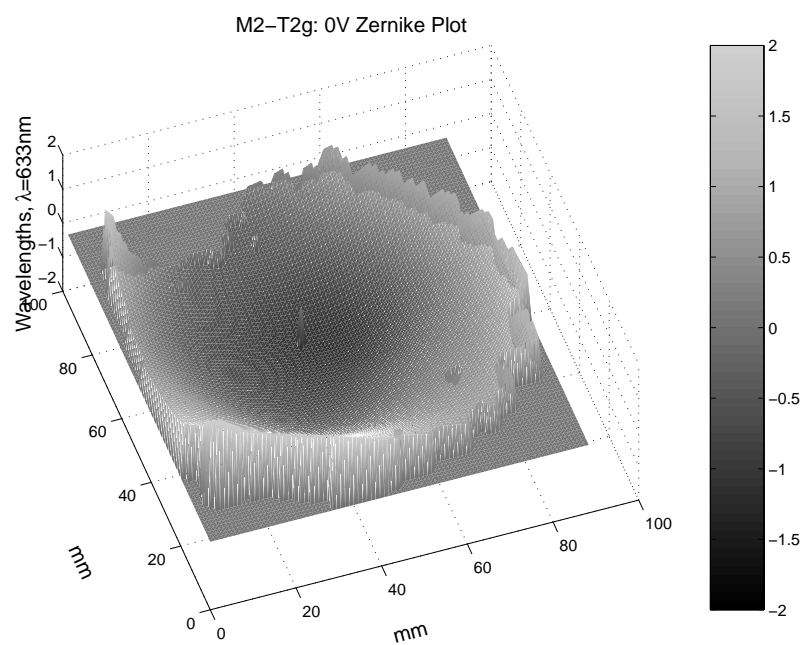
Figure 4.61   M2 at 0V after applying negative voltage (Zernike).

4-39
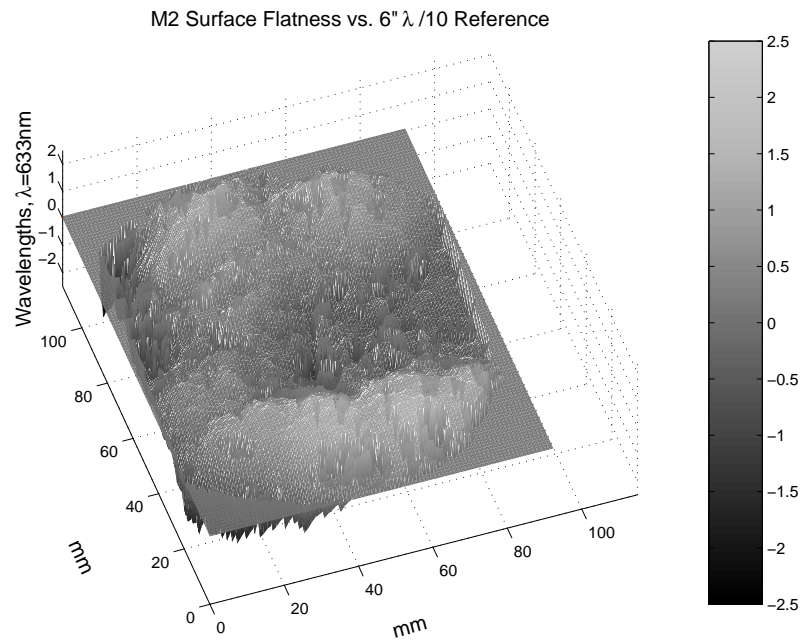
Figure 4.62   M2 surface flatness, after Test 2 actuation (3.95λ PV, 0.63λ RMS).
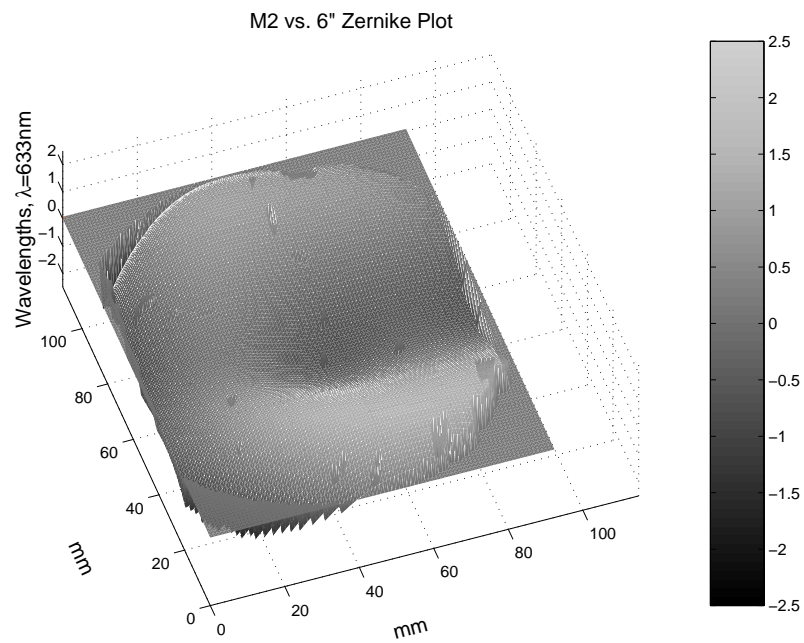
Figure 4.63   M2 surface flatness, after Test 2 actuation (Zernike).
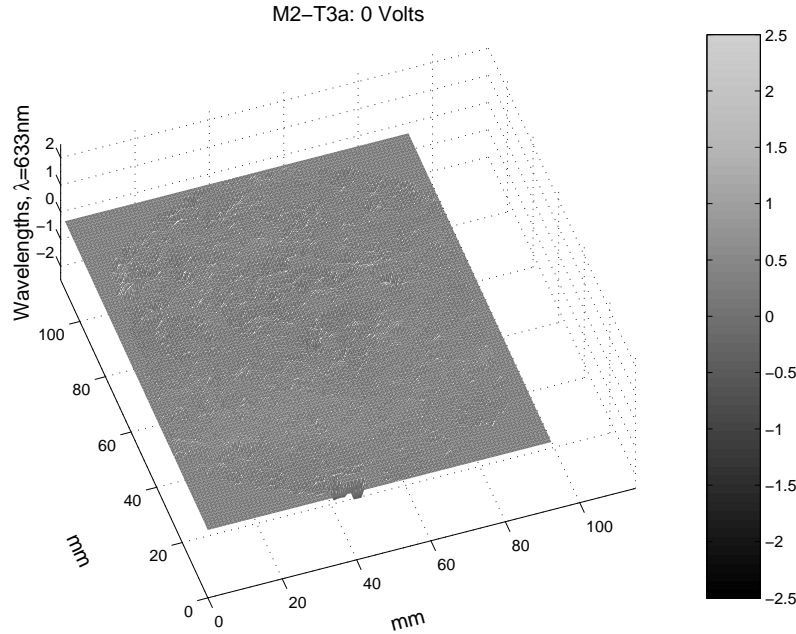
Figure 4.64   M2 self-referenced surface flatness (0.59λ PV, 0.07λ RMS).

4.64). Each of the 7 control regions were then actuated in turn using -600V, causing the selected region to deform upward. The un-actuated regions in each test were connected to ground. The actuated regions varied in magnitude from 3λ to over 5λ PV. Figures 4.65 through 4.76 show the surface flatness and plots of the associated Zernike polynomials for each of the outer regions.

Upon actuation, each region deformed the mirror surface according to the pattern etched on the control surface. During testing of region 3 (see Figure 4.69), surface deformation was also visible in region 1. This deformation was visible during the testing of regions 4-6 as well, although the magnitude decreased slightly during each subsequent test. The cause of the deformation is unknown, but it was probably due to charge leakage from the actuated electrodes or a short in the electrical leads.

After the outer regions of M2 had been tested, region 7 was tested with -600V as well. The center region deflected upward as expected, comparing favorably with previous actuation of the same region. Compare Figures 4.77 and 4.78 with Figures
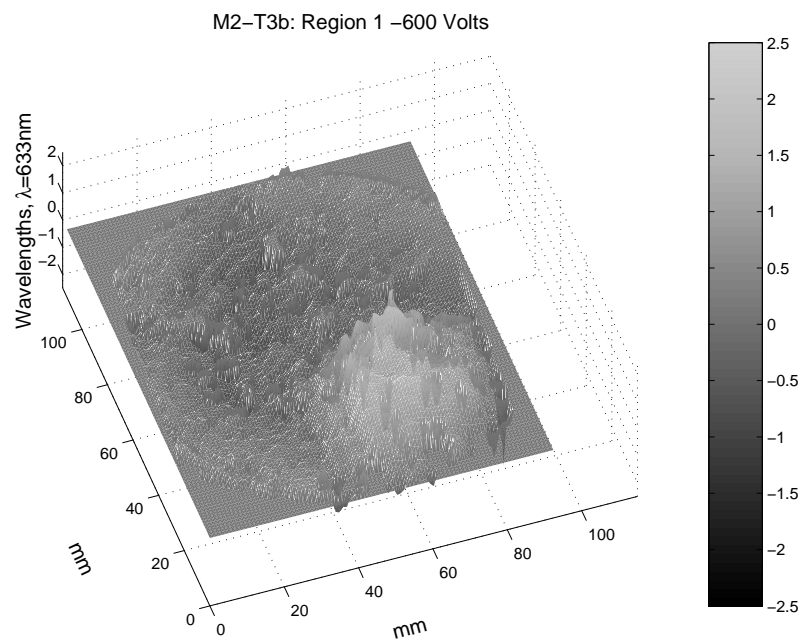
Figure 4.65   M2 Region 1 actuated with -600V (4.47λ PV, 0.53λ RMS).
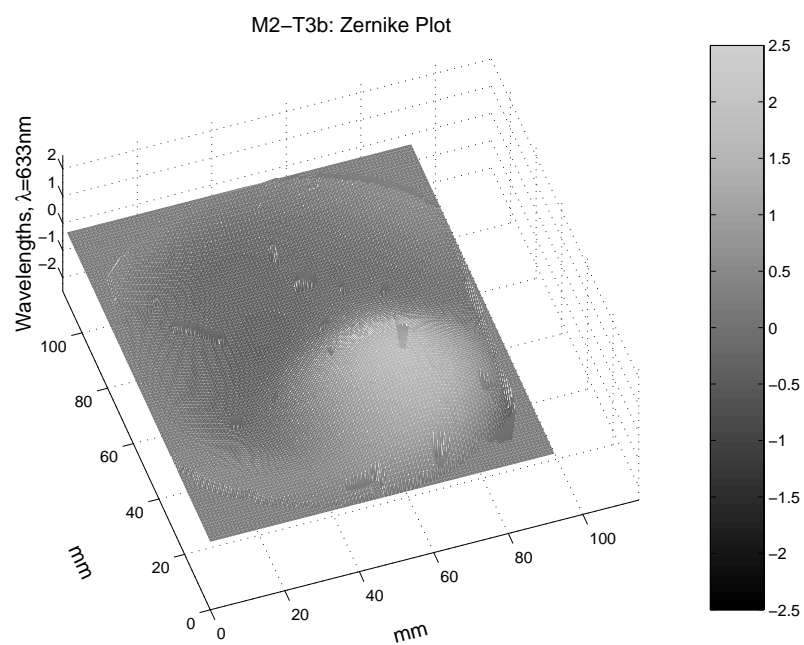
Figure 4.66   M2 Region 1 actuated with -600V (Zernike).
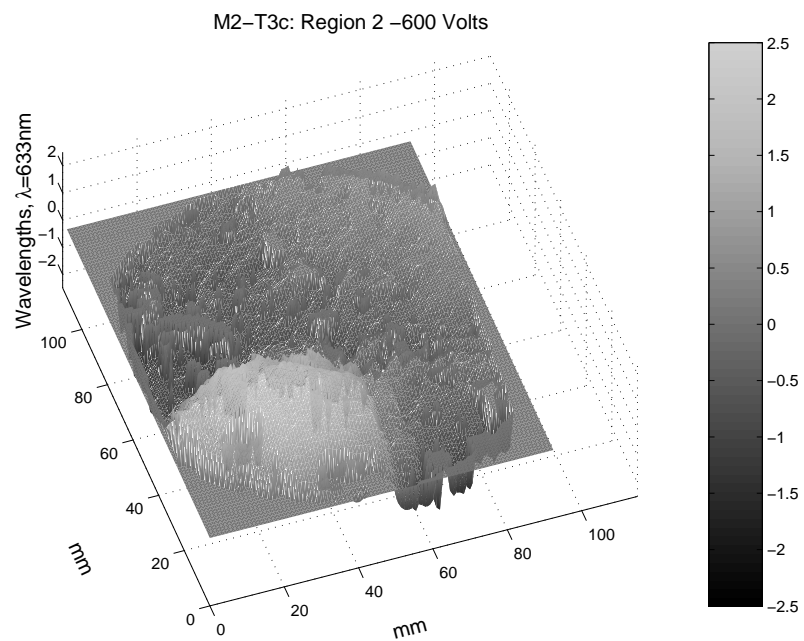
Figure 4.67   M2 Region 2 actuated with -600V (3.65λ PV, 0.81λ RMS).
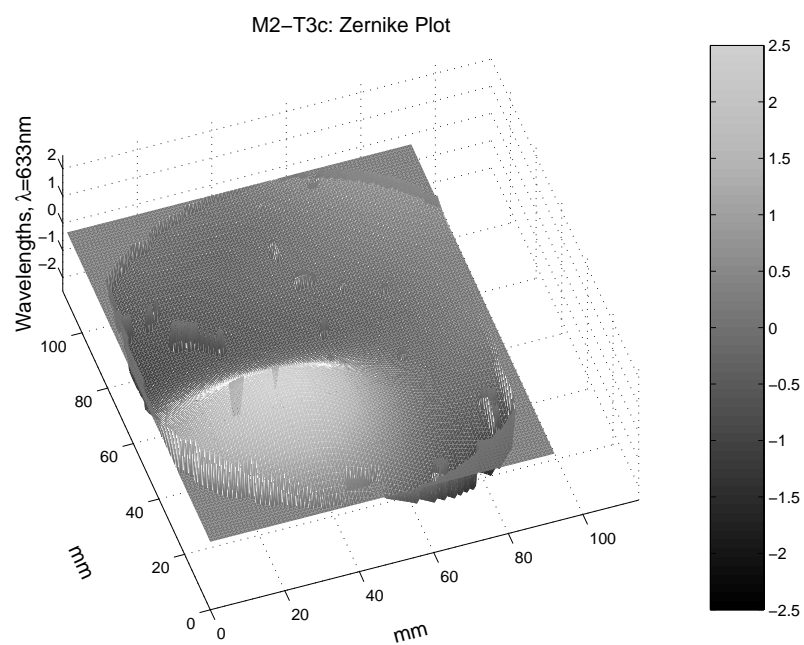
Figure 4.68   M2 Region 2 actuated with -600V (Zernike).
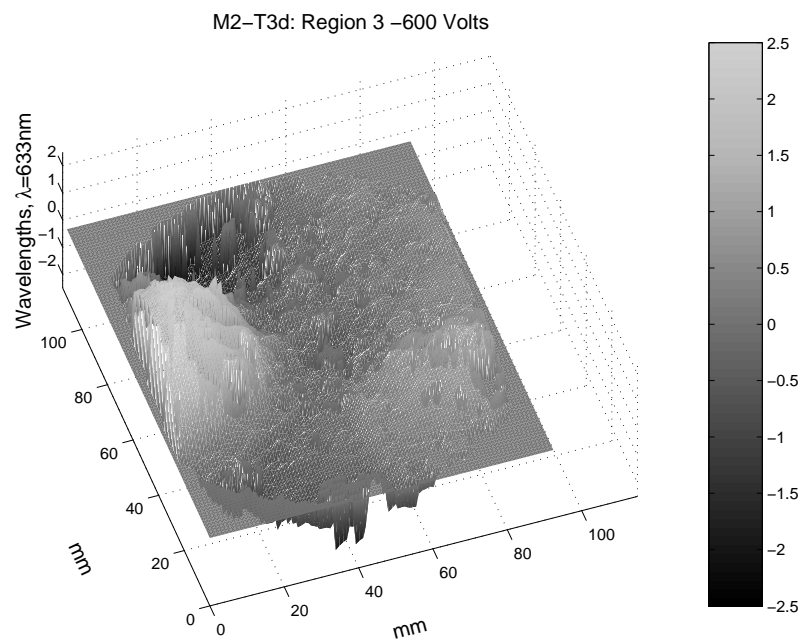
Figure 4.69   M2 Region 3 actuated with -600V (4.80λ PV, 0.91λ RMS).
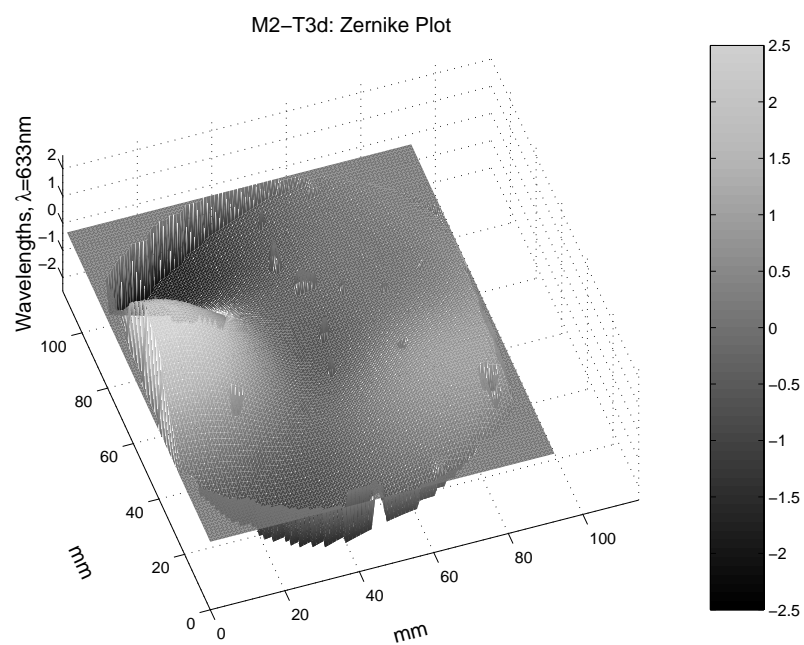
Figure 4.70   M2 Region 3 actuated with -600V (Zernike).

4-44
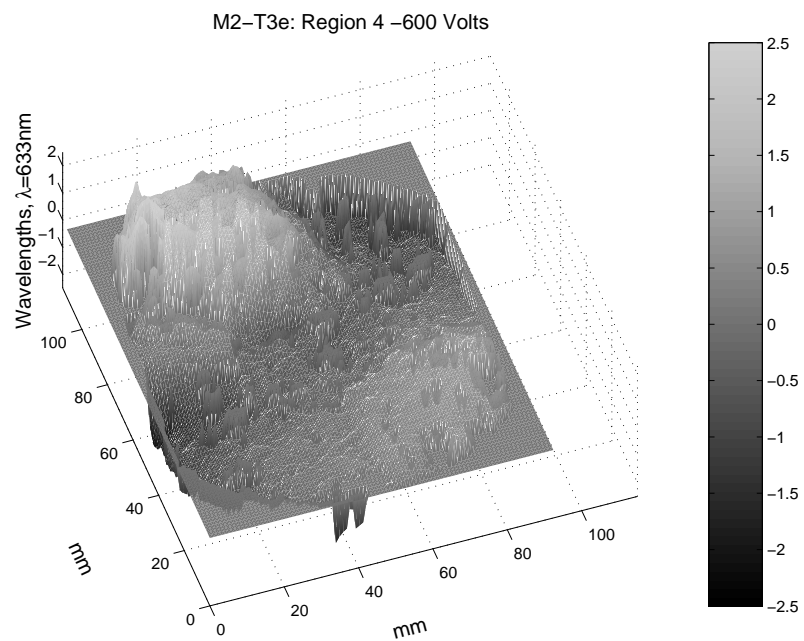
Figure 4.71   M2 Region 4 actuated with -600V (5.38λ PV, 0.90λ RMS).
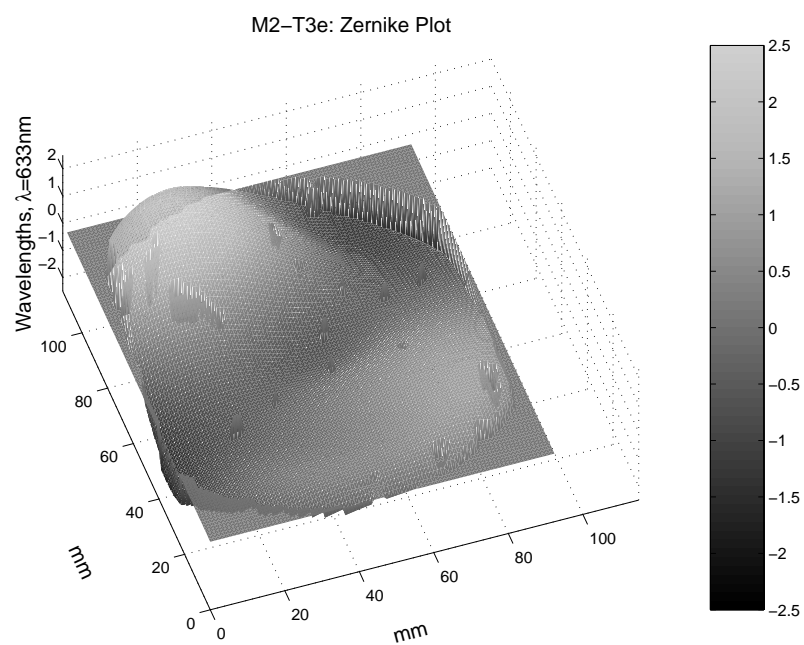
Figure 4.72   M2 Region 4 actuated with -600V (Zernike).
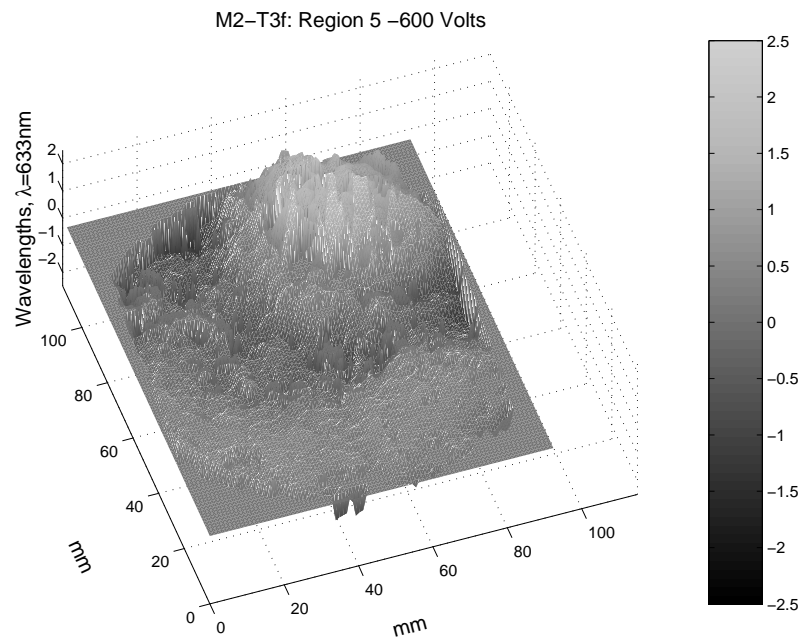
Figure 4.73   M2 Region 5 actuated with -600V (3.45λ PV, 0.61λ RMS).
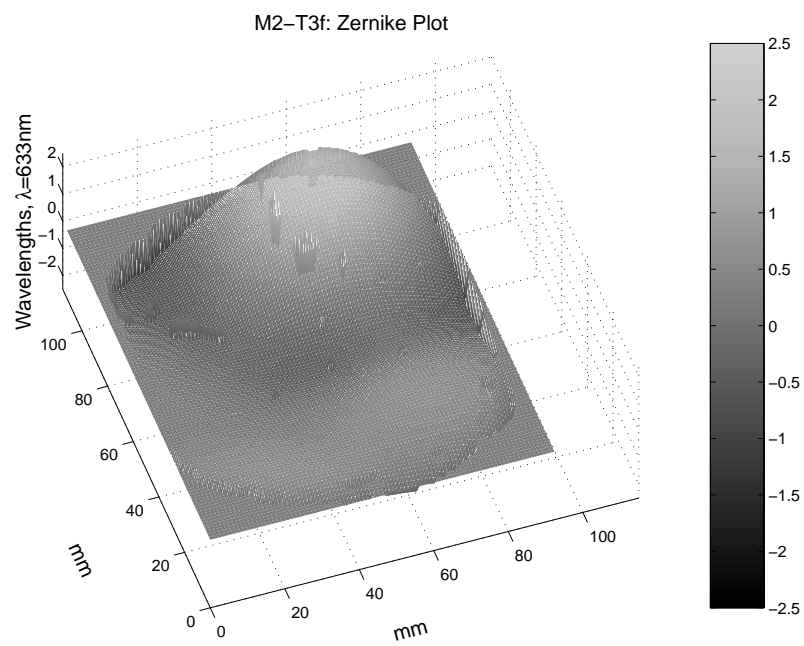
Figure 4.74   M2 Region 5 actuated with -600V (Zernike).
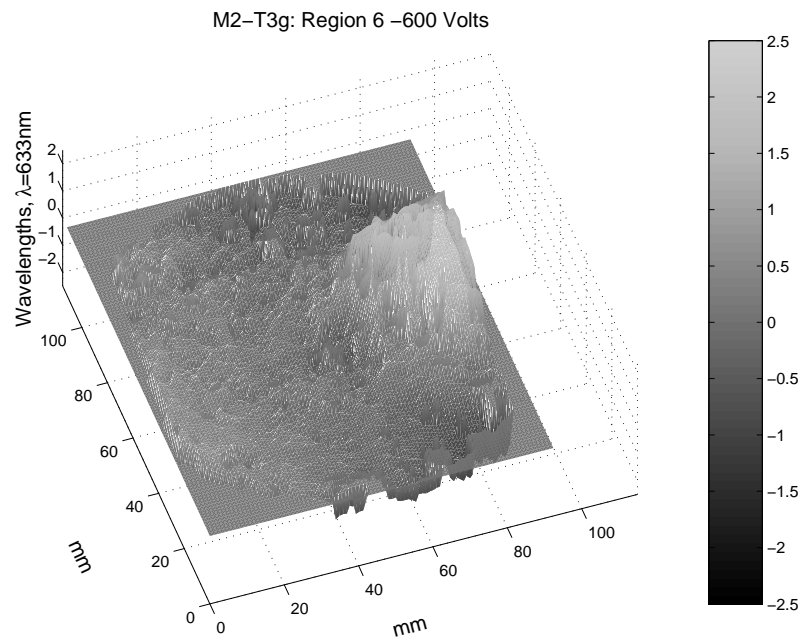
Figure 4.75   M2 Region 6 actuated with -600V (3.52λ PV, 0.63λ RMS).
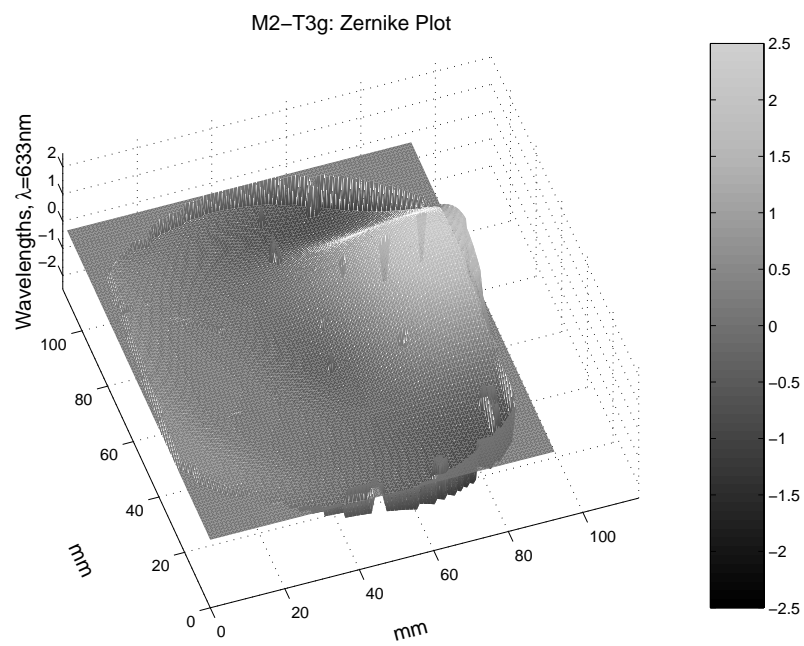
Figure 4.76   M2 Region 6 actuated with -600V (Zernike).

4-47
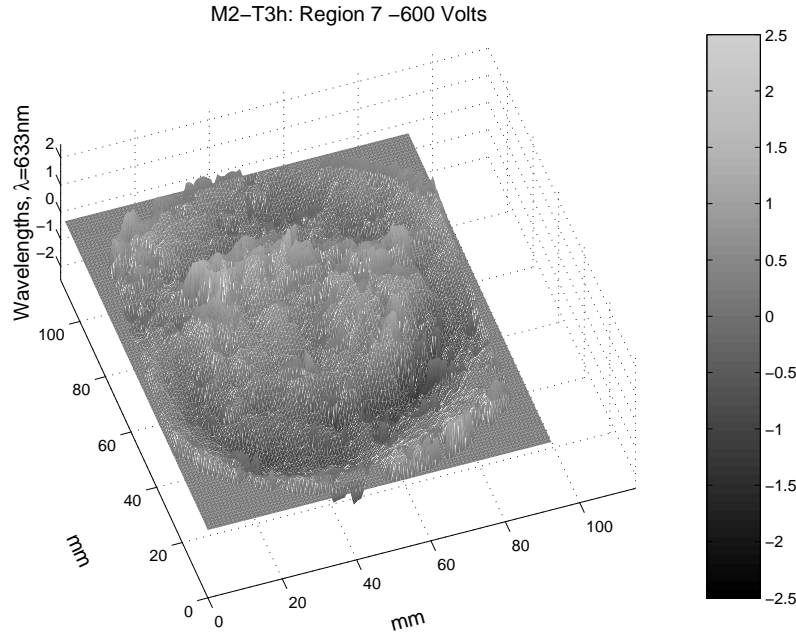
Figure 4.77   M2 Region 7 actuated with -600V (3.06λ PV, 0.50λ RMS).

4.45 and 4.46. The surface deflection is similar, although the earlier test resulted in a slightly higher (3.40λ PV versus 3.06λ PV) and narrower deformation pattern.

A final test of mirror M2 consisted of connecting the leads for regions 1,3, and 5 to the power supply and applying -600V to the three regions simultaneously. The remaining leads were connected to ground. Figures 4.79 and 4.80 show the surface deflection of these three regions. The mirror surface was deformed only in the actuated regions, indicating that any combination of actuators could be used to effect desired changes in the mirror surface. An analysis of the Zernike coefficients for this test revealed that the primary polynomials represented were numbers 10 and negative 19 (see Appendix C for Zernike polynomial definitions and plots), indicating that higher-order surface control was achieved using this control pattern. Actuating the outer regions simultaneously could provide low-order global curvature control similar to that achieved with the M1 control pattern.

The tests conducted on mirror M2 proved that isolated regions of the mirror could be controlled by actuating specific regions of the PVDF control layer. The

M2−T3h: Zernike Plot
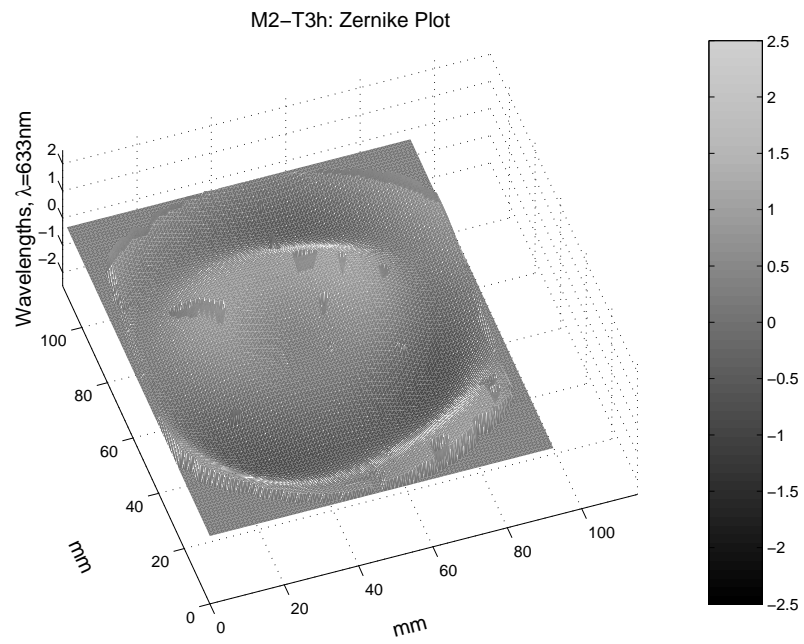
Figure 4.78   M2 Region 7 actuated with -600V (Zernike).

M2−T3j: Regions 1,3,5 −600 Volts
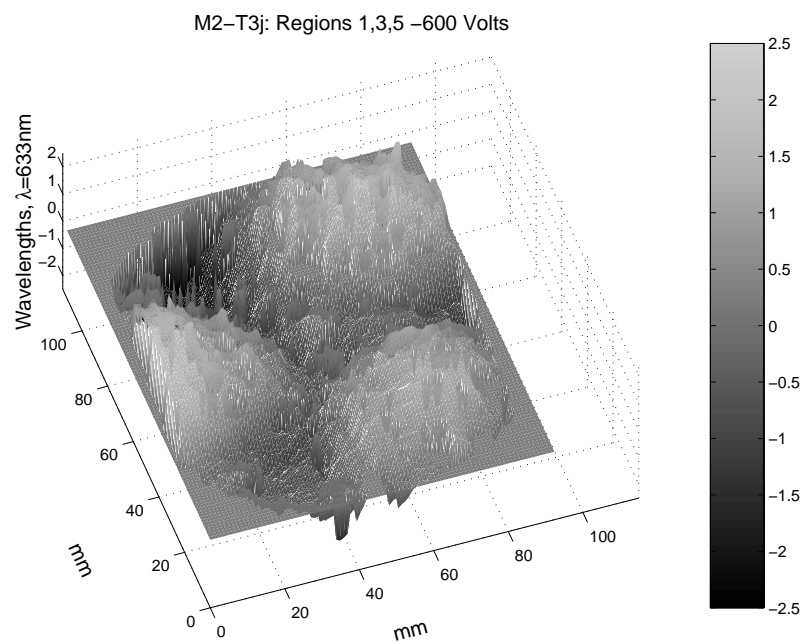
Figure 4.79   M2 Regions 1, 3, and 5 actuated with -600V (4.43λ PV, 0.99λ RMS).
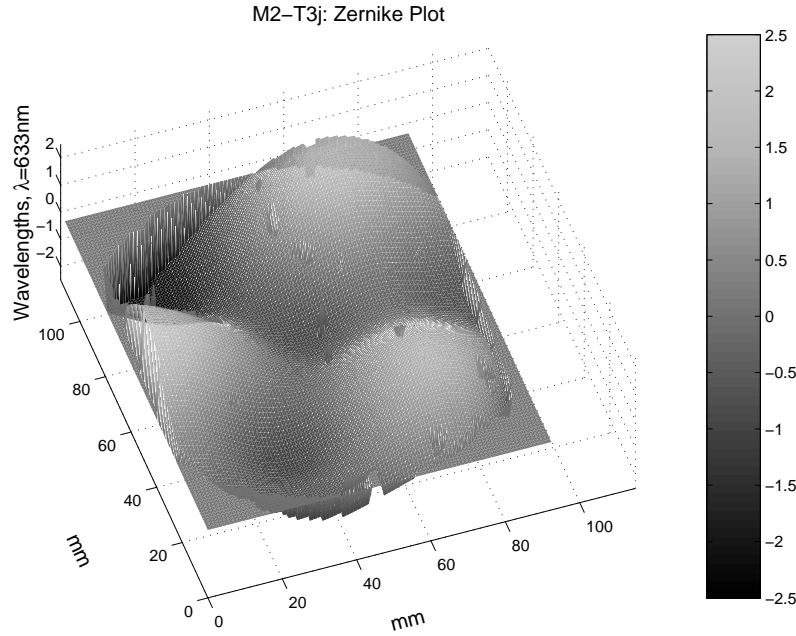
Figure 4.80   M2 Regions 1, 3, and 5 actuated with -600V (Zernike).

magnitude of the controlled displacements, as high as 5.38λ PV, were greater than the absolute surface roughness of 3.95λ PV. This indicates that membrane mirror surface figure can be corrected and controlled using a layer of PVDF with an etched control pattern. Combined with the results from the tests on M1, these experiments offer proof that membrane optics are viable in the near future. Large aperture remote sensing satellites could utilize these membranes for the primary optics, taking advantage of their very low areal density ($<2\mathrm{kg/m}^2$ for the prototype) to save weight. The flexible nature of the membranes could allow them to be rolled or folded for deployment, enabling the use of existing launch vehicles. After deployment, low- and high-order control of the membrane surface can be achieved using systems similar to those developed during this research.

4.4   Stiff Mirror S1

The first stiff mirror, S1, was originally constructed to develop manufacturing techniques for future piezo-controlled test mirrors. Upon mirror completion, however, tests were conducted to determine the level of control achieved using the speaker-type
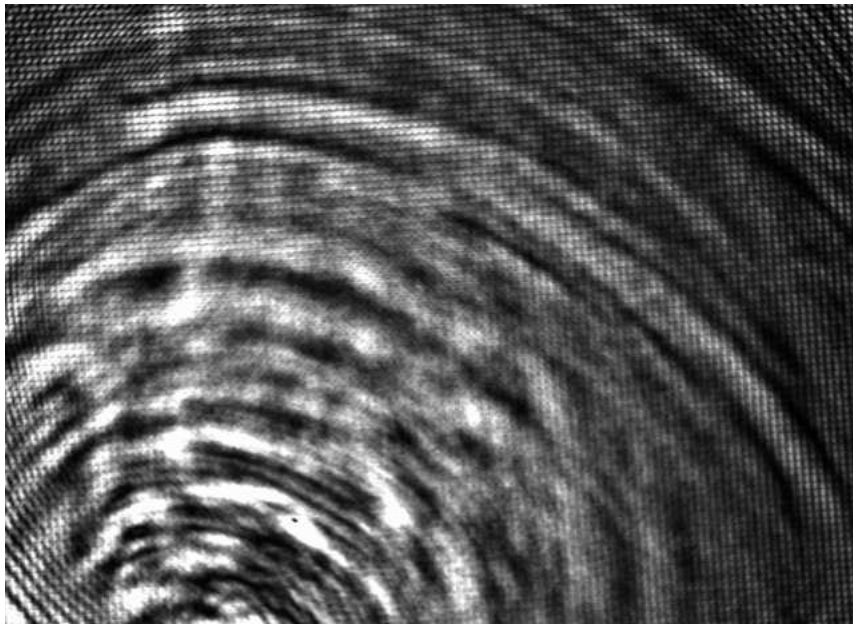
Figure 4.81   S1 surface reflection. Note ripples due to polymer flow.

piezo element. Initial surface flatness tests were conducted on S1 using a 1" test beam
and the 133μm MLM. The first measurement was taken after two layers of RTV615
were applied, but prior to any reflective coating. The surface flatness was measured
to be 1.45λ PV (0.30λ RMS).

After a gold reflective coating was applied, the surface reflection showed rippling
where the polymer was poured into the mirror form. The surface was then measured
to be 0.92λ PV (0.14λ RMS). The difference in surface flatness is likely due to a
slightly different test spot location. The test setup was changed to allow a 2" section
of the mirror to be tested by expanding the 1" test beam with a pair of lenses. Figure
4.81 shows the surface reflection of S1 as recorded by the WaveScope® using this
setup. Note the presence of the MLM grid (133μm for each lenslet) near the edges of
the image.

4.4.1   S1 Test 3.   Test 3 was conducted using a 2" test beam with the
480μm MLM. The test beam return slightly overfilled the WaveScope® aperture,

4-51
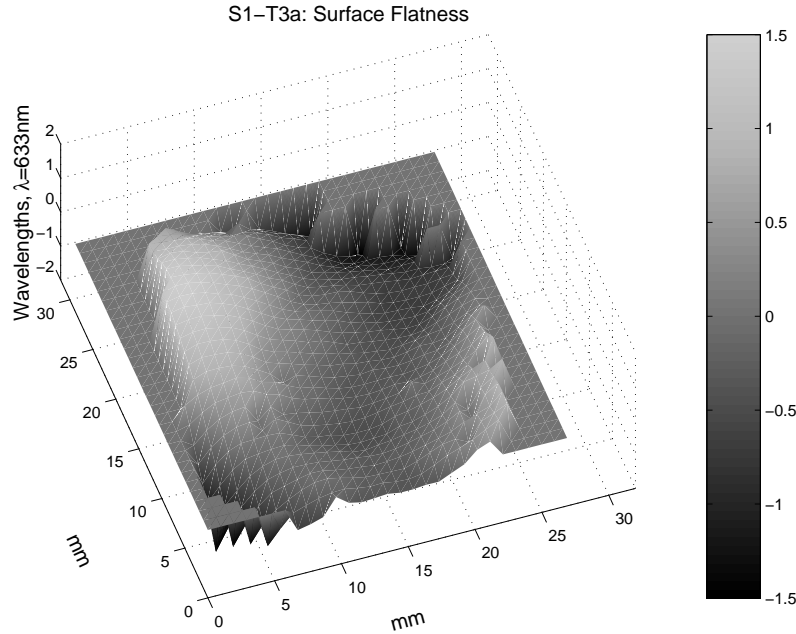
Figure 4.82   Surface Flatness of mirror S1 (3.42λ PV, 0.63λ RMS).

resulting in a 3cm by 2.5cm test region being recorded. The surface flatness of the test region was recorded to be 3.42λ PV (0.63λ RMS), as shown in Figure 4.82.

Note the "high spots" on the mirror surface. Based on the location of the spots and the polymer flow pattern, the lower of the two spots (on the lower right) was caused by the initial pouring of the polymer (the surface plot is rotate 90° counterclockwise from Figure 4.81). The mirror was then tipped to ensure the polymer flowed to the opposite side of the mirror. The higher spot, in the upper left, was created when the mirror was tipped. These surface problems are caused primarily due to the viscosity and handling time of this polymer. Mirror S1 was the second mirror poured using the same batch of resin and may have begun to thicken due to the time elapsed since mixing.

Mirror S1 was tested using the self-referenced 0V state shown in Figure 4.83. Voltage was applied to the piezo, causing it to bend into a bowl shape. Figures 4.84 and 4.85 show the surface deflection at +16V and -16V, respectively. Figures 4.86 and 4.87 show the surface deflection at +30V and -30V, respectively. Note that the
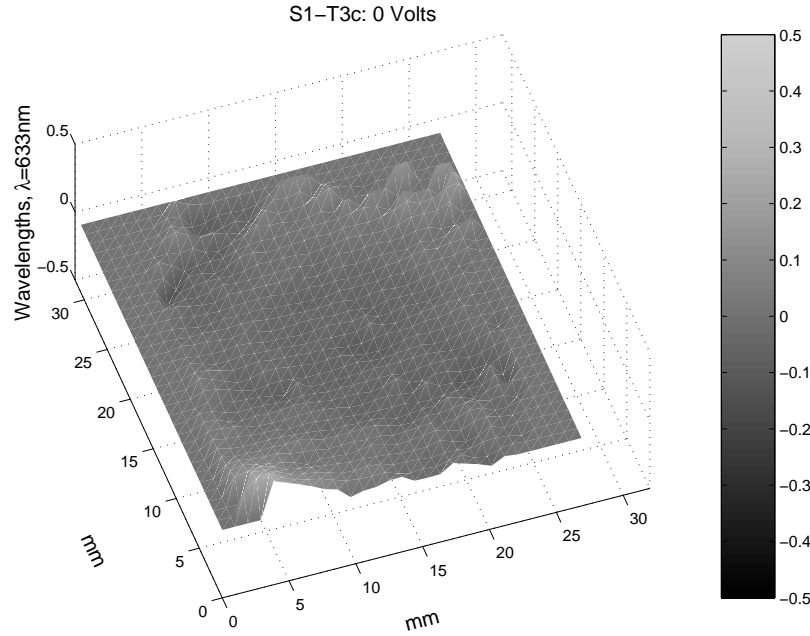
Figure 4.83   S1 self-referenced surface flatness (0.38λ PV, 0.05λ RMS).

response to negative voltage is less noticeable than the response to positive voltage. Maximum deflection of the surface was recorded at over one wavelength with +30V applied to the piezo.

4.4.2   S1 Test 4.   To increase fidelity of the surface flatness measurements, the 480μm MLM was replaced with the 133μm MLM for Test 4. The surface flatness, referenced to a λ/20 flat mirror, was recorded to be 3.65λ PV (0.60λ RMS), as shown in Figure 4.88. The surface shape was the same as that measured in Test 3, but the affect of the ripples was more apparent with the higher fidelity MLM. The ripples were not very large relative to the surface flatness, but they caused a large gradient in the reflectivity. The resulting brightness variation prevented the WaveScope® from recording data at both the rippled and non-rippled regions.

The WaveScope® was re-calibrated, and the self-referenced 0V surface flatness was measured to be 1.45λ PV (0.19 λ RMS). Upon analyzing test results, a slight astigmatism was noticed in the 0V reference test (see Figure 4.89) . Consequently, the surface deflection caused by the piezo actuator in Test 4 is difficult to delineate from
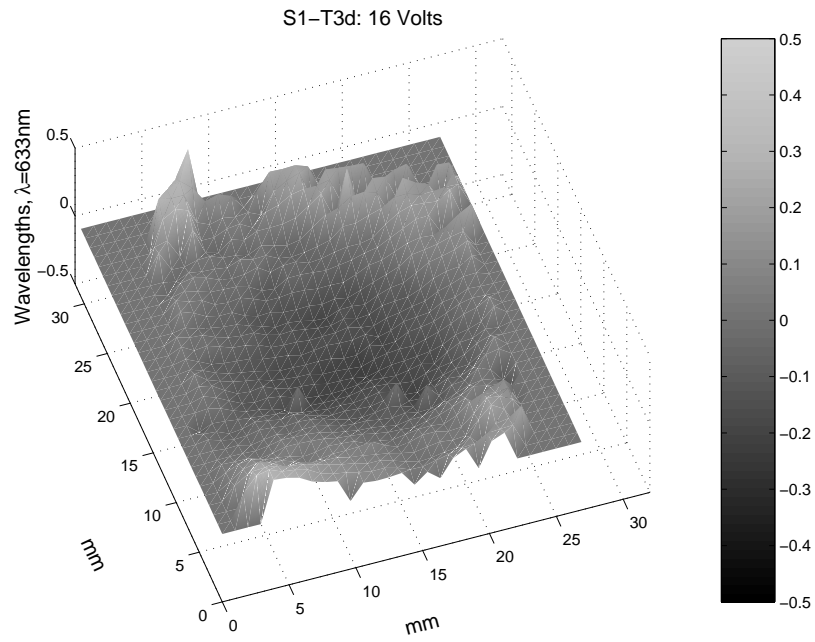
Figure 4.84   S1 actuated with 16V (0.74λ PV, 0.12λ RMS).
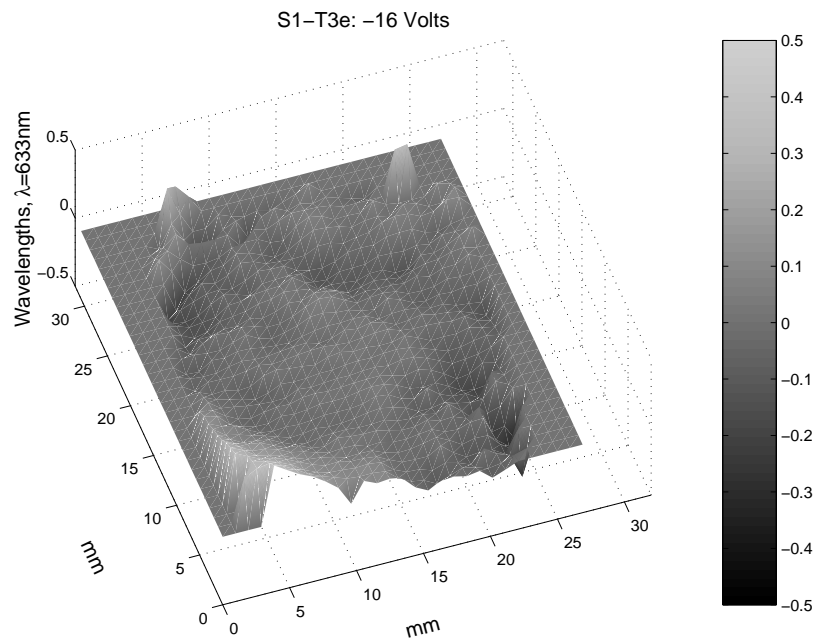
Figure 4.85   S1 actuated with -16V (0.74λ PV, 0.09λ RMS).
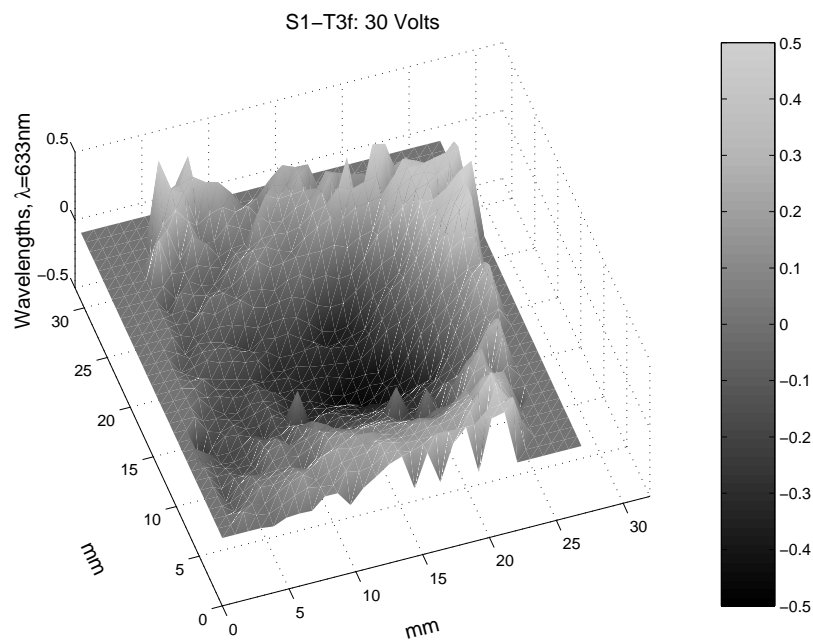
Figure 4.86   S1 actuated with 30V (1.09λ PV, 0.22λ RMS).
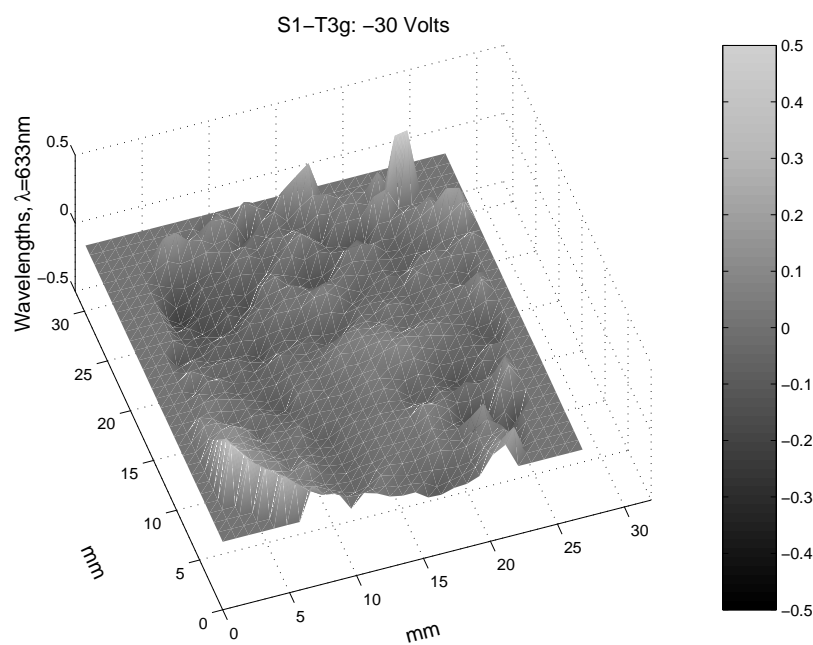
Figure 4.87   S1 actuated with -30V (0.70λ PV, 0.08λ RMS).
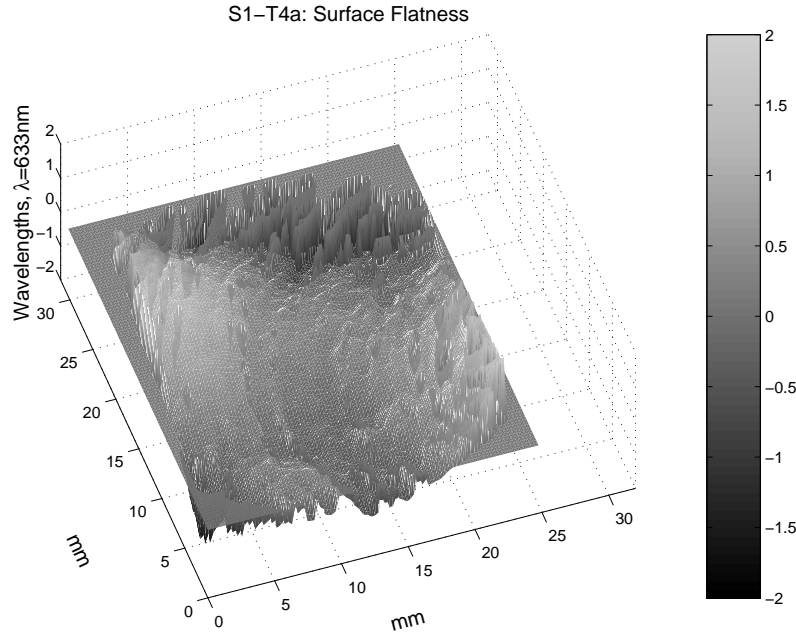
Figure 4.88   S1 surface flatness (3.65λ PV, 0.60λ RMS).

the astigmatism. The source of the observed astigmatism was undetermined. Figures 4.90 and 4.91 show the surface flatness measured at +30V and -30V, respectively.

To help discern the actual surface deflection, the 0V data was subtracted from the +30V and -30V test data. The results show the piezo actuator region more clearly than the recorded data. Figures 4.92 and 4.93 show the maximum downward at +30V and maximum upward deflection at -30V, respectively. Figures 4.94 and 4.95 show the Zernike polynomial plots for easier comparison of the actuated surface shapes.

Although the surface flatness was not ideal (due to uneven pouring of the top polymer layer), the actuation of the piezo element produced visible surface deformation. Although the deformation clearly increased as applied voltage increased, the magnitude of the positive voltage actuation was greater than the negative voltage actuation. This may be caused by the bi-material properties of the brass/ceramic piezo element or by mechanical interaction of the piezo with the stiff substrate.
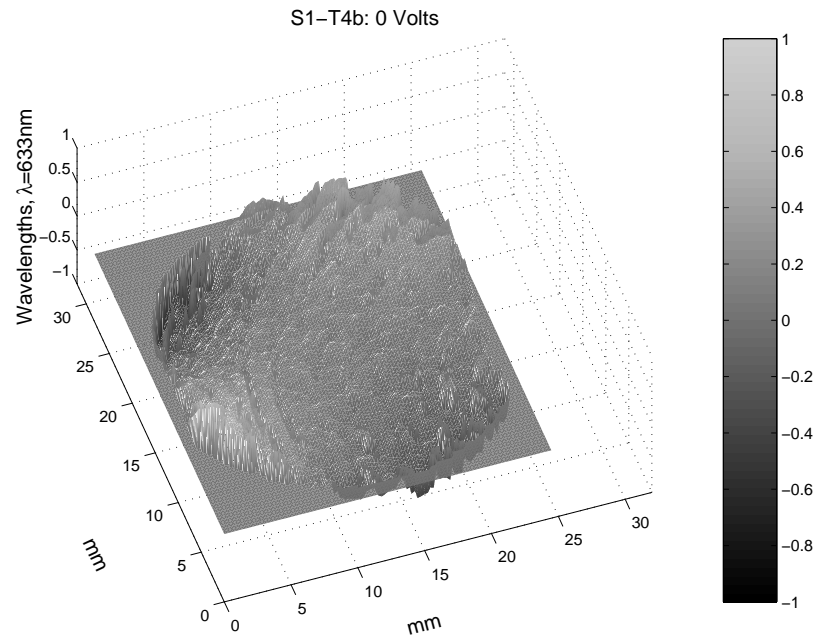
Figure 4.89   S1 self-referenced surface flatness (1.45λ PV, 0.19λ RMS).
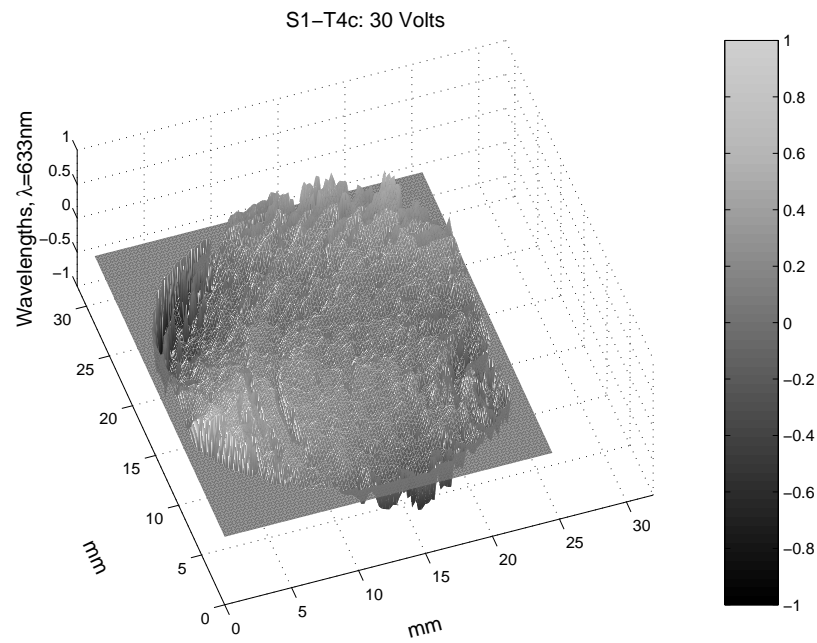
Figure 4.90   S1 actuated with 30V (1.48λ PV, 0.19λ RMS).
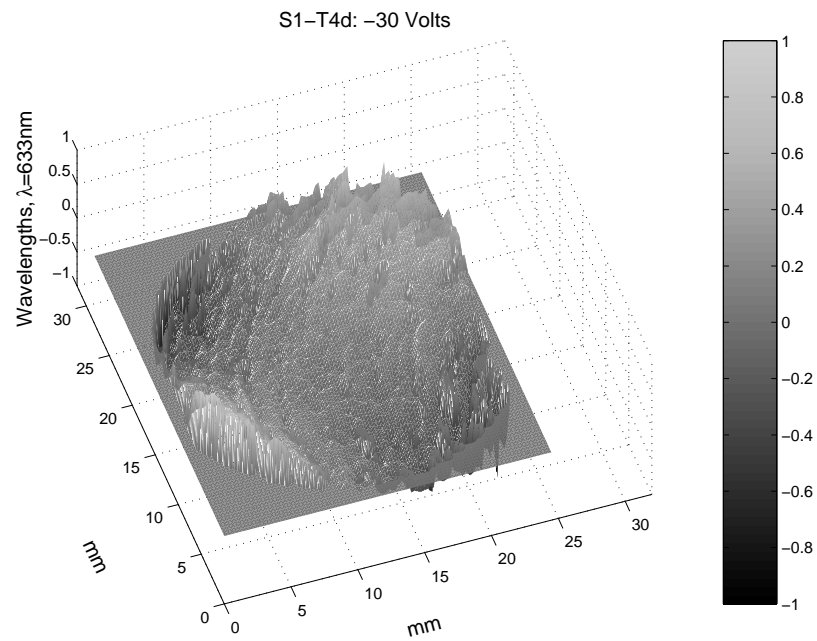
Figure 4.91   S1 actuated with -30V (1.78λ PV, 0.25λ RMS).
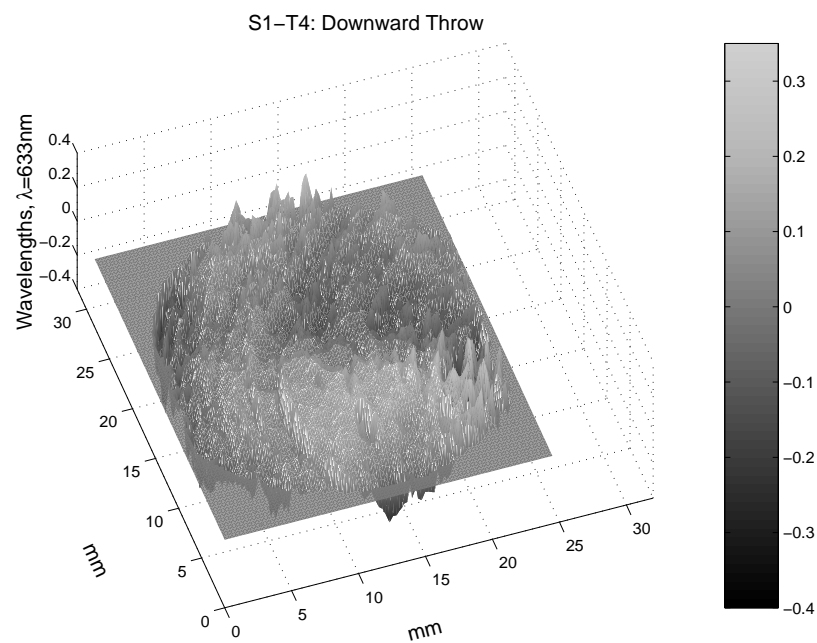
Figure 4.92   Maximum downward deflection of S1 (0.70λ PV).
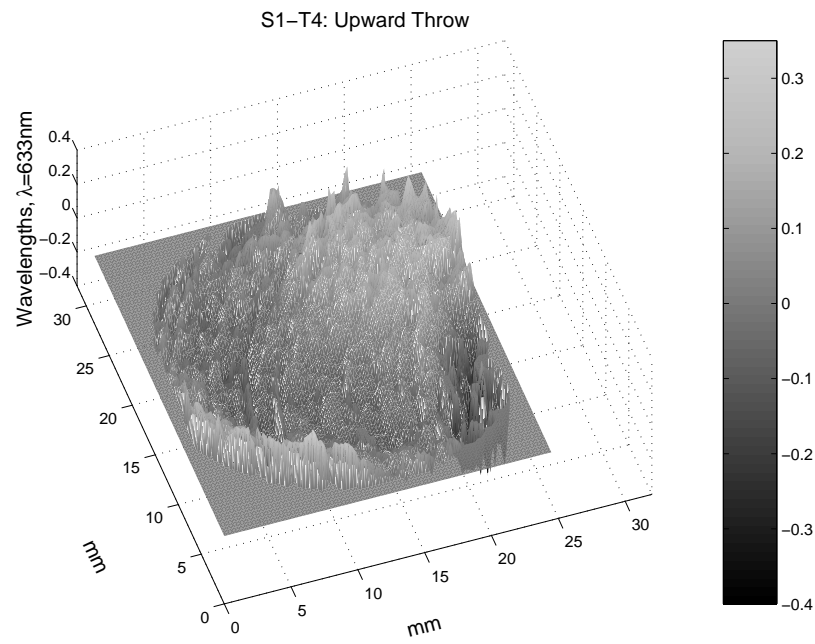
Figure 4.93   Maximum upward deflection of S1 (0.74λ PV).
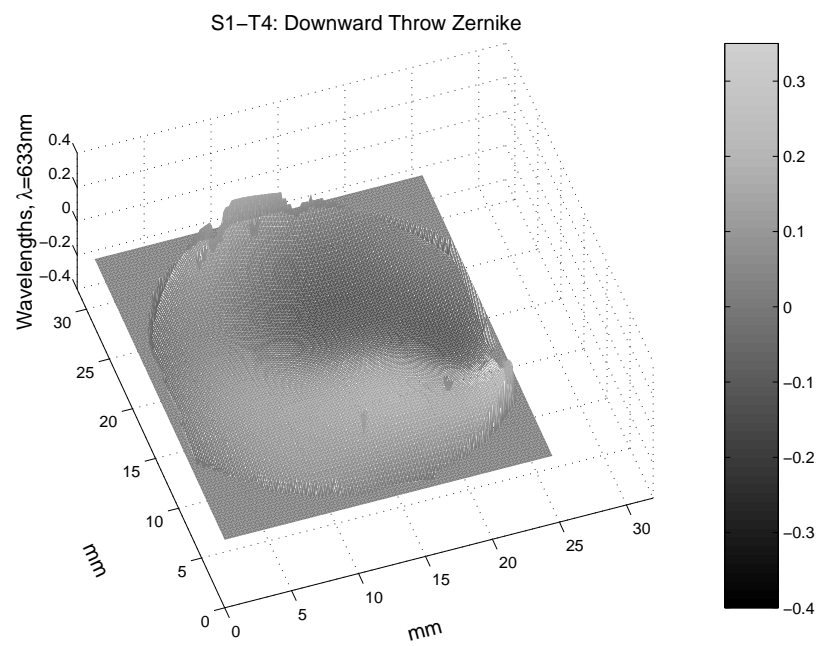
Figure 4.94   Maximum downward deflection of S1 (Zernike).
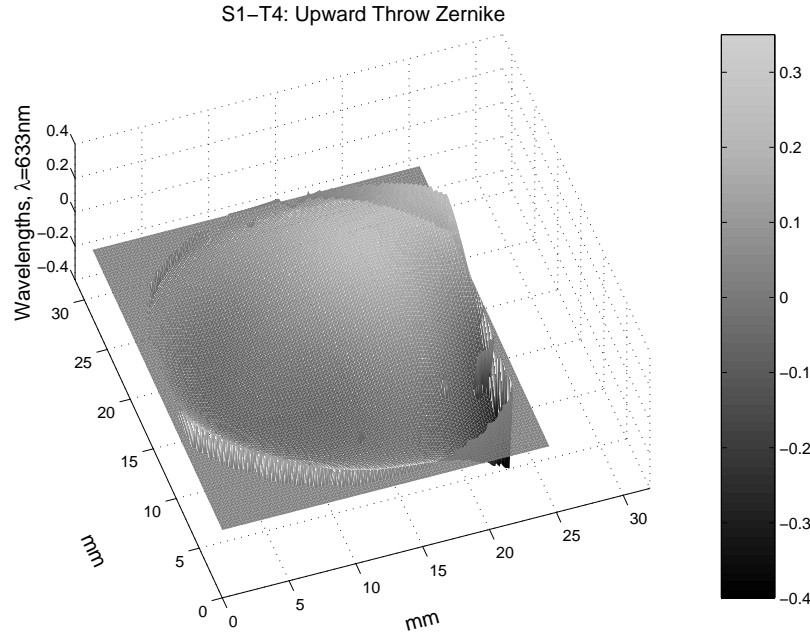
Figure 4.95   Maximum upward deflection of S1 (Zernike).

4.5   Stiff Mirror S2

The great tragedy of Science: the slaying of a beautiful hypothesis by an ugly fact. Thomas Huxley (1825-1895)

Mirror S2 was constructed to test the use of piezoceramic actuators mounted to a stiff substrate for controlling polymer optical surfaces. An actuator thickness of 3mm was chosen based on sensor availability. After the actuators were mounted to the copper substrate, several layers of RTV656 were applied to create a flat optical surface. After several polymer layers, the surface appeared flat to the naked eye. Placing the mirror in the test setup revealed that flaws still remained in the surface. The surface reflection showed a bright ring between the the disk and washer actuators, indicating a depression at that location (see Figure 4.96). A ring was also visible outside the washer actuator.

Possible explanations for the surface flaws included temperature changes between the manufacturing and testing labs, and resin curing problems. To attempt to alleviate temperature problems, a final layer of RTV656 was applied in the test

4-60
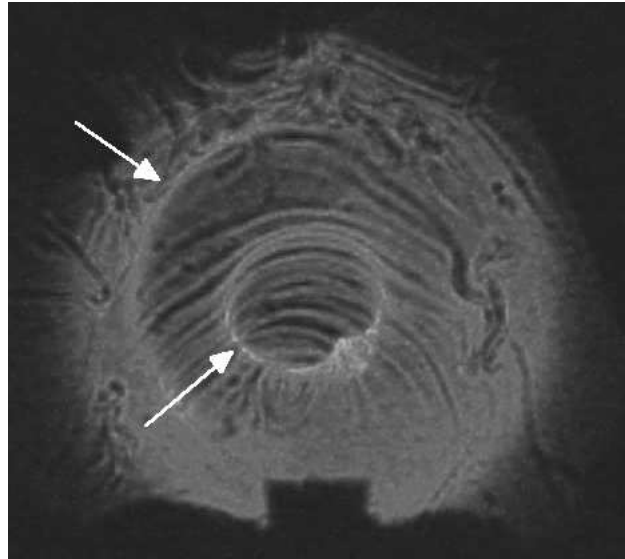
Figure 4.96   Reflection from S2. Note circular flaws.

lab. The resin cured after 24 hours and appeared to have a flat surface. However, upon placing the mirror in the test setup, the circular flaw between the actuators was still evident. An attempt to test the mirror using the WaveScope® showed that the flaw was too large to produce valuable results. Voltage was applied to the piezos to determine if the flaw was correctable using the built-in actuators. The diameter of the circular flaw reflection changed size slightly as the voltage applied to the interior washer was increased, and some changes in the overall reflection were visible when voltage was applied to the interior disk. No changes were apparent when voltage was applied to the rear actuators.

Because mirror S2 was un-coated during the WaveScope® tests, the reflection was too dim to attempt interferometry. A gold vapor deposit coating was applied to the mirror to enhance reflectivity. Upon removal of the mirror from the vacuum chamber, the circular flaw was easily visible to the naked eye. The magnitude of the flaw decreased over time, until it was barely visible a few hours later. The mirror was placed in the test setup and a Twyman-Green interferometry setup was constructed using the available optics equipment [17]. Although the reflection was enhanced by the gold coating, the mirror exhibited an overall curvature that prevented collimation

4-61
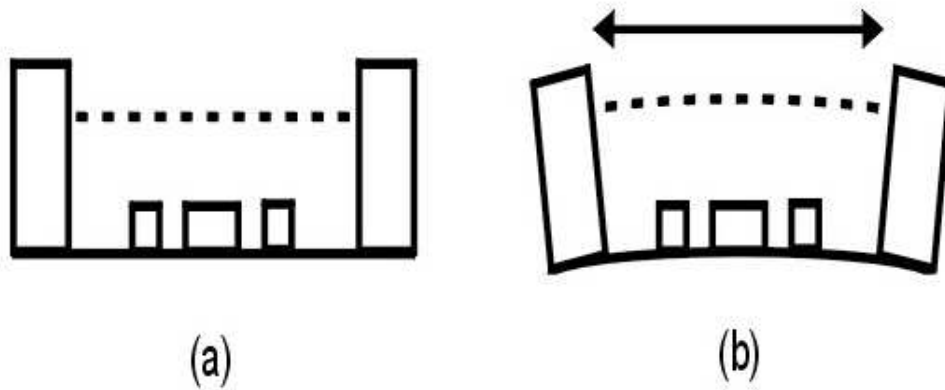
Figure 4.97   Bending in S2 caused by temperature: (a) Neutral temperature; (b) Mounting ring expanded.

of the test reflection. As a result, the beam reflected from the mirror expanded as it returned from the test section, making interferometric testing impossible.

The relative failure of mirror S2 emphasizes the importance of considering material properties when constructing composite mirrors. In this case, the polymer had a relatively high coefficient of thermal expansion (CTE) compared to the ceramic. This and possible resin curing problems may have resulted in the surface flaws on S2. In addition, the aluminum ring had a different CTE than the copper-clad fiberglass plate. Thus, temperature changes may have also resulted in bending of the mirror substrate, giving the mirror a global curvature that prevented testing. Figure 4.97 shows a cross-section of mirror S2. Figure 4.97a shows the system at a neutral temperature. Because of the CTE difference between the ring and the copper plate, temperature changes may cause bending to occur as shown in Figure 4.97b. To alleviate these problems with future piezoceramic-actuated polymer mirrors, thinner actuators (< 1mm) should be used to minimize CTE mismatch problems. In addition, a highly flexible material, such as paper or thin plastic, should be used to retain the resin instead of a solid aluminum ring.

4.6 Summary

Two PVDF-actuated membrane mirrors and two piezo-actuated stiff mirrors were constructed as described in Chapter Three. The mirrors were tested using an AOA WaveScope® Shack-Hartmann sensor. Surface measurements were recorded for each mirror, in both actuated and neutral states.

The membrane mirrors showed excellent results, proving that both zonal and global control of membrane surfaces is possible using the techniques developed during this research. The displacement achieved was localized to the specific regions actuated and had a magnitude great enough to correct local surface flaws and global figure error.

The first stiff mirror tested showed that some surface control is possible using piezoceramic actuators. Because the actuator was very thin compared to the mirror thickness, the magnitude of the displacement achieved was limited to about one wavelength. The mirror deformation was, however, localized to the actuator region, suggesting that greater surface control is possible using these actuators. Mirror S2 utilized thicker ceramic actuators, which provided much more displacement than the piezo element used in S1. However, the actuator thickness, coupled with CTE mismatch issues, created large flaws on the mirror surface. Although these flaws prevented surface flatness measurements, localized movement of the mirror surface was observed in the test reflection when the actuators were energized. The results suggest that future mirrors using thinner actuators could validate the ceramic/polymer combination for lightweight controllable optical surfaces. These systems offer an advantage over similar, glass-based active mirrors in that polishing time is eliminated. Such systems could be used as active secondary mirrors in large telescopes or for beam control in airborne or space-based laser applications.

V. Conclusions and Recommendations

Science is facts; just as houses are made of stones, so is science made of facts; but a pile of stones is not a house and a collection of facts is not necessarily science.

Henri Poincare (1854-1912)

5.1 Conclusions

The objective of this research was to design, construct, and test mirrors using smart structures technology to determine the viability of using imbedded actuators for the control of polymer optical surfaces. Two PVDF-controlled membrane mirrors and two piezoceramic-controlled mirrors with stiff copper-clad board substrates were constructed. Two different polymers, GE Silicones® RTV615 and RTV656, were used for the optical surfaces of the mirrors. Different control patterns were designed for each mirror to determine the effect of control layer shape on the optical surface deformation. All mirrors exhibited local deformation closely correlated to the control layer pattern, proving that mirror surface control is possible using these polymer-based imbedded actuator systems.

Membrane mirrors M1 and M2 produced excellent results, proving that local and global control of PVDF-based optical membranes is possible. Mirror M1, which had a surface flatness of 6.6λ PV (1.6λ RMS) and an areal density of 3.55kg/m^2, showed a controlled surface deflection of 5.37λ PV in the inner region and 13.6λ PV in the outer region at a control voltage of 300V. The surface deflection of M1 was greater at higher voltages (18.6λ PV at maximum), but the shape was uncontrolled due to charge leakage from faulty electrodes. The observed surface deformation proved that global curvature control is possible using this technique.

Mirror M2 had the lowest areal density, at less than 2kg/m^2, and showed dramatic results in local mirror surface control. The overall surface flatness of the mirror was 3.9λ PV (0.63λ RMS). Highly localized surface deformation was observed in

the actuated regions ranging from 3.1λ PV to 5.4λ PV at -600V. The complex etch pattern allowed desired regions of the mirror surface to be deformed independently, proving that the PVDF membrane can also be used to provide high-order mirror surface control. In both mirrors, surface control was on the same order of magnitude as the mirror surface flatness, suggesting that mirror flaws could be corrected using these systems.

The stiff piezo-controlled mirrors also exhibited some surface deformation. Mirror S1, which had a flatness of 3.6λ PV (0.6λ RMS), showed measurable surface control using a simple piezo speaker element. The maximum surface deflection observed was 1.1λ PV at 30V. Mirror S2 was constructed to test thicker piezoceramic actuators, which should produce greater surface deflection and thus provide more control. Unfortunately, problems with the mirror design (most notably CTE mismatch between materials) prevented achieving a surface flat enough to test using either interferometry or Shack-Hartmann sensing. Changes to voltage applied to the actuators did, however, produce observable changes in the surface reflection. Thus, surface deformation was also achieved using the piezo-actuated polymer mirrors.

The results gathered from these experiments prove the viability of polymer-based adaptive mirrors. These mirrors could be integrated with a wavefront sensor in a closed-loop system, allowing active control of the mirror surfaces. The low- and high-order control achieved with the very lightweight membrane mirrors suggests that large-aperture membrane-based remote sensing satellites are feasible in the near future.

5.2   Lessons Learned

The initial problems encountered during this research were a result of polymer material properties. RTV615 and RTV656 were chosen for the optical surfaces because they exhibit low cure shrinkage and cure with a fairly flat optical surface [14]. Due to their high viscosity, however, bubbles became easily entrapped in the polymer. Experimentation revealed that placing the polymers in a vacuum chamber to remove

the bubbles sometimes prevented them from curing properly. Thus, bubbles induced during mixing were removed using a centrifuge, and bubbles that remained after the mirror was poured were removed using a dental pick or disposable eyedropper.

Another important breakthrough occurred in the PVDF membrane etching procedures. Although the process would be tedious for complex etch patterns and inefficient for mass production, etching the control patterns by hand was far superior to previously attempted methods [17]. Applying the etchant with a cotton swab allowed complete removal of the electrode coating where necessary, without impacting the overall conductivity of the PVDF membrane. Thus, control regions were easily isolated using this technique. For larger scale or mass-produced membranes, a screen printing process can be used to create the electrodes, ensuring precision and repeatability.

Problems encountered with mirror S2 emphasized the importance of thermal stability in optical systems. While polymer layering has been proven to mitigate mirror substrate flaws [14], very large surface features (relative to the wavelength) may be an issue if the polymer and the substrate have a different CTE. In the case of S2, temperature changes may have resulted in the observed local deformation near the actuators. In addition, CTE differences between the aluminum mounting ring and the copper-clad fiberglass substrate likely caused bending to occur, resulting in global curvature.

5.3 Recommendations for Further Study

Several key areas of further study were identified during this research effort. The greatest challenge to designing and manufacturing controllable polymer optical systems lies in proper material selection. Polymers with low viscosity, low cure shrinkage, low CTE, and a smooth surface cure must be developed to improve mirror construction. Commercially available or specially engineered polymers that meet these requirements will enable production of larger optical surfaces with fewer flaws.

The composite mirror systems themselves must also be designed to minimize the effects of temperature and humidity variation.

In addition to material selection, mirror systems with real-time surface figure feedback offer significant potential for future research. Connecting the WaveScope® to the control layer in a feedback loop would establish the viability of membrane optics for use in an active system. This would also enable testing of the membrane mirrors in a dynamic environment, which would be required for future production systems.

Combining the benefits of inexpensive polymer surfaces with the strength and stability of stiffer substrates opens yet another area for further research. Proper design of such a bi-material system could enable more intelligent mirrors, with surface control circuitry etched onto silicon wafers, which are then coated with a polymer optical layer. These systems would offer the benefit of controllability without the cost and effort associated with polishing the surface to optical tolerances.

5.4 Summary

This research has shown that polymer-based optics with imbedded actuators offer the possibility of reduced-weight, highly controllable mirrors. The development of large-aperture, deployable membrane optical systems is dependent on the ability to control the membrane surface. Experiments performed during this research proved that membrane surfaces can be controlled to the tight tolerances required by optical systems through the use of piezoelectric polymer layers. In addition, lessons learned in production of active polymer mirrors with stiff substrates may lead to the development of low-cost, lightweight replacements for large-aperture adaptive mirrors.

Appendix A. Lab Notes

These lab notes were recorded journal-style throughout the experimentation process. Toward the end, journal writing was postponed in lieu of thesis writing, and later entries were simply included in Chapter Three rather than in the journal. As a result, the lab notes were re-ordered by topic rather than the original chronological order. Comments in italics were added after all experiments were complete.

A.1 Membrane Mounting

Before attempting to etch the PVDF, I thought it would be a good idea to mount a "blank" PVDF membrane to get familiar with the process. This mirror will also be used to test polymer adhesion. Here are the steps I followed:

1. Cut a square piece of PVDF from the roll (as wide as the roll).

2. Place the aluminum stretching ring, o-ring side up, on the table.

3. Place the square of PVDF centered on top of the o-ring.

4. Set the 0.5" thick aluminum ring on top of the PVDF membrane.

5. Pull the membrane tight around the edge of the stretching ring.

6. Set the four clamps "upside down" with the plastic piece flat on the table.

7. Open the clamps one at a time and put the stretching assembly in the clamps.

8. Tighten the clamps slightly until the PVDF membrane begins to stretch.

9. Pull any remaining wrinkles out of the membrane and then tighten the clamps a little at a time, going around in a circle.

10. Apply epoxy (work fast if it's the 5-minute kind) to the inner groove of the 6" diameter mounting ring.

11. Invert the ring and place it centered on the stretched PVDF membrane.

12. Place the 0.5" thick aluminum disc on top of the mounting ring as a weight to increase the tension until the epoxy is set (overnight).

   Note: This mounted membrane was later etched and it became M1.
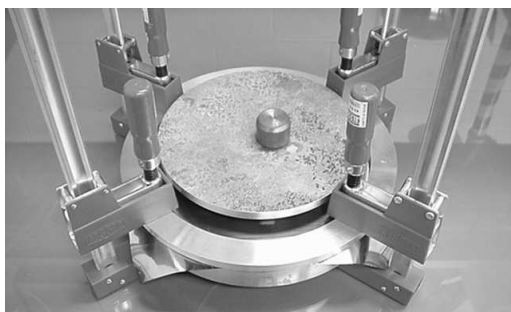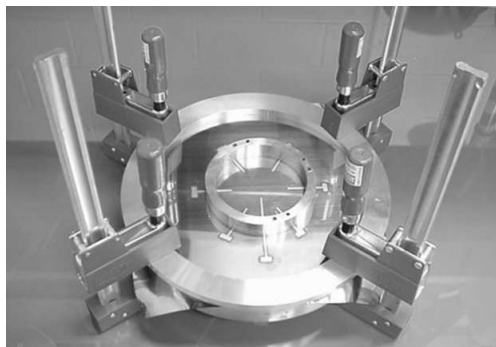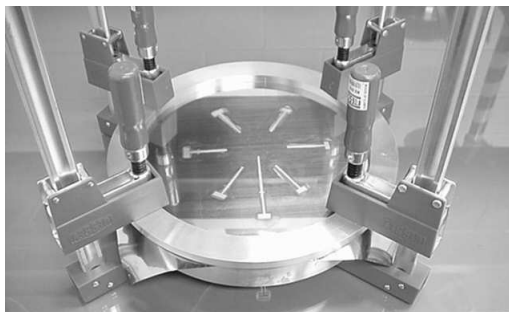
A.2 PVDF and Copper Etching

In order to determine etching time and procedures, I bought a circuit etching kit from Radio Shack® for \$15. The kit included:

- 6 oz. Ferric Chloride etching solution ($FeCl_3$)

- 2 plastic trays for etching the boards

- 1 etch-resistant pen (Sharpie® marker)

- 4 oz. bottle of etch-resistant pen remover (rubbing alcohol)

- 2 double-sided copper clad boards

- Instructions for using the kit

I also bought an additional 16 oz. bottle of etchant ($3.49), a larger copper clad board than the ones in the kit ($2.49), and a piezo element ($1.49).

After reading the instructions and the warnings on the bottle of etchant, and noting that it should be chemically similar to but slightly less reactive than hydrochloric acid (HCl), I set up three experiments.

A.2.1   Experiment 1 - Etching the copper board.   For the first experiment I wanted to see how long it would take to etch the copper clad board. I chose a concentric ring pattern similar to the one I will use for the stiff piezo controlled mirror. For the pattern mask, I covered both sides of the copper board with Contact® decorative covering (a nice floral pattern that coincidentally lines our kitchen drawers). Then, I drew the pattern onto the mask and retraced it with a razor knife. Peeling away the appropriate sections left the copper surface exposed for etching. I also thought I would test the pen, so I wrote my initials on the copper surface with the super-duper etch resistant Sharpie® marker. The instructions in the kit said it would take twenty minutes and half the small bottle of etchant. Understanding the chemical reaction, however, I improved the process. Covering the other side of the board, which did not need to be etched, sped things up a little and required about half as much etchant. Upon putting the board into the tray of etchant (don't forget the gloves!), the copper surface immediately turned black. I took a cotton swab and rubbed the surface of the copper to remove the black precipitate and agitate the solution. This reduced the etching time to about 6 minutes. Upon removal from the etchant, I rinsed the board in running water and then peeled off the etch mask. The pattern looked great, and the mask prevented the etchant from affecting the covered areas. The pen was less successful, although it still worked. It looked like some of the pen marks rubbed off when I was agitating the solution. Then, I disposed of the used etchant according to the manufacturer's directions (i.e. flushed it down the toilet).

Finally, I wiped down the surface of the board with isopropanol (the etch-resistant pen remover) to remove the pen marks and any residue left from the mask adhesive.

A.2.2   Experiment 2 - Testing the PVDF.   Since the PVDF has a thinner coating than the copper board, I expected that the etching time would be shorter, although I didn't know how the nickel-copper or the silver would react to the Ferric Chloride. I had two samples of PVDF: an 8.5x11" sheet of silver- coated PVDF and a scrap of the nickel-copper coated PVDF that I'll use for the thesis work (since it comes on a long roll). I put a drop of etchant on each sample to see what would happen. I expected to see the same black precipitate form on the surface that I saw with the copper, but no reaction was apparent. I took a cotton swab to wipe up the drop, and when I did I noticed that the metal surface on each of the films had been dissolved. Apparently, the coatings are so thin that the metal is instantly dissolved upon contact with the etchant. As a result, I discovered that the PVDF could be "etched" by dipping a cotton swab into the etchant and merely wiping the metal coating off. Upon this discovery, I set up my third experiment.

A.2.3   Experiment 3 - Etching the PVDF.   Since the "etching" process was practically instantaneous, I decided that using the pen would be the best way to mask off the PVDF. I drew a test pattern on the silver PVDF sheet that included two concentric ring patterns similar to the copper board and one tessellating hexagonal pattern. I then removed the silver coating using the process developed previously. It worked as expected, but some of the pen marks were removed, messing up one of the patterns. I discovered that a bit more etchant and less vigorous "scrubbing" with the cotton swab remedied this problem. After trying to pat off the PVDF with a paper towel, I discovered that the etchant doesn't absorb very well. Resorting back to the directions, I rinsed the sheet in the sink, which thoroughly removed the remaining etchant without smearing the pattern further. I then removed the coating on the back side of the sheet for visual effect, although in practice only one side needs to be etched (the other will be ground).

Having improved my technique, I proceeded to design a more complicated "captain's wheel" pattern on the scrap PVDF. The design is similar to one currently used for PZT bimorph adaptive secondary mirrors. Once the pattern was drawn out, the coating was removed (this time without smudging it). Upon rinsing the PVDF, I discovered what nickel-copper means: the film has a copper coating on it (visible through the clear PVDF from the back side after the top coating is removed) with a nickel coating on top. I'm not sure what the purpose of the dual-metal coating is (maybe copper is cheaper than silver, but the copper oxidizes, so they coat the outside with nickel?). I also removed half of the coating from the back of the pattern for display purposes.

A.2.4   Bonus Experiment - Piezo Mirror.   With the etching procedures down, I decided to start building a piezo mirror that I could use to work out how to make the stiff piezo controlled mirror for the thesis. I cut the remaining copper clad board into a 3" square. Then I disassembled the piezo element to remove the brass/ceramic piece from its plastic housing. I drilled a hole in the copper board for the piezo wires and glued the brass side of the piezo down to the center of the board with epoxy. I then cut a 0.5" thick section from the center of a 2.5" diameter plastic water bottle and glued it down to serve as a form for the liquid polymer to be poured over the piezo element. The result will be a round polymer mirror with imbedded piezo actuator that has wires coming out the back for the voltage to be applied (30 V max). Polymer and reflective coating to be applied at a later date.

A.2.5   Other ideas / initial observations.   Here are some things I thought of while working:

- Interestingly, ordinary rubbing alcohol removes "permanent" Sharpie® pen marks from smooth surfaces quite well.

- The 16 oz. bottle of etchant will be more than enough for my entire thesis work.

- The Ferric Chloride (or Ferrochloric Acid, as it could be called) isn't quite as nasty as I thought. Although the reaction produces gaseous chlorine, the amount involved is minute enough not to be noticed. It will, however, burn the skin, stain almost anything, and react to most metals (though none of these were actually tested today). It can be neutralized by diluting with a baking soda solution (tested) which produces CO_2, NaCl (probably) and some kind of nasty brown iron precipitate.

- The photoresist process *(or screen printing)*would be useful for making multiple copies of a complicated pattern on the PVDF. For a few simple designs, however, the manual procedure developed today saves a lot of time and materials.

- A more complicated and precise mask could be made for the copper board by covering it with Con-tact® paper and using the laser engraver at the skills development center to cut the mask (it wouldn't go through the copper if I polished it up so that it was shiny).

- If necessary, the PVDF could be etched after it was stretch-mounted to the aluminum ring.

A.3   M1 Construction Notes

A.3.1   5 Nov 01.   I checked on the PVDF membrane that I mounted last week, and it looks fine. I removed it from the stretching assembly and cut the excess PVDF away from the diameter mounting ring, leaving a tab on one side to make contacts for the wires. With the success of the PVDF etching experiments, I decided to go ahead and etch a control pattern on the PVDF. Typically, this would be done prior to mounting, but this will test the viability of etching the mounted membrane. I decided to etch the front surface of the membrane, which will leave the rear surface intact and grounded to the metal mounting ring. Additionally, I think it would be best to pour the polymer onto the "back" side of the membrane. This will allow the mounting ring to also serve as the form to contain the liquid polymer. The finished

mirror could then be safely placed "face-down" to keep dust off without marring the reflective surface.

A.3.2 6 Nov 01.   Today I poured the polymers into the test membrane and piezo mirrors. First I spray painted the PVDF membrane navy (I didn't have black) because it's reflective and the polymer is transparent. The vapor coating isn't completely opaque, so the paint will keep the second-surface interference down during testing. I probably should have painted the piezo mirror too, since it's got a shiny copper surface, but I'll just have to wait and see how it works. For these mirrors, I used GE Silicones® RTV615. It's a two-part resin with very low cure shrinkage and a good surface flatness. Here are the procedures for pouring the mirrors:

1. Prep the surface by applying the primer to ensure adhesion (if required - it depends on the polymer being used).

2. Pour half of the required polymer (by weight) into a clean plastic disposable container.

3. Pour half of the curing agent (10% of polymer by weight for RTV615) into the container.

4. Add the remaining polymer followed by the remaining curing agent. For these mirrors, I used 90 grams of polymer (and 9 grams of curing agent).

5. Mix it with a wooden spatula for about 15-20 minutes, making sure to scrape the sides well.

6. For small quantities, use vacuum debulking to remove the bubbles. For this larger quantity, I poured the resin into 6 plastic disposable test tubes and ran them in the centrifuge for 15 minutes.

7. Make sure that the mirrors are on a level surface, and that the membrane is supported by the mounting ring only. *Note: This procedure was later changed to support the membrane on a flat piece of glass*

8. I poured three test tubes (about 45 grams) into the membrane mirror, making sure not let it form bubbles, and then tilted the mirror until the polymer coating was even (about 1/8 inch thick).

9. I used two of the test tubes (about 30 grams) for the piezo mirror, forming a thicker mirror to help cover the wires and piezo transducer (about 1/4 inch thick).

10. Using light reflecting off the surface of the liquid polymer, it is possible to see bubbles floating up to the surface. Use a dental pick to remove these bubbles (if possible). For the membrane mirror, there was a piece of fuzz stuck in it that I couldn't get out. It will show up in the tests, unless I decide to pour another layer on top of this one.

    Note: See Chapter 3 for pictures of the finished mirrors.

Next, I'll have to wait for the polymer to cure (overnight) and then either add another layer or go ahead and put the reflective coating on them. Later the same day, I also crated three templates that I'll use to trace etch patterns on the PVDF to be sent to SRS for coating. I'll probably use the same ones for my own mirrors, which will be built using the same process as above (unless I run into any problems with the test mirror).

A.3.3   26 Nov 01.   Today I poured the second layer on M1 and S1. There were a lot of bubbles in M1, probably due to dust on the surface. With the RTV615, bubbles were always a problem. In the past, experiments have shown that applying a vacuum to this particular polymer after it was poured produced an uneven surface upon cure. So, the bubbles were removed with a dental pick one at a time or dragged to the edge of the mirror where they would not affect the test section.

A.4   Membrane Control Pattern Etching

A.4.1   8 Nov 01.   Now that the etching process for the PVDF was established, I made three etched membranes to send to SRS. They will coat the membranes

with CP1, a space qualified polymer. When they are returned, I will mount and test them using the same test setup as the mirrors I build.

Note: These membranes were never returned. Apparently SRS had trouble coating them with their polymers.

First, I designed three etch patterns using Corel PrintHouse® and printed them on photo paper. Then, I cut the patterns out with an x-acto® knife to create templates for the etching. I used a Sharpie® marker to draw the patterns on the PVDF using the templates as a guide. The covered areas represented regions of the membrane that would be left after the etching. Then, I used a cotton swab dipped in etchant to wipe away the metal coating surrounding the pattern. In order to save time and clean-up effort, I did not remove all of the metal, only enough to electrically isolate the control regions. Next, I removed the etchant by sopping it up with a slightly damp cotton ball. To minimize the spread of the etchant and avoid rubbing off the protective pattern, it was important to continually rotate the cotton ball to a clean part of the ball. Once the etchant was wiped up, I cleaned the surface again with a damp cotton ball. Lastly, I removed the etching pattern with cotton balls saturated with rubbing alcohol. I noticed that the rubbing alcohol did not work as well as the cleaner included in the etching kit. This was probably due to the fact that rubbing alcohol is only 70% isopropyl alcohol, versus 100% in the kit. The pattern can still be cleaned off easily, but the alcohol needs to "soak in" for a second or so before wiping the pattern off. Any other organic solvent would probably work (such as MEK, acetone, or methanol) but I haven't tried any of these to see if they adversely affect the PVDF.

I did have some problems with the marker "bleeding" under the template and messing up the pattern. These areas were either cleaned up prior to etching using a cotton swab slightly damp with alcohol, or fixed after the etching by manually reapplying the marker to the control areas and touching up the flaws with a cotton swab dipped in etchant.

The entire etching process requires a steady hand, but for these experiments the PVDF membranes produced will be more than sufficient. If more complicated and precise patterns are required in the future, the patterns could be printed on a transparency for use in applying a photoresist to the membranes. The etching could then be done by hand or by submersion for several seconds in a container of etchant.

Note: According to the PVDF manufacturer, complex patterns could also be applied using a screen-printing process.

A.5   Testing M1

A.5.1   7 Nov 01.   After the resins had cured, David and I did a quick check to make sure that the membrane mirror was flat (the piezo mirror has bubbles in it and needs another layer). Using laser light that had been passed through a spatial filter, we reflected the light off the polymer surface. The reflection was smooth and circular, with one noticeable defect (from the flaw described earlier). We also reflected collimated light off the mirror and then checked the reflection for collimation. The reflected light was fairly well collimated over the 1-inch area covered by the beam.

We decided to take the mirror over to the optics lab at AFIT to test the full aperture. I mounted the mirror in the 6" mount and set up the optics to test it using the WaveScope. Because the mirror had not yet been coated, the reflection was too dim to test it using interferometry. The WaveScope, however, measures the test image and reference image at different times and the laser intensity can be varied between tests. Because the test image was very dim, it was difficult to align the mirror such that the reflection entered the WaveScope. We noticed that the beam reflected off of the mirror was not collimated, which made it impossible to test in the current configuration. The mirror had a slight convex shape, causing the reflected beam to diverge over the beam path. We theorized that the weight of the liquid polymer had caused the membrane to sag slightly. The polymer the cured with a flat surface on the curved membrane. When the mirror was turned vertical, the membrane returned

to its original flat shape, causing the polymer to bulge outward. This problem could be corrected in the following ways:

1. Test the mirror in the horizontal position.

2. Set the mounting ring on a flat surface to support the membrane before pouring the polymer.

This particular mirror could be corrected by setting it on a flat surface and pouring another layer of polymer on top.

A.5.2   9 Nov 01.   Today, I decided to change the optics setup to allow testing of the mirror with the WaveScope. In order to overcome the slight curvature of the mirror, I used the 1" collimated beam, unexpanded, to test a 1" section of the mirror directly. I removed the expansion lens and 1" 45° turning mirror so that the test beam was not turned toward the 12" parabolic mirror. Instead, I used a 2" mirror at 45° to turn the beam from the beam splitter directly to the test mirror. I also shortened the reference path accordingly. Since the test beam was brighter, I attempted to again test the surface using interferometry. The first result showed a straight fringe pattern, indicating a very flat but tilted surface. Upon occlusion of the test beam, however, the pattern remained. The source of the fringes was determined to be internal reflections within the 2" cube beam splitter. Thus, the cube beam splitter was replaced with a 3" circular wedge beam splitter. The 1/2" thick wedge has one transparent surface and one partially reflective surface that is almost parallel to it. The two surfaces are a few arcseconds from parallel, just enough prevent internal reflections. Exchanging the beam splitters eliminated the fringes. Another attempt at interferometry revealed that the test beam was still too much dimmer than the reference beam to get a good fringe pattern.

Testing the mirror with the WaveScope in several different locations showed that it had a surface flatness varying from 0.062μm to 0.12μm RMS($\lambda/10$ to $\lambda/5$). An area near a visible flaw in the mirror was measured to 4μm peak-to-valley, but

the WaveScope gave errors that the intensity gradient was to large for a valid measurement. Thus, local surface flatness of the mirror is good enough for testing. With another, more carefully applied coating, the mirror could be used for thesis testing.

A.5.3 14 Nov 01.   Today I hooked up the membrane test mirror to a frequency generator to attempt to measure the surface deflection of the mirror. I again used a 1" collimated beam to measure a section of the mirror's surface. This time, with careful adjustment, I was able to discern a fringe pattern. The pattern had very little contrast due to the low intensity of the beam reflected by the test mirror, but it clearly showed five or six fairly symmetric concentric rings. Thus the primary abberation is defocus, which was seen earlier in the expansion of the collimated test beam. I then used the WaveScope's camera display function to show the interference pattern on the computer screen. Although the fringes seemed stable on the paper propped in front of the WaveScope opening, the computer image oscillated a bit. Due to vibration of the membrane, movement of the fringe pattern (inward and outward movement of the circles from changes in focus or curvature of the mirror) was very noticeable. The total oscillation was about two or three rings in amplitude. I again measured several 1" sections of the mirror surface and found surface flatness from 0.062μm near the center of the mirror to 0.15μm about halfway between the center and the edge.

I put the test spot on an area of the mirror that was between two of the PVDF control regions so that the mirror deflection could be measured. As a first check, I put up the fringe pattern I had observed before. Applying voltage at varying frequencies from 1-10 Hz caused no apparent change in the already oscillating fringe pattern. The voltage was reaching the membrane, since the control tab could be seen oscillating at the same frequency as the output. Increasing the frequency to 1-10 kHz produced audible tones, again verifying that the membrane was being energized. I then switched to using the WaveScope for Hartmann sensing and measured the surface deformation.

The surface shape did not appear to move as a result of the PVDF membrane. Even in live data gathering mode, the surface appeared constant.

To determine if the effect from the PVDF membrane was global and not noticeable on the local level, I decided to test the entire membrane surface for deflections due to the control layer. I removed the spatial filter, collimating lens, beam splitter, and turning mirror from the optical path. Then, I aimed the raw laser light at the center of the membrane mirror and replaced the spatial filter. Thus, the entire aperture of the mirror was illuminated with "clean" laser light. The circular image reflected on the wall showed one local surface flaw (mentioned previously) and a kind of "swirly" texture to the overall surface (causing the surface quality variations noticed in prior testing). Applying voltage to the PVDF layer again showed no deviation in the mirror's surface. Two theories so far on why the mirror seems to be unaffected by the control layer:

1. The PVDF is stretched so tightly that it prevents visible movement of the PVDF (i.e. stress induced by the voltage is overwhelmed by tension in the PVDF membrane).

2. The polymer layer is so thick (about 2 mm) that any sub-λ movement of the PVDF membrane is not translated through to the mirror surface.

Note: In future tests, displacement of the membrane surface due to applied voltage was observed and recorded.

A.5.4 16 Nov 01. Tests performed on the first membrane mirror, M1.

M1 = Mirror 1 - PVDF with circular test pattern, 1 layer clear RTV615, convex curvature.

Test 2 - check for PVDF control by self-reference in WaveScope. All tests are 5 tests averaging 5 frames at 30Hz each. λ = 633 nm = 0.633 microns.

Test 2a: check surface flatness at test region by using reference flat.

A-14

Test 2b: check surface flatness in self reference test (just to see what happens).

Test 2c: re-calibrate and run 2b again to check results.

Test 2d: voltage applied - polarity and magnitude unknown (several hundred V).

Test 2e: voltage applied - magnitude unknown (several hundred V), polarity opposite Test 2d.

Test 2a		Test 2b		Test 2c	
PV μm	RMS μm	PV μm	RMS μm	PV μm	RMS μm
0.3405	0.0623	0.0974	0.0124	0.0637	0.0106
0.3366	0.0597	0.0878	0.0134	0.0676	0.0121
0.3220	0.0609	0.1000	0.0121	0.0654	0.0106
0.3416	0.0621	0.1071	0.0121	0.0751	0.0114
0.3418	0.0628	0.1048	0.0124	0.0638	0.0108

Test 2d		Test 2e	
PV μm	RMS μm	PV μm	RMS μm
0.3655	0.0608	0.3843	0.0705
0.3445	0.0578	0.3857	0.0711
0.3498	0.0587	0.3775	0.0711
0.3513	0.0597	0.3955	0.0706
0.3392	0.0561	0.3934	0.0705

A.5.5   19 Nov 01.   Test 3, M1 - Now I have a volt meter and can apply a specific voltage. In addition, I was playing with the mirror and testing the voltage on different parts of the mirror. I found that while 300-400 volts was being applied at the electrodes, only about 20 V made it to the mirror. Recalling some arcing during the preliminary testing, I suspected that some of the metal coating on the PVDF had vaporized, reducing the conductivity of the material. Upon inspection, some of the leads from the electrode to the control regions looked like they had been damaged. Measuring the voltage on either side of the damaged area showed 300V on one side and 20V on the other. Repairs were made with conducting copper tape, which may or may not affect the mirror surface. Subsequent testing of the mirror will be done in other regions of the mirror. Depending on the results from test 3, it is likely that the voltages in Test 2 were on the order of tens of volts, not hundreds of volts.

Test three will be done with controlled, specific voltages on mirror 1.

Test 3a: Absolute surface flatness of membrane mirror 1.

Test 3b: Surface flatness self-referenced.

Test 3c: Positive 100 volts.

Test 3a		Test 3b		Test 3c	
PV μm	RMS μm	PV μm	RMS μm	PV μm	RMS μm
0.4055	0.0742	0.1205	0.0166	0.1640	0.0259
0.3791	0.0705	0.1329	0.0156	0.1629	0.0234
0.3910	0.0719	0.0814	0.0150	0.1263	0.0219
0.3997	0.0760	0.0864	0.0156	0.1364	0.0266
0.3936	0.0727	0.0897	0.0143	0.1582	0.0240

Test 3d: Positive 200 volts.

Test 3e: Positive 300 volts.

Test 3f: Positive 400 volts.

Test 3d		Test 3e		Test 3f	
PV μm	RMS μm	PV μm	RMS μm	PV μm	RMS μm
0.1877	0.0298	0.1725	0.0287	0.2071	0.0341
0.1557	0.0268	0.2050	0.0308	0.2131	0.0350
0.1572	0.0268	0.1880	0.0311	0.1756	0.0336
0.1547	0.0275	0.1640	0.0305	0.1964	0.0318
0.1500	0.0275	0.1829	0.0283	0.1833	0.0329

Test 3g: Positive 500 volts.

Test 3h: 0V surface flatness, after voltage applied.

Test 3i: Negative 100 volts. Membrane response drastically reduced to pos or neg voltage. Test surface flatness again after activation.

Test 3j: Absolute surface flatness after voltage applied (0v). Surface flatness not adversely affected by actuation. Try again.

Test 3k: Negative 600 volts.

Test 3l: Positive 600 volts

Test 3g		Test 3h		Test 3i	
PV μm	RMS μm	PV μm	RMS μm	PV μm	RMS μm
0.2169	0.0396	0.1062	0.0143	0.0696	0.0122
0.2038	0.0401	0.0949	0.0148	0.0895	0.0139
0.2267	0.0392	0.0810	0.0122	0.1034	0.0129
0.2045	0.0383	0.0828	0.0124	0.1143	0.0136
0.2148	0.0374	0.1142	0.0158	0.1138	0.0155

Test 3j		Test 3k		Test 3l	
PV μm	RMS μm	PV μm	RMS μm	PV μm	RMS μm
0.3636	0.0661	0.1960	0.0343	0.3294	0.0442
0.3683	0.0656	0.1947	0.0334	0.3382	0.0453
0.3769	0.0682	0.1728	0.0331	0.3140	0.0425
0.3733	0.0667	0.1657	0.0317	0.3116	0.0413
0.3607	0.0657	0.1761	0.0343	0.3166	0.0412

A.5.6   20 Nov 01.   Today I tried testing M1 using the 12" parabolic mirror to get the full aperture of the membrane mirror. I had the mirror set up in the mount vertically, but the surface shape displayed by the WaveScope oscillated between concave and convex as the membrane surface vibrated back and forth. I think that the membranes will have to be tested in the horizontal position. I tried testing M1 in the horizontal position with no success. The membrane shape was too deformed to produce a good image, with a large variation in brightness across the surface.

A.5.7   9 Dec 01.   After the second layer and a gold reflective coating were applied, the mirror was re-tested in the horizontal position, with a 5x4 inch section illuminated.

Test 4, 6": 6" reference flat - note astigmatism (unknown source).

Test 4a: Surface flatness - may have errors due to large wavefront gradient.

Test 4b: Surface flatness - recalibrated using T4a reference and new test calibration. Large intensity gradient required manual exposure at 1/1000. Many interior points were eliminated due to brightness.

Test 4, 6"		Test 4a		Test 4b	
PV μm	RMS μm	PV μm	RMS μm	PV μm	RMS μm
1.9475	0.2360	6.5266	1.0349	4.1915	0.7791
1.8645	0.2242	6.9009	1.0213	4.1731	0.7838
1.9274	0.2321	6.3874	0.9629	4.1931	0.7822

Test 4c: Self-referenced surface flatness - manual calibration due to intensity gradient.

Test 4d: Self-referenced surface flatness - after membrane sat "right side up" for an hour.

Test 4e: Inner circle region 300V.

Test 4c		Test 4d		Test 4e	
PV μm	RMS μm	PV μm	RMS μm	PV μm	RMS μm
0.6914	0.0768	0.5445	0.0533	3.6098	0.5648
0.7604	0.0823	0.4688	0.0487	3.5291	0.5503
0.7089	0.0765	0.5211	0.0503	3.0559	0.5294

Test 4f: Inner region 600V.

Test 4g: Re-test 0V after applying positive voltage.

Test 4h: Inner region - Neg 300V.

Test 4f		Test 4g		Test 4h	
PV μm	RMS μm	PV μm	RMS μm	PV μm	RMS μm
9.1605	1.4301	2.2119	0.2696	2.6516	0.3674
11.2784	1.4382	1.9391	0.2687	2.8684	0.3861
10.8787	1.4170	1.7249	0.2754	2.3842	0.3671

Test 4i: Inner region - Neg 600V.

Test 4j: Re-test 0V after applying negative voltage.

Test 4k: Re-calibrated, then tested self-referenced (0v).

Test 4l: Middle ring 300V.

Test 4i		Test 4j		Test 4k	
PV μm	RMS μm	PV μm	RMS μm	PV μm	RMS μm
4.5264	0.5983	1.6546	0.2876	0.5310	0.0686
4.3685	0.6062	1.8238	0.2984	0.7777	0.0881
4.4905	0.6029	1.8177	0.2902	0.5376	0.0645

Test 4l		Test 4m		Test 4n	
PV μm	RMS μm	PV μm	RMS μm	PV μm	RMS μm
8.9226	1.4350	11.8606	2.1174	2.3739	0.3772
7.9676	1.4334	11.4114	2.1150	2.4244	0.3728
8.9052	1.4582	12.0262	2.1002	2.3850	0.3735

Test 4m: Middle ring 600V.

Test 4n: Re-test 0v after applying positive voltage.

Test 4o: Middle ring - Negative 300V.

Test 4p: Middle ring - Negative 600V.

Test 4q: Middle ring - 0v re-check after applying negative voltage.

Test 4o		Test 4p		Test 4q	
PV μm	RMS μm	PV μm	RMS μm	PV μm	RMS μm
3.2507	0.5666	6.7818	1.1288	1.8962	0.2140
3.2606	0.5727	6.7912	1.1388	2.2368	0.2234
3.1997	0.5723	6.7382	1.1628	2.0268	0.2158

A.6   M2 Construction and Testing

A.6.1   18 Nov 01.   Today I made membrane mirror two (M2). The second membrane and all subsequent membrane mirrors will be made from a different roll of PVDF than the first mirror. The second roll is thicker than the first and should have a greater piezoelectric effect. The second membrane has a different etch pattern (see Figure 3.12).

A.6.2   19 Nov 01.   This morning I poured the first layer of mirror M2. Instead of suspending the mounting ring and pouring the polymer on top, I placed

the mirror on top of a flat 7" diameter piece of glass to support the membrane until the polymer cures.

A.6.3   9 Dec 01.
Performed Test 1 on M2. Single layer of RTV615, uncoated, with 7 control regions. Tested in full aperture with the 133μm MLM.

Test 1a: Surface flatness - self-referenced - 0V.

Test 1b: Re-calibrated due to spike in center, repeated T1a. Spike still there, but less tall.

Test 1c: Middle region 300v.

Test 1a		Test 1b		Test 1c	
PV μm	RMS μm	PV μm	RMS μm	PV μm	RMS μm
1.2435	0.0550	0.3104	0.0308	1.5373	0.1744
1.2769	0.0609	0.6483	0.0336	1.5047	0.1722
1.0907	0.0634	0.3845	0.0314	1.3881	0.1682

Test 1d: Middle region 600v.

Test 1e: 0v re-check after applying positive voltage.

Test 1f: Negative 300V.

Test 1d		Test 1e		Test 1f	
PV μm	RMS μm	PV μm	RMS μm	PV μm	RMS μm
2.0188	0.1926	1.6689	0.1186	1.4467	0.2311
2.0669	0.1925	1.6990	0.1275	1.3981	0.2277
2.0343	0.1853	1.5773	0.1240	1.6908	0.2243

Test 1g: Negative 600V.

Test 1h: Re-check 0v after negative voltage applied.Still looks relatively flat. The actuation must affect the calibration (since the reference is pre-actuation). More accurate results (in terms of magnitudes only) may be achieved by recalibrating between test runs.

	Test 1g		Test 1h
PV μm	RMS μm	PV μm	RMS μm
2.1055	0.2998	2.1895	0.1884
1.9522	0.2988	2.3127	0.1904
2.3960	0.3006	2.1724	0.1811

A.6.4   10 Dec 01.   Spent some time importing the data from M2, test 1 into MATLAB®. Performed Test 2 to check the response of two side actuators.

Test 2a: Self-reference - 0V.

Test 2b: Positive 300V.

Test 2c: Positive 600V.

	Test 2a		Test 2b		Test 2c
PV μm	RMS μm	PV μm	RMS μm	PV μm	RMS μm
0.4089	0.0568	1.9081	0.2699	2.7880	0.4649
0.4177	0.0543	1.8091	0.2636	2.9596	0.5082
0.4693	0.0550	1.7613	0.2663	2.7099	0.4604

Test 2d: 0V recheck after positive voltage applied. Appears to be some residual shape change.

Test 2e: Negative 300V

Test 2f: Negative 600V (accidentally named M2_T2e_Neg_600v on disk).

	Test 2d		Test 2e		Test 2f
PV μm	RMS μm	PV μm	RMS μm	PV μm	RMS μm
1.5266	0.2191	2.2719	0.2956	3.0375	0.4845
1.4085	0.1916	2.2280	0.3174	3.5966	0.4972
1.3860	0.1853	2.1520	0.3079	3.3346	0.4862

Test 2g: Recheck 0v (accidentally named M2_T2f_0v on disk). Looks like there is some "sag" in the membrane - maybe due to heating?

Test 2h: Recalibrated and tested at 0v.

Test 2d		Test 2e	
PV μm	RMS μm	PV μm	RMS μm
2.5103	0.3959	1.1963	0.0773
2.9158	0.4817	0.4735	0.0621
2.9632	0.4879	0.4717	0.0352

Test 3a: 0v.

Test 3b: Region 1 Neg 600V.

Test 3c: Region 2 Neg 600V.

Test 3a		Test 3b		Test 3c	
PV μm	RMS μm	PV μm	RMS μm	PV μm	RMS μm
0.3587	0.0419	2.9496	0.3321	2.2858	0.5123
0.3499	0.0436	2.8035	0.3289	2.3067	0.5060
0.4131	0.0435	2.7401	0.3361	2.3347	0.5105

Test 3d: Region 3 Neg 600V.

Test 3e: Region 4 Neg 600V.

Test 3f: Region 5 Neg 600V.

Test 3a		Test 3b		Test 3c	
PV μm	RMS μm	PV μm	RMS μm	PV μm	RMS μm
3.0409	0.5773	3.5366	0.5783	2.1768	0.3831
2.9807	0.5691	3.3535	0.5636	2.1813	0.3870
3.0870	0.5733	3.3227	0.5643	2.1694	0.3862

Test 3g: Region 6 Neg 600V.

Test 3h: Region 7 Neg 600V.

Test 3i: Regions 1,3,5 Neg 600V Regions 2,4,6,7 Pos 600V. This combination didn't work very well - the center region bled into the outer regions.

Test 3j: Regions 1,3,5 Neg 600V. Much better!

	Test 3g		Test 3h		Test 3i
PV μm	RMS μm	PV μm	RMS μm	PV μm	RMS μm
2.2649	0.4038	1.9857	0.3235	4.2378	0.7726
2.2167	0.3964	1.9370	0.3135	4.2954	0.7684
2.2025	0.4029	1.8820	0.3074	4.2295	0.7766

	Test 3j
PV μm	RMS μm
2.7910	0.6223
2.7961	0.6294
2.8268	0.6290

A.6.5   22 Jan 02.   I decided to test all of the control regions of M2 separately at -600V. First, though, I tested the surface flatness of M2 compared to a small $\lambda/20$ reference flat and the 6" $\lambda/10$ reference flat placed in the test setup.

Test 3 $\lambda/20$:   Compared to 2" flat mirror.

Test 3 6" $\lambda/10$:   Compared to 6" flat mirror placed in test setup.

	Test 3 $\lambda/20$		Test 3 6" $\lambda/10$
PV μm	RMS μm	PV μm	RMS μm
3.7545	0.7403	2.4754	0.4008
3.7610	0.7395	2.4866	0.4001
3.7638	0.7406	2.5303	0.3996

A.7   S1 Construction and Testing

Note: Initial construction notes are recorded in earlier sections.

A.7.1   27 Nov 01.   Today I tested S1 to check the surface flatness. The test was made on a 1" section of the surface near the middle of the specimen with the 133 μm MLM.

A.7.2   28 Nov 01.   Today I coated S1 with a reflective coating of gold to enhance the reflectivity and test the coating process on RTV615. The mirror was first attached to a stand that allowed it to be suspended in the top of the vacuum

S1 Surface Flatness

PV μm	RMS μm
1.3308	0.2619
1.0150	0.2091
0.8351	0.1826
0.7032	0.1519
0.7162	0.1358

chamber. Then, a tungsten wire basket electrode was placed in the bottom of the vacuum chamber and connected to the power supply. A 3mm length of gold wire was placed in the basket, taking care to place the wire such that it would not fall out of the basket once the vacuum chamber was reassembled. The bell jar was replaced on the machine and the air was pumped out of the chamber. Once a suitable vacuum was achieved, current was applied to the basket. The gold melted and "wicked" into the wire basket. Then the current was increased until the wire glowed white hot. After a few seconds, the current was reduced to make sure that the gold had all evaporated. When the vacuum chamber was opened the gold had covered all of the exposed surfaces, including the mirror surface. The gold surface was not thick enough to be opaque, but the reflectivity was greatly enhanced. Prior testing revealed that most other metals, including aluminum and copper, did not produce a good coating on this polymer.

A.7.3   29 Nov 01.   Today I tried to test S1 in full-aperture mode. The reflected image was too small and distorted using the 12" parabolic mirror. I determined that the best solution would be to try to test the mirror using a 2" beam of collimated light instead of the 12" beam. I spent the rest of the day and the next several days experimenting with the setup.

A.7.4   5-6 Dec 01.   Spent two days locating source of fringes (Newton's rings due to edge diffraction). Re-built system and decided to use a shorter reference leg or simply place the reference flat in the test leg slightly in front of the test speci-

men. Of course, this won't work for interferometry, but it's fine for the WaveScope. Arranged the setup for testing S1.

A.7.5 7 Dec 01. Test 2 - Two layers of RTV615, with gold reflective coating. One inch aperture measured.

Test 2 - Surface flatness, measured against 1/20 wave reference.

S1 Test 2

PV μm	RMS μm
0.5654	0.0879
0.5860	0.0852
0.5902	0.0901

Test 3 - Same mirror, different setup - two inch aperture measured. Lowered brightness tolerance to include more points.

Test 3a: Surface flatness over aperture.

Test 3b: Surface flatness, self-reference.

Test 3c: Switched to 5 frames at 0.2 second intervals to average better (vs. 30 Hz) - 0V.

Test 3a		Test 3b		Test 3c	
PV μm	RMS μm	PV μm	RMS μm	PV μm	RMS μm
2.1744	0.4007	0.2960	0.0403	0.2607	0.0334
2.1585	0.4013	0.2827	0.0378	0.2469	0.0332
2.1602	0.3996	0.2989	0.0421	0.2090	0.0304

Test 3d: +16 volts.

Test 3e: -16 volts

Test 3f: +30 Volts.

Test 3g: -30 Volts.

Due to the apparent ineffectiveness of negative voltage, a re-calibration was done and the specimen was retested at 0, 30, -30 volts.

Test 3d		Test 3e		Test 3f	
PV μm	RMS μm	PV μm	RMS μm	PV μm	RMS μm
0.4304	0.0757	0.4817	0.0613	0.7654	0.1524
0.5514	0.0923	0.4383	0.0564	0.6219	0.1299
0.4164	0.0668	0.4797	0.0591	0.6866	0.1392

Test 3g	
PV μm	RMS μm
0.4291	0.0499
0.4613	0.0536
0.4454	0.0516

Test 3h: 0 Volts - Self-referenced calibration.

Test 3i: +30 Volts.

Test 3j: -30 Volts.

Test 3h		Test 3i		Test 3j	
PV μm	RMS μm	PV μm	RMS μm	PV μm	RMS μm
0.1817	0.0258	0.5097	0.0672	0.4861	0.0520
0.1826	0.0245	0.5361	0.0679	0.4531	0.0486
0.1911	0.0251	0.5372	0.0696	0.4574	0.0483

Test 4 - repeated test 3 with the 133 μm MLM. Should give more accuracy.

Test 4 flat: $\lambda/20$ flat mirror - self referenced in 2" setup. Note 45° astigmatism - source unknown (lenses, maybe?).

Test 4a: Surface flatness (using $\lambda/20$ reference.

Test 4b: Self-referenced (0V)surface flatness.

Test 4c: +30 Volts.

Test 4d: -30 Volts.

Test 4 flat (again):   Well, after all this testing (Test 4 - I flipped the last expanding lens and the 2" collimation looks cleaner. Still has astigmatism.

Test 4 flat		Test 4a		Test 4b	
PV μm	RMS μm	PV μm	RMS μm	PV μm	RMS μm
0.5331	0.0742	2.3249	0.3810	0.9049	0.1176
0.4947	0.0740	2.2907	0.3760	0.9327	0.1257
0.5316	0.0733	2.3109	0.3762	0.9272	0.1225

Test 4c		Test 4d		Test 4 λ/20	
PV μm	RMS μm	PV μm	RMS μm	PV μm	RMS μm
0.8572	0.1110	1.1137	0.1552	0.5456	0.0798
0.9652	0.1238	1.1629	0.1598	0.5425	0.0811
0.9919	0.1268	1.1042	0.1639	0.5438	0.0740

A.8   Testing Alternate Polymers

A.8.1   30 Nov 01.   Today David and I experimented with the new polymers. One is a two-part gray polymer, RTV627. This polymer was very thin, like cream, compared to RTV615, which had a honey-like viscosity. Since the polymer had a filler, bubbles induced by stirring were removed by placing the polymer in the vacuum chamber for several minutes. The polymer was poured into an aluminum mold with tape along the edges to hold the polymer in. A few bubbles formed on the surface, but they were popped with a sharp dental pick.

The other polymer tested was a very thin, clear hardcoat that cures upon exposure to ultraviolet light (UVHC8558). Due to its low viscosity and the quick cure time, this polymer may be perfect for thin polymer mirrors. Unfortunately, the UV lamp that we tried wasn't powerful enough to fully cure the polymer. It solidified into a gummy substance, but the surface remained liquid. Also, this polymer is very nasty (from the safety label, "may cause burns that are not immediately obvious or painful").

A.8.2   3 Dec 01.   The RTV627 test sample showed numerous bubbles that had popped on the surface creating a sort of "orange peel" texture. Not the best for mirrors, but between the flaws the overall surface seemed flat. I poured another coat on top of the first one to see if the second layer would have better results. Hypothesizing that the bubbles were introduced when the liquid polymer

flowed over the aluminum substrate's surface flaws, another test sample was made and the bubbles were removed in the vacuum chamber. The air pressure was reduced to less than 0.05 Torr. Bubbles formed around the taped edges and some bubbles appeared in the interior of the test area. The test sample was left in the chamber for about 20 minutes. During this time, the bubbles around the edge slowed but remained constant. The bubbles in the interior continued to appear at the rate of about 1 every twenty seconds. The bubbles left dark spots on the surface of the polymer, probably caused by the filler. Upon removal of the test sample, the surface seemed to have residual flaws from the bubbles that did not appear to settle out. It is possible that the prolonged exposure of the polymer to very low pressures affected the curing of the polymer (maybe evaporation of some of the constituents, thus altering the composition of the polymer).

A.8.3   4 Dec 01.   Today I looked at the second RTV627. Looks like flat paint.

A.8.4   11 Dec 01.   Made first test sample of RTV656.

A.8.5   12 Dec 01.   Made a second test sample of RTV656.

A.8.6   13 Dec 01.   Tested the conductive spray paint. It wasn't. Only very high voltages made it through, and then at reduced amounts over the input voltages. 600v applied = 100v across. Poured another layer of RTV656 on top of paint, and some parts of the paint lifted where bubbles came up during evacuation. Looks like the conductive paint may not work. The second sample of RTV656 looked pretty good, with minimal surface flaws (no bubbles, only some minor deviation due to submerged block).

A.9   S2 Construction and Testing

A.9.1   11 Dec 01.   Made baseplate for S2. Mounted piezoceramics with leads on front of S2. Made a bunch of copper tape leads for the membrane mirrors. Made first test sample of RTV656.

A.9.2   12 Dec 01.   Mounted piezoceramics on rear of S2. Made a second sample of RTV656.

A.9.3   13 Dec 01.   Tested the conductive spray paint. It wasn't. Only very high voltages made it through, and then at reduced amounts over the input voltages. 600v applied = 100v across. Soldered copper tape to front of piezos on S2 to ground them to front surface and metal ring (since the conductive paint layer won't work for grounding the top piezo surfaces).

A.9.4   14 Dec 01.   Intended to pour S2 today, but I couldn't get a key to the materials cabinets. Instead, I spent the entire afternoon working on the code to import the surface data, smooth the surface by averaging the surrounding points, and plot the Zernike polynomials.

Note: Further description of S2 construction and testing attempts recorded in Chapter 3.

Appendix B. Example MATLAB® Code

B.1   Test Data Plot Example

```
% M2_T1a_0v
% Mon Dec 10 21:42:00 2001
% Zygo Zernike Coefficients
% Obscuration Ratio = 0.0000
% Index Coefs(microns) Equation
clear
z=[
    1     0.000111  % rcos(t) (X Tilt)
    2    -0.017736  % rsin(t) (Y Tilt)
    3     0.000000  % 2r^2-1 (Focus)
    4     0.002374  % r^2cos(2t) (0 Astigmatism)
    5     0.060935  % r^2sin(2t) (45 Astigmatism)
    6     0.063945  % (3r^2-2)rcos(t) (X Coma)
    7    -0.017444  % (3r^2-2)rsin(t) (Y Coma)
    8     0.011925  % 6r^4-6r^2+1 (Spherical)
    9     0.048998  % r^3cos(3t)
   10     0.015642  % r^3sin(3t)
   11     0.051215  % (4r^2-3)r^2cos(2t)
   12     0.047111  % (4r^2-3)r^2sin(2t)
   13     0.056155  % (10r^4-12r^2+3)rcos(t)
   14    -0.014347  % (10r^4-12r^2+3)rsin(t)
   15     0.003686  % 20r^6-30r^4+12r^2-1
   16     0.042861  % r^4cos(4t)
   17    -0.016271  % r^4sin(4t)
   18     0.015161  % (5r^2-4)r^3cos(3t)
   19    -0.006705  % (5r^2-4)r^3sin(3t)
   20    -0.001297  % (15r^4-20r^2+6)r^2cos(2t)
   21     0.037905  % (15r^4-20r^2+6)r^2sin(2t)
   22     0.012681  % (35r^6-60r^4+30r^2-4)rcos(t)
   23    -0.022015  % (35r^6-60r^4+30r^2-4)rsin(t)
   24    -0.001044  % 70r^8-140r^6+90r^4-20r^2+1
   25     0.016246  % r^5cos(5t)
   26     0.029928  % r^5sin(5t)
   27     0.027668  % (6r^2-5)r^4cos(4t)
   28     0.010367  % (6r^2-5)r^4sin(4t)
   29    -0.008846  % (21r^4-30r^2+10)r^3cos(3t)
   30     0.002812  % (21r^4-30r^2+10)r^3sin(3t)
   31    -0.002484  % (56r^6-105r^4+60r^2-10)r^2cos(2t)
   32    -0.002624  % (56r^6-105r^4+60r^2-10)r^2sin(2t)
   33     0.015239  % (126r^8-280r^6+210r^4-60r^2+5)rcos(t)
   34    -0.010192  % (126r^8-280r^6+210r^4-60r^2+5)rsin(t)
   35     0.001073  % 252r^10-630r^8+560r^6-210r^4+30r^2-1
```

```
];

data=textread('M2_T1a_0v.dat', '%f');
% factor(length(data))  % [ 2     3     5     11     31]
data(5353)=0; % remove bad data points >10*surrounding points
data(5463)=0;
data(5464)=0;
rows=110;        % size of data matrix determined by factoring
cols=93;         %    the raw data column [rows*cols = length(data)]
smoothlevel=1;    % increase this for smoother plots
pupil=47;        % manually adjust the Zernike scaling - approx cols/2
shift=[3 0];     % shifts the Zernike location within the pupil, in mm
MLM=0.133;       % MLM lenslet size, in millimeters
ratio=7.6327;    % test beam expansion ratio
trim=1;          % 1 trims data outside test pupil, 0 plots all
makeplots        % this plots the data, Zernike, and smoothed data
```

B.2 makeplots.m Subroutine

```
% makeplots.m subroutine

z=z(:,2);

% Converts the data from a column to a matrix of size [rows,cols]
for j = 1:cols
   data_surf(1:rows,j)=data((j-1)*rows+1:j*rows);
end

% Trims matrix to exactly fit the data pupil, removes empty rows/cols
% near the edges.
if trim==1
   temp=zeros(rows+2,cols+2);
   temp(2:rows+1,2:cols+1)=data_surf;
   data_surf=temp;
   while (sum(data_surf(2,:))==0&sum(diff(data_surf(2,:)))==0)
     data_surf(2:size(data_surf,1)-1,:)=data_surf(3:size(data_surf,1),:);
   end
   r=2;
   while (sum(data_surf(r,:))~=0|sum(diff(data_surf(r,:)))~=0)
      r=r+1;
   end
   data_surf=data_surf(1:r,:);
   while (sum(data_surf(:,2))==0&sum(diff(data_surf(:,2)))==0)
     data_surf(:,2:size(data_surf,2)-1)=data_surf(:,3:size(data_surf,2));
   end
   c=2;
   while (sum(data_surf(:,c))~=0|sum(diff(data_surf(:,c)))~=0)
      c=c+1;
   end
   data_surf=data_surf(:,1:c);
   rows=size(data_surf,1);
   cols=size(data_surf,2);
end

% Converts from microns to wavelengths
data_surf=data_surf./(0.633);

% Converts data shift from millimeters to data points (lenslets)
shift=round(shift/(MLM*ratio));

% Calculates the Zernike plot surface
```

```matlab
zsurface = myzern(z,[rows cols], pupil, shift);

% Converts the Zernike height from microns to wavelengths
array=zsurface;
array=array./(0.633);

% Plots the Zernike surface
figure(1)
surf([0:size(array,2)-1]*MLM*ratio,[0:size(array,1)-1]*MLM*ratio,array);
view([-19,68])
%axis([0 110 0 110 -1 1.5]) % Adjust this or use autoscaling as needed
colormap(copper)
colorbar
shading interp
xlabel=('Surface Location - mm');
ylabel=('Surface Location - mm');
zlabel=('Surface Height - Wavelengths (633nm)');

% Plots the data surface
figure(3)
surf([0:cols-1]*MLM*ratio,[0:rows-1]*MLM*ratio,data_surf);
view([-19,68])
%axis([0 110 0 110 -1 1.5])
colormap(copper)
colorbar
shading interp

% Calculates the smoothed data surface
smooth_data = interpolate2(data_surf,smoothlevel);

% Plots the smooth data
figure(4)
surf([0:cols-1]*MLM*ratio,[0:rows-1]*MLM*ratio,smooth_data);
view([-19,68])
%axis([0 110 0 110 -1 1.5])
colormap(copper)
colorbar
shading interp

% Calculates the data mask for the Zernike
mask=zeros(rows, cols);

for r=1:rows
```

```matlab
    for c=1:cols
        if smooth_data(r,c)~=0
            mask(r,c)=1;
        end
    end
end

% Gets the axis size from the first Zernike plot so they match
figure(4)
H=axis;
figure(2)

% Plots the masked Zernike surface
surf([0:size(array,2)-1]*MLM*ratio,[0:size(array,1)-1]*MLM*ratio,array.*mask);
view([-19,68])
axis(H);
%axis([0 110 0 110 -2 2])
colormap(copper)
colorbar
shading interp
```

B.3 Interpolation Subroutine

```
function [data]= interpolate2(d,weight)
%function [data]= interpolate2(d,weight)
%
% Where d is a matrix of the surface data, weight is how much
% value to place on the neighboring points, and tolerance sets
% how much variation in the data is acceptable before it's thrown
% out.  This function basically "smooths out" data that is
% "choppy".  For qualitative use only!!!
%

% If weight isn't specified, set it to 1
if nargin < 2
    weight = 1;
end

rows = size(d,1);
cols = size(d,2);

data=d;

for r = 2:rows-1
   for c = 2:cols-1
      neighbors = d(r-1,c-1)+d(r+1,c-1)+d(r-1,c+1)
                      +d(r+1,c+1)+d(r-1,c)+d(r+1,c)+d(r,c+1)+d(r,c-1);
      if neighbors~=0
        neighbors=neighbors/8;
        data(r,c)=(d(r,c)+weight*neighbors)/(1+weight);
      end
    end
end
```

B.4 Zernike Plotting Subroutine

```
function [zernsurf] = myzern(zernpoly,sz,pupil,shift)
%function [zernsurf] = myzern(zernpoly,sz,pupil,shift)
%
% Where zernsurf is the surface represented by the Zernike
% polynomial (in column form, up to order 35). The coefficients
% of the polynomial are contained in the 'zernpoly' variable
% and the output surface is a matrix of size [row col] with pupil
% radius 'pupil' in the same units as 'sz'.  The surface can be
% shifted by the amount in rows and cols, 'shift' = [0 0]
% is unshifted.
%
% Copyright 2002 - Michael Sobers - All rights reserved.

% Ensures the Zernike coefficient vector is at lest 35 long
if length(zernpoly)<35
   zernpoly(35)=0;
end

% If the user inputs a row vector, this converts it to column
if size(zernpoly,1)<2
   zernpoly=zernpoly';
end

% If sz is unspecified, this sets it to 30-square
if nargin<2
   sz=[30 30];
end

row=sz(1);
col=sz(2);

% Determines the odd/even nature of row/col and finds the
% center and selects the pupil radius, if unspecified
if mod(row,2)==0
   even=1;
   if nargin<3
      pupil=row/2-0.5;
   else
      if pupil==0
         pupil=row/2-0.5;
      end
   end
```

```
else
    even=0;
    if nargin<3
        pupil=row/2-1;
    else
        if pupil==0
            pupil=row/2-0.5;
        end
    end
end

% If the shift is unspecified, sets it to zero
if nargin<4
    shift=[0 0];
end

% Calculates the Zernike surface from the coeffiecients
if even
  center=[0.5+row/2 0.5+col/2]+shift;
  for i = 1:row
     for j = 1:col
         xpos = i-center(1); %0.5-row/2;
         ypos = j-center(2); %0.5-col/2;
         r = sqrt(xpos^2+ypos^2)/pupil;
         if r<=1
           t = atan2(ypos,xpos);
           polyvalue = [ r*cos(t);r*sin(t);2*r^2-1;
             (r^2)*cos(2*t);(r^2)*sin(2*t);(3*r^2-2)*r*cos(t);
             (3*r^2-2)*r*sin(t);6*r^4-6*r^2+1;r^3*cos(3*t);
             r^3*sin(3*t);(4*r^2-3)*r^2*cos(2*t);
             (4*r^2-3)*r^2*sin(2*t);(10*r^4-12*r^2+3)*r*cos(t);
             (10*r^4-12*r^2+3)*r*sin(t);20*r^6-30*r^4+12*r^2-1;
             r^4*cos(4*t);r^4*sin(4*t);(5*r^2-4)*r^3*cos(3*t);
             (5*r^2-4)*r^3*sin(3*t);(15*r^4-20*r^2+6)*r^2*cos(2*t);
             (15*r^4-20*r^2+6)*r^2*sin(2*t);
             (35*r^6-60*r^4+30*r^2-4)*r*cos(t);
             (35*r^6-60*r^4+30*r^2-4)*r*sin(t);
             70*r^8-140*r^6+90*r^4-20*r^2+1;
             r^5*cos(5*t);r^5*sin(5*t);(6*r^2-5)*r^4*cos(4*t);
             (6*r^2-5)*r^4*sin(4*t);(21*r^4-30*r^2+10)*r^3*cos(3*t);
             (21*r^4-30*r^2+10)*r^3*sin(3*t);
             (56*r^6-105*r^4+60*r^2-10)*r^2*cos(2*t);
             (56*r^6-105*r^4+60*r^2-10)*r^2*sin(2*t);
```

```
                     (126*r^8-280*r^6+210*r^4-60*r^2+5)*r*cos(t);
                     (126*r^8-280*r^6+210*r^4-60*r^2+5)*r*sin(t);
                     252*r^10-630*r^8+560*r^6-210*r^4+30*r^2-1];
             zernsurf(i,j)=sum(zernpoly.*polyvalue);
           else
            zernsurf(i,j)=0;
           end % if r<=1
       end % for j = 1:col
   end % for i = 1:row

 else
   center=[(row+1)/2 (col+1)/2]+shift;
   for i = 1:row
       for j = 1:col
           xpos = i-center(1); %(row+1)/2;
           ypos = j-center(2); %(col+1)/2;
           r = sqrt(xpos^2+ypos^2)/pupil;
           t = atan2(ypos,xpos);
           if r<=1
             polyvalue = [ r*cos(t);r*sin(t);2*r^2-1;
               (r^2)*cos(2*t);(r^2)*sin(2*t);(3*r^2-2)*r*cos(t);
               (3*r^2-2)*r*sin(t);6*r^4-6*r^2+1;r^3*cos(3*t);
               r^3*sin(3*t);(4*r^2-3)*r^2*cos(2*t);
               (4*r^2-3)*r^2*sin(2*t);(10*r^4-12*r^2+3)*r*cos(t);
               (10*r^4-12*r^2+3)*r*sin(t);20*r^6-30*r^4+12*r^2-1;
               r^4*cos(4*t);r^4*sin(4*t);(5*r^2-4)*r^3*cos(3*t);
               (5*r^2-4)*r^3*sin(3*t);(15*r^4-20*r^2+6)*r^2*cos(2*t);
               (15*r^4-20*r^2+6)*r^2*sin(2*t);
               (35*r^6-60*r^4+30*r^2-4)*r*cos(t);
               (35*r^6-60*r^4+30*r^2-4)*r*sin(t);
               70*r^8-140*r^6+90*r^4-20*r^2+1;
               r^5*cos(5*t);r^5*sin(5*t);(6*r^2-5)*r^4*cos(4*t);
               (6*r^2-5)*r^4*sin(4*t);(21*r^4-30*r^2+10)*r^3*cos(3*t);
               (21*r^4-30*r^2+10)*r^3*sin(3*t);
               (56*r^6-105*r^4+60*r^2-10)*r^2*cos(2*t);
               (56*r^6-105*r^4+60*r^2-10)*r^2*sin(2*t);
               (126*r^8-280*r^6+210*r^4-60*r^2+5)*r*cos(t);
               (126*r^8-280*r^6+210*r^4-60*r^2+5)*r*sin(t);
               252*r^10-630*r^8+560*r^6-210*r^4+30*r^2-1];
             zernsurf(i,j)=sum(zernpoly.*polyvalue);
                 else
             zernsurf(i,j)=0;
           end % if r<=1
```
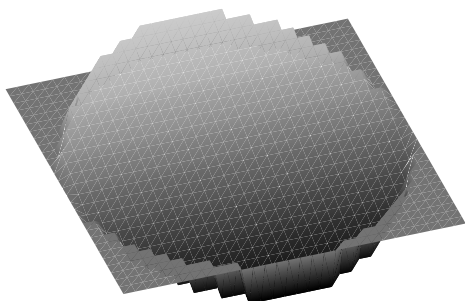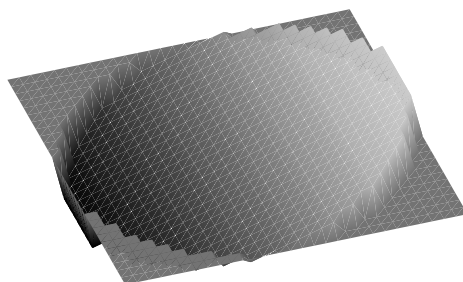
```
      end % for j = 1:col
   end % for i = 1:row
end % if even, else
```

Appendix C. Zernike Polynomials

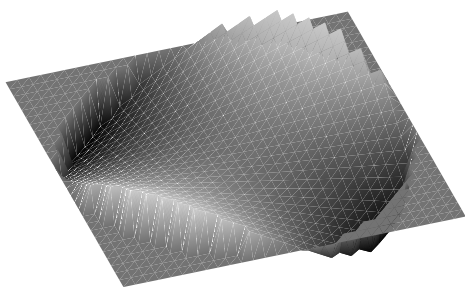Zernike 1: rcos(t) (X Tilt)

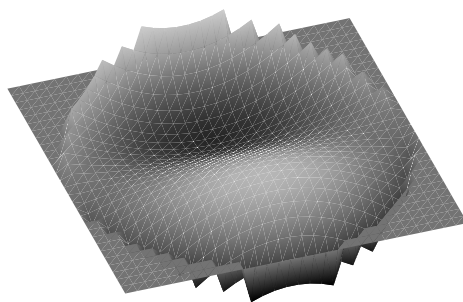Zernike 2: rsin(t) (Y Tilt)

Zernike 3: $2r^2-1$ (Focus)
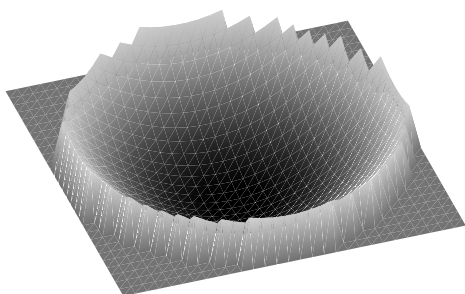
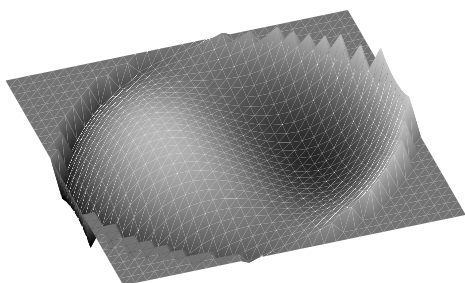Zernike 4: $r^2\cos(2t)$ (0 Astigmatism)
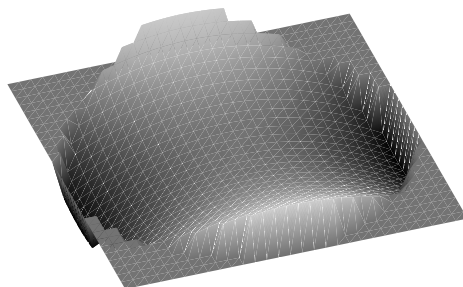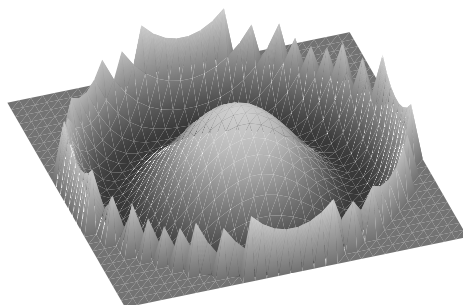
Zernike 5: $r^2\sin(2t)$ (45 Astigmatism)
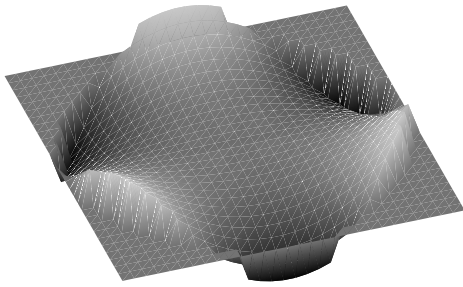
Zernike 6: $(3r^2-2)r\cos(t)$ (X Coma)
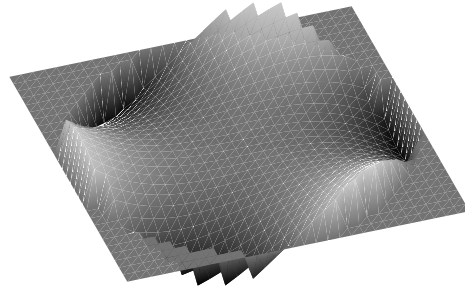
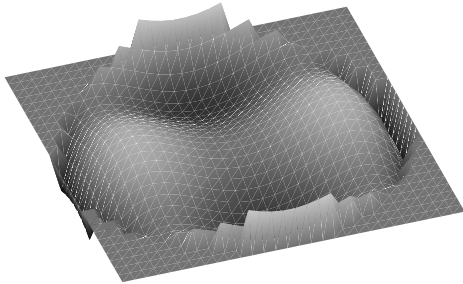Zernike 7: $(3r^2-2)r\sin(t)$ (Y Coma)

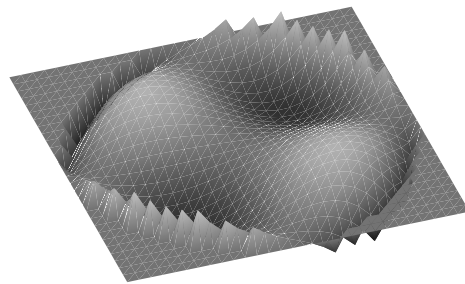Zernike 8: $6r^4-6r^2+1$ (Spherical)
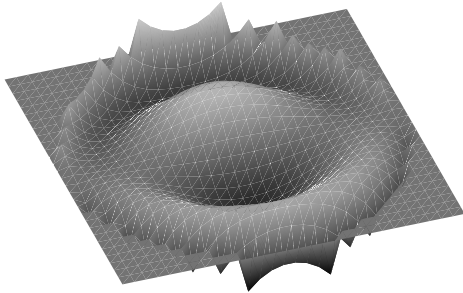
Zernike 9: $r^3\cos(3t)$
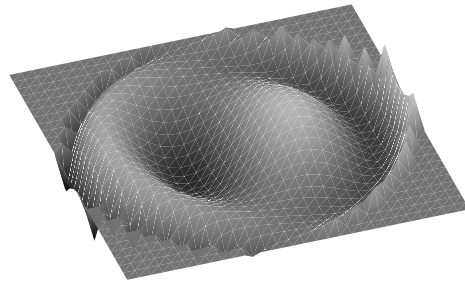
Zernike 10: $r^3\sin(3t)$

Zernike 11: $(4r^2-3)r^2\cos(2t)$

Zernike 12: $(4r^2-3)r^2\sin(2t)$

Zernike 13: $(10r^4-12r^2+3)r\cos(t)$

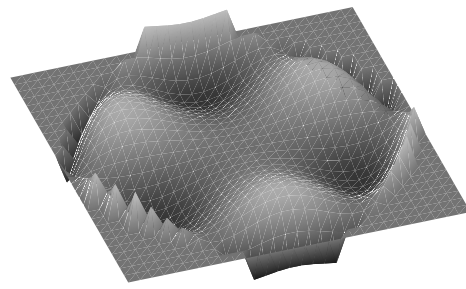Zernike 14: $(10r^4-12r^2+3)r\sin(t)$

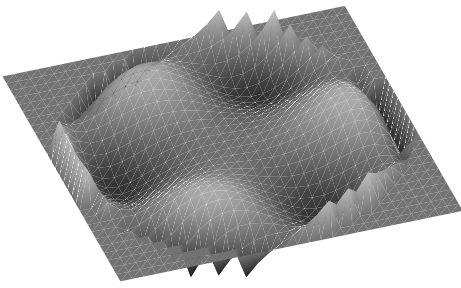Zernike 15: $20r^6-30r^4+12r^2-1$
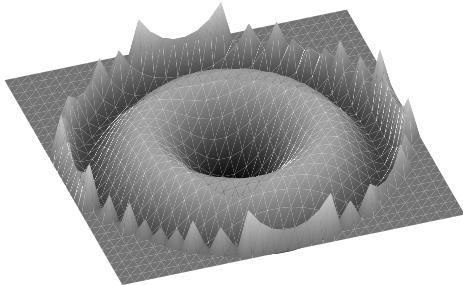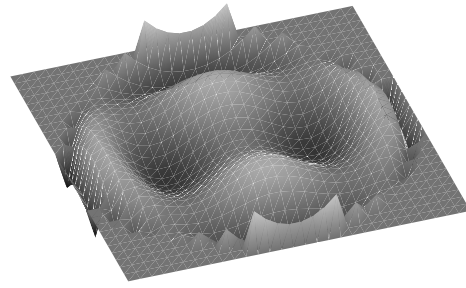
Zernike 16: $r^4\cos(4t)$
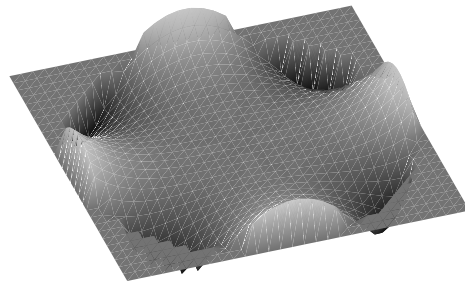
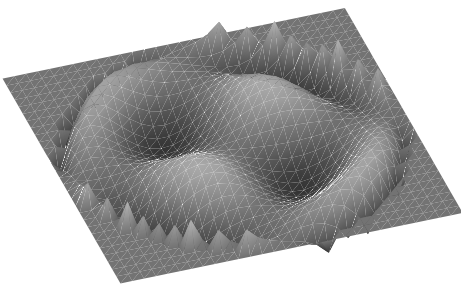Zernike 17: $r^4\sin(4t)$
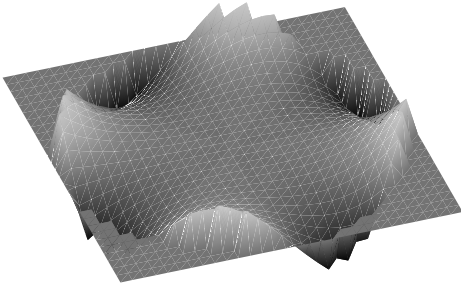
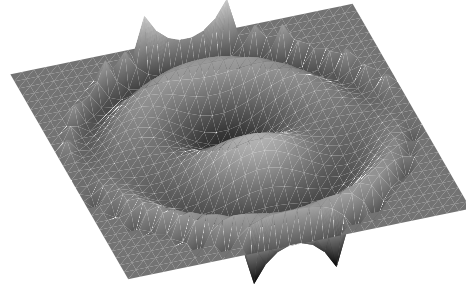Zernike 18: $(5r^2-4)r^3\cos(3t)$

Zernike 19: $(5r^2-4)r^3\sin(3t)$
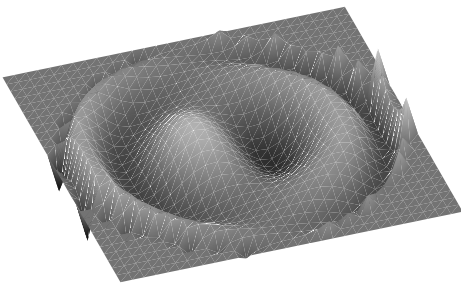
Zernike 20: $(15r^4-20r^2+6)r^2\cos(2t)$
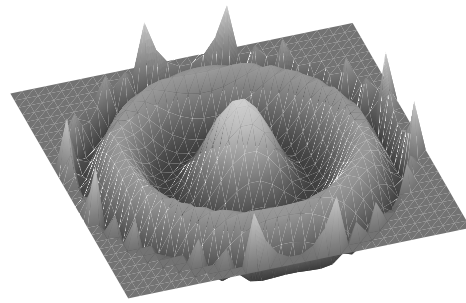
Zernike 21: $(15r^4-20r^2+6)r^2\sin(2t)$

Zernike 22: $(35r^6-60r^4+30r^2-4)r\cos(t)$

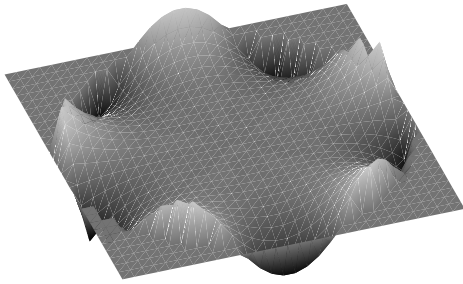Zernike 23: $(35r^6-60r^4+30r^2-4)r\sin(t)$

Zernike 24: $70r^8-140r^6+90r^4-20r^2+1$

C-4

Zernike 25: $r^5\cos(5t)$

Zernike 26: $r^5\sin(5t)$
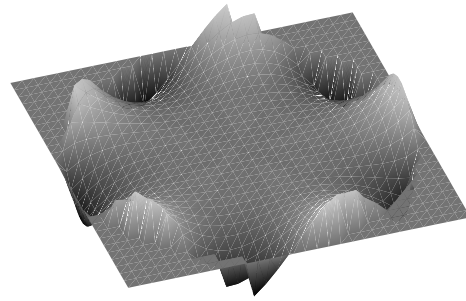
Zernike 27: $(6r^2-5)r^4\cos(4t)$
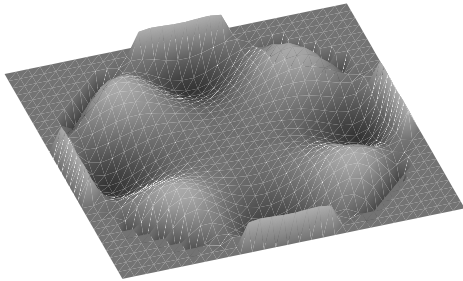
Zernike 28: $(6r^2-5)r^4\sin(4t)$
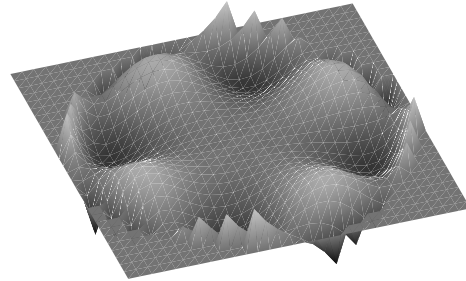
Zernike 29: $(21r^4-30r^2+10)r^3\cos(3t)$
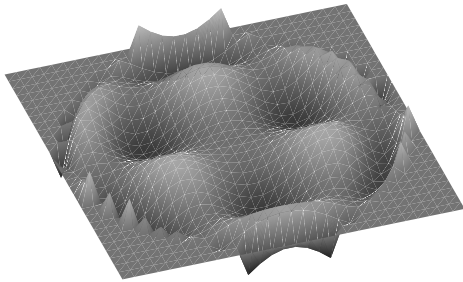
Zernike 30: $(21r^4-30r^2+10)r^3\sin(3t)$
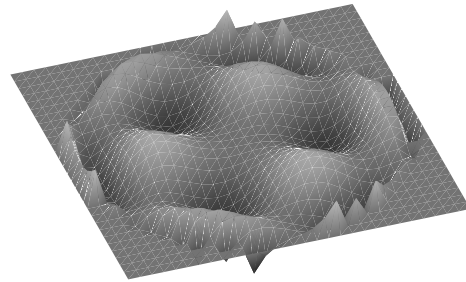
Zernike 31: $(56r^6-105r^4+60r^2-10)r^2\cos(2t)$
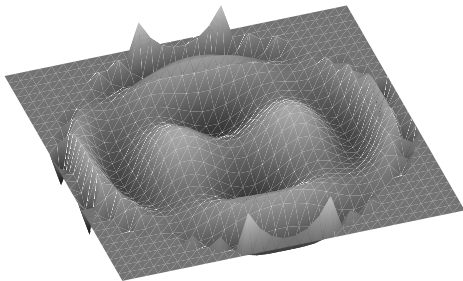
Zernike 32: $(56r^6-105r^4+60r^2-10)r^2\sin(2t)$
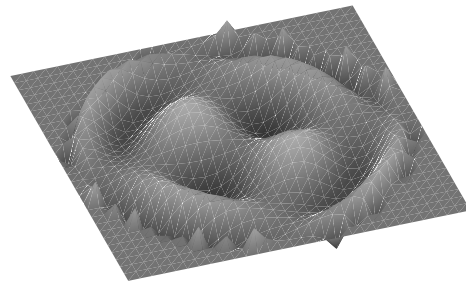
Zernike 33: $(126r^8-280r^6+210r^4-60r^2+5)r\cos(t)$

Zernike 34: $(126r^8-280r^6+210r^4-60r^2+5)r\sin(t)$

Zernike 35: $252r^{10}-630r^8+560r^6-210r^4+30r^2-1$

Bibliography

1. Burge, J. H. and others. "Active mirror technology for large space telescopes." *UV, Optical, and IR Space Telescopes and Instruments 4013*, edited by James B. Breckinridge and Peter Jakobsen. 640–648. Bellingham WA: SPIE, 2000.

2. Dierickx, P. and others. "The 8.2 metre primary mirrors of the VLT." *Adaptive Optics and Optical Structures 1271*, edited by R. K. Tyson and J. Schulte in den Bäumen. 266–274. Bellingham WA: SPIE, 1990.
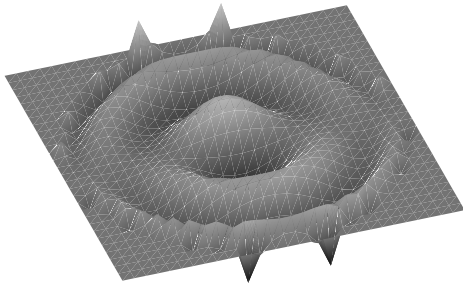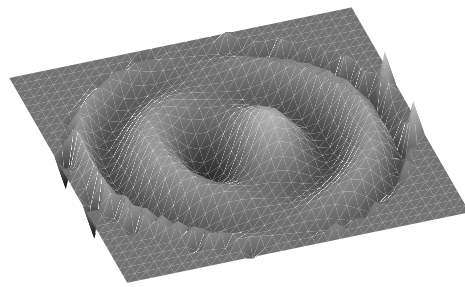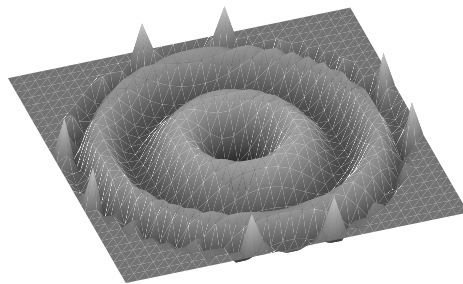
3. Dornheim, Michael A., "Inflatable Structures Taking Flight." http://mike.lgarde.com/programs/iaearticle/awarticle.html.

4. Forbes, F. F. "Bimorph PZT active mirror." *Active telescope systems 1114*, edited by François J. Roddier. 146–151. Bellingham WA: SPIE, 1989.

5. Grahne, Mark S. and David P. Codogan. "Deployment Control Mechanisms and Packaging Methodologies for Inflatable and Membrane Space Structures." *Gossamer Spacecraft: Membrane and Inflatable Structures Technology for Space Applications 191*. Progress in Astronautics and Aeronautics, edited by Christopher H. Jenkins, chapter 4, 417–431, Reston, VA: The American Institute of Aeronautics and Astronautics, Inc., 2001.

6. Grätzer, George. *Math into LaTeX* (3 Edition). Boston: Birkhäuser-Springer, 2000.

7. Jagourel, P. and P. Madec. "Adaptive optics: a bimorph mirror for wavefront correction." *Adaptive Optics and Optical Structures 1271*, edited by R. K. Tyson and J. Schulte in den Bäumen. 160–171. Bellingham WA: SPIE, 1990.

8. Lehman, D. H. and others. "Precision segemented reflectors for space applications." *Adaptive Optics and Optical Structures 1271*, edited by R. K. Tyson and J. Schulte in den Bäumen. 191–203. Bellingham WA: SPIE, 1990.

9. Maji, A. K. and M. A. Starnes. "Shape Measurement and Control of Deployable Membrane Structures," *Experimental Mechanics*, *40*(2):154–159 (June 2000).

10. Marker, D. K. and others. "Fundamentals of Membrane Optics." *Gossamer Spacecraft: Membrane and Inflatable Structures Technology for Space Applications 191*. Progress in Astronautics and Aeronautics, edited by Christopher H. Jenkins, chapter 4, 111–201, Reston, VA: The American Institute of Aeronautics and Astronautics, Inc., 2001.

11. Martin, H. M. and D. S. Anderson. "Techniques for optical fabrication of a 2mm-thick adaptive secondary mirror." *Adaptive optical systems and aplications 2534*, edited by Robert K. Tyson and Robert Q. Fugate. 134–139. Bellingham WA: SPIE, 1995.

12. Mather, John and others. "Next Generation Space Telescope." *UV, Optical, and IR Space Telescopes and Instruments 4013*, edited by James B. Breckinridge and Peter Jakobsen. 2–16. Bellingham WA: SPIE, 2000.

13. Meinel, A. B. and others. "Wavefront control of large optical systems." *Adaptive Optics and Optical Structures 1271*, edited by R. K. Tyson and J. Schulte in den Bäumen. 180–190. Bellingham WA: SPIE, 1990.

14. Mollenhauer, David and John Camping, "Multi-Layered Polymer Mirror Experiment." American Institute of Aeronautics and Astronautics, AIAA Paper 2001-1341, 2001.

15. Vdovin, G. V. and others. "Technology, characterization, and applications of adaptive mirrors fabricated with IC-compatible micromachining." *Adaptive optical systems and aplications 2534*, edited by Robert K. Tyson and Robert Q. Fugate. 116–129. Bellingham WA: SPIE, 1995.

16. Wada, B. K. and others. "Adaptive Structures." *Selected Papers on Smart Structures for Spacecraft MS 167*. SPIE Milesone Series, edited by Alok Das and Ben Wada, chapter 1, 3–20, Bellingham WA: SPIE, 2001.

17. Wagner, John W. *Optical Metrology of Active Membrane Mirrors*. MS thesis, Air Force Institute of Technology, Wright-Patterson AFB, March 2000.

18. Wertz, James R. and Wiley J. Larson. *Space Mission Analysis and Design* (3 Edition). Boston: Microcosm Press and Kulwer Adacemic Publishers, 1999.

19. "WaveScope® Operator's Manual." Adaptive Optics Associates, 1999.

Vita

First Lieutenant D. Michael Sobers, Jr., was born in Lafayette, Louisiana. He attended Baton Rouge Magnet High School and he received an Air Force ROTC scholarship to the Georgia Institute of Technology upon graduation. While at Georgia Tech, he majored in Aerospace Engineering and received his Bachelor of Aerospace Engineering degree in June, 1998.

His first Air Force assignment was Training Systems Engineer for the C-130 H2 Weapon System Trainer at the Training Systems Product Group, Aeronautical Systems Center, Wright-Patterson AFB, Ohio. He provided technical oversight in the development and testing of the flight characteristics for the C-130 H2 trainer and was responsible for final approval of the trainer's flight model. He then transitioned to Joint STARS Flight Crew Training System Lead Engineer, where he was responsible for the development of the Request For Proposal and the solicitation and acquisition of the Joint STARS Flight Crew Training System.

In August 2000, he began the Graduate Astronautical Engineering program at the Air Force Institute of Technology. Upon graduation, he will be reassigned to the Air Force Research Laboratory Advanced Composites Office at Hill AFB, Utah.

REPORT DOCUMENTATION PAGE

Form Approved
OMB No. 074-0188

The public reporting burden for this collection of information is estimated to average 1 hour per response, including the time for reviewing instructions, searching existing data sources, gathering and maintaining the data needed, and completing and reviewing the collection of information. Send comments regarding this burden estimate or any other aspect of the collection of information, including suggestions for reducing this burden to Department of Defense, Washington Headquarters Services, Directorate for Information Operations and Reports (0704-0188), 1215 Jefferson Davis Highway, Suite 1204, Arlington, VA 22202-4302. Respondents should be aware that notwithstanding any other provision of law, no person shall be subject to an penalty for failing to comply with a collection of information if it does not display a currently valid OMB control number. **PLEASE DO NOT RETURN YOUR FORM TO THE ABOVE ADDRESS.**

1. REPORT DATE (DD-MM-YYYY)	2. REPORT TYPE	3. DATES COVERED (From – To)
26-03-2002	Master's Thesis	Aug 2000 – Mar 2002

4. TITLE AND SUBTITLE

SMART SRUCTURES FOR CONTROL OF OPTICAL SURFACES

5a. CONTRACT NUMBER

5b. GRANT NUMBER

5c. PROGRAM ELEMENT NUMBER

6. AUTHOR(S)

Sobers, Jr., D. Michael, First Lieutenant, USAF

5d. PROJECT NUMBER
02185

5e. TASK NUMBER

5f. WORK UNIT NUMBER

7. PERFORMING ORGANIZATION NAMES(S) AND ADDRESS(S)

Air Force Institute of Technology
Graduate School of Engineering and Management (AFIT/ENY)
2950 P Street, Building 640
WPAFB OH 45433-7765

8. PERFORMING ORGANIZATION REPORT NUMBER

AFIT/GA/ENY/02-2

9. SPONSORING/MONITORING AGENCY NAME(S) AND ADDRESS(ES)

AFOSR/NA Structural Mechanics
Attn: Mr. Daniel Segalman
801 North Randolph Street   COMML: 703-696-7259
Arlington, VA 22203   e-mail: Daniel.Segalman@afosr.af.mil

10. SPONSOR/MONITOR'S ACRONYM(S)

11. SPONSOR/MONITOR'S REPORT NUMBER(S)

12. DISTRIBUTION/AVAILABILITY STATEMENT

APPROVED FOR PUBLIC RELEASE; DISTRIBUTION UNLIMITED.

13. SUPPLEMENTARY NOTES

.

14. ABSTRACT

The development of lightweight, large-aperture optics is of vital importance to the Department of Defense and the US Air Force for advancing remote sensing applications and improving current capabilities. Synthetic polymer optics offer weight and flexibility advantages over current generation glass mirrors, but require active control to maintain tight surface figure tolerances. This research explores the feasibility of using imbedded piezoelectric materials to control optical surfaces. Membrane-based and stiff piezo-controlled mirrors were constructed to develop and validate control techniques. Test results verified that surface control on the order of tens of wavelengths is possible using these systems.

15. SUBJECT TERMS

Adaptive Optics, Membrane Optics, PVDF Control, Polymer Mirror, Smart Structures, Flexible Mirror

16. SECURITY CLASSIFICATION OF:			17. LIMITATION OF ABSTRACT	18. NUMBER OF PAGES	19a. NAME OF RESPONSIBLE PERSON
a. REPORT	**b. ABSTRACT**	**c. THIS PAGE**	UU	173	Gregory S. Agnes, Maj, USAF (ENY)
U	U	U			**19b. TELEPHONE NUMBER** (Include area code) (937) 255-6565, ext 4317; e-mail: Gregory.Agnes@afit.edu

Standard Form 298 (Rev. 8-98)
Prescribed by ANSI Std. Z39-18

Form Approved
OMB No. 074-0188